



POLITECNICO DI TORINO

**Tesi di Laurea Magistrale in
Ingegneria Energetica e Nucleare**

Specializzazione in Tecnologie e Applicazioni Nucleari

**Treatment Planning in Proton Therapy using
VPatient 3D and Monte Carlo Simulation**

Candidato

Isabel De Pasquale

Relatori

Prof. Gianni Coppa (*DET*)

Dott.ssa Faiza Bourhaleb (*I-See s.r.l.*)

Anno Accademico 2021 - 2022

A mia nonna Abieh

Sommario

La radioterapia è una terapia medica che si erge sull'utilizzo delle radiazioni ionizzanti per il trattamento di masse tumorali. Essa si è evoluta nel tempo sia dal punto di vista dei campi applicativi che dal punto di vista tecnologico, ovvero nell'ottimizzazione del trattamento e nell'utilizzo di particelle più efficienti, come i protoni e gli ioni carbonio.

La sua prescrizione si fonda su una serie di passaggi eseguiti da medici e tecnici specialisti che ne definiscono l'adeguatezza nel caso specifico da trattare.

La seguente tesi si occupa innanzitutto di esplicitare le basi teoriche della radioterapia, dalla definizione di radiazione sino al concetto di cellula e pone una particolare attenzione sulla loro interazione e sugli effetti che derivano da questa.

In collaborazione con l'azienda *I-See Computing* sono stati approfonditi gli aspetti più tecnici che si celano dietro la protonterapia, come la programmazione, la modellazione e l'ottimizzazione di un piano di trattamento radioterapico. Tutto ciò è stato possibile grazie al paziente virtuale VPatient 3D sviluppato dalla *I-See* in collaborazione con il *National Institute of Nuclear Physics*.

Il primo accento è stato posto sul processo di generazione di immagini CT artificiali, il quale è costituito da due fasi, nella prima fase viene modellato il tumore all'interno del VPatient e nella seconda fase il software genera le immagini delle sezioni del tumore.

Il lavoro svolto nella seguente tesi riguarda l'elaborazione delle immagini CT migliorandone il contrasto ed effettuando dei controlli di qualità.

Tra le altre applicazioni offerte dall'*I-See Computing* troviamo 4SeePlan, sistema di pianificazione del trattamento, che permette al privato di poter simulare e ottimizzare online un piano di trattamento tramite il metodo Monte Carlo.

In quest'ultimo caso è stato possibile grazie all'interfaccia 4ToGo analizzare le discrepanze che definiscono il divario che si cela tra la Fast Optimization e il Metodo Monte Carlo.

Inoltre, è stata effettuata un'analisi sull'effettiva efficienza di una tecnica novizia al mondo della protonterapia, ovvero il trattamento tumorale attraverso più campi di irradiazione.

Abstract

Radiotherapy is a medical therapy that stands on the use of ionizing radiation for the treatment of tumour masses. It has evolved over time both in terms of its fields of application but also from a technological point of view, i.e. in the optimization of treatment and in the use of more efficient particles, such as protons and carbon ions.

Its prescription is based on a series of steps performed by doctors and technical specialists that define its suitability in the specific case to be treated.

The following thesis deals first of all with the explanation of the theoretical basis of radiotherapy, from the definition of radiation to the concept of the cell and pays particular attention to their interaction and to the effects resulting from this.

In collaboration with the company *I-See Computing* have been deepened the more technical aspects behind the proton therapy, such as programming, modelling and optimization of a radiotherapy treatment plan. This was made possible thanks to the VPatient 3D, developed by *I-See* in collaboration with the *National Institute of Nuclear Physics*.

The first emphasis was on the process of generating artificial CT images, which consists of two phases, in the first phase the tumour is modelled within VPatient and in the second phase the software generates images of the tumour sections.

The work carried out in the following thesis concerns the processing of CT images by improving the contrast and performing quality control.

Among the other applications offered by *I-See Computing* it's possible to find 4SeePlan, a treatment planning system that allows the individual to be able to simulate and optimize online a treatment plan through the Monte Carlo method.

In the latter case it was possible, thanks to the 4ToGo interface, to analyse the discrepancies that define the gap between Fast Optimization and the Monte Carlo Method.

In addition, an analysis was carried out on the effective efficiency of a novice technique in the world of proton therapy, that is the tumour treatment through multiple fields of irradiation.

Contents

List of Figures.....	1
List of Tables.....	6
Introduction	7
Physics principles of ionizing radiation.....	9
1.1 Classification of ionizing radiations	11
1.2 Ionizing radiation field	15
1.3 Dosimetric quantities	17
1.4 Coefficients of interactions of radiations with matter	19
Radiobiology	22
2.1 Hints of cell biology	23
2.1.1 Cell structure and function	23
2.1.2 Cell life cycle.....	24
2.2 Radiobiological phases	25
2.2.1 Physical phase.....	25
2.2.2 Chemical and biochemical phase	26
2.2.3 Biologic phase	28
2.2.4 Clinical phase	30
Radiotherapy.....	31
3.1 Bragg's peak.....	32
3.2 Radiotherapy Center	35
3.2.1 Particles accelerator.....	37
3.2.1.1 Cyclotron	37
3.2.1.2 Synchrotron	38
3.2.1.3 LINAC	39
3.2.2 Transmission lines	40
3.2.3 Treatment room	41
Head and neck cancers	41
Pelvic and abdominal tumours	42
Eye cancers	43

Treatment planning.....	45
4.1 Computed Tomography	46
4.1.1 X-ray tube	47
4.1.2 CT Detectors.....	49
4.1.3 Attenuation coefficient	50
4.1.4 Hounsfield units.....	51
4.1.5 CT machinery	56
4.1.6 CT treatment.....	57
4.1.7 Imaging acquisition	58
4.2 Magnetic Resonance Imaging	61
4.2.1 MR machinery	61
4.2.2 MR treatment.....	65
4.3 DICOM.....	65
4.4 Contouring.....	65
4.5 Treatment Planning.....	67
4.5.1 Fast Optimization	67
4.5.2 Monte Carlo Simulation	69
4.5.3 Treatment Planning Output	71
VPatient3D	74
5.1 Anthropomorphic Phantom	74
5.2 Virtual Patient 3D.....	79
5.3 DICOM CT Generation	80
5.3.2 Case 1: Brain	83
5.3.3 Case 2: Prostate	89
5.3.4 Case 3: Left Lung	94
Workflow VPatient.....	99
6.1 4SeePlan	99
6.1.1 Comparative analysis between Fast Optimization and Monte Carlo simulation	101
Isodose.....	103
DVHs.....	107
Evaluation Indices	112

Comments	113
6.1.2 Study analysis on a new tumour treatment technique	114
Isodose	117
DVHs	118
Evaluation Indices	119
Comments	120
Conclusions	121
Bibliography	123
Appendix	128

List of Figures

Figure 1	Incidence and mortality depending on the World Area relative to 2020.[1]	7
Figure 2	Incidence and the mortality depending on the type of cancer relative to 2020.[1].....	7
Figure 3	Directly and Indirectly ionizing radiation. [4]	11
Figure 4	Impact parameter for charged particles through a medium, Soft Collisions. [5].....	12
Figure 5	Impact parameter for charged particles through a medium, Hard Collisions. [5].....	12
Figure 6	Impact parameter for charged particles through a medium, Bremsstrahlung. [5].....	12
Figure 7	Bremsstrahlung radiation. [6]	13
Figure 8	Photoelectric effect. [7].....	13
Figure 9	Compton scattering. [7]	14
Figure 10	Pair production. [7]	14
Figure 11	Characterizing radiation field at a point P in terms of the radiation traversing the spherical surface S. [5].....	15
Figure 12	Cell nucleus, Chromosomes and DNA.	23
Figure 13	DNA Replication. [16].....	24
Figure 14	Energetic domains of photoelectric effect, Compton effect and pair production in function of the energy of the radiation and of the atomic number of the absorber. [13].....	25
Figure 15	(a) Direct and Indirect radiation damage to the DNA. (b) Cell DNA damage due to radiation. [26]	27
Figure 16	Direct and Indirect DNA damage due to ionizing radiation. [18]	28
Figure 17	Absorbed radiation in function of the thickness of the tissue for X-rays, protons and carbon ions. [27].....	33
Figure 18	Comparison between the use of protons, carbon ions and photos to treats brain tumours, lung and rectum intestine tumour. [27]	34
Figure 19	Dose distribution for a photons radiation with 10 windows of access and protons radiation with 3 windows of access. [28].....	34

Figure 20	Spread-Out Bragg Peak. [28].....	35
Figure 21	Number of radiotherapy machines per 1000 cancer patients. [29]	35
Figure 22	Scheme of a hadrontherapy centre. [32]	36
Figure 23	Scheme of a cyclotron. [34].....	37
Figure 24	Picture and scheme of Synchrotron situated in CNAO. [35].....	39
Figure 25	LINAC [36].....	39
Figure 26	Isocentric and eccentric gantry. [39].....	41
Figure 27	Patient Positioning System. [40].....	41
Figure 28	Optical Tracking System. [40].....	42
Figure 29	Patient Verification System. [40].....	42
Figure 30	Carbon fiber bed in CAPH room. [40].....	43
Figure 31	Patient Positioning System. [40].....	44
Figure 32	Eye Tracking System. [40]	44
Figure 33	X-ray tube scheme. [45].....	47
Figure 34	Detector.....	49
Figure 35	Scheme of interaction between the X-Ray beam and the target.	50
Figure 36	Value of the HU according to the mass density. [55]	52
Figure 37	First and second CT generation. [58].....	56
Figure 38	Third and fourth CT generation. [58]	57
Figure 39	System Source – Detector.[61]	58
Figure 40	Reference system of the patient and the device. [61]	59
Figure 41	Reference system of the patient, the device and the X-ray. [61]	59
Figure 42	Source shape function. [61]	60
Figure 43	Open and Closed Magnetic Resonance Imaging. [66].....	64
Figure 44	Volume defined in Radiotherapy by ICRU 50/62/83. [41].....	66
Figure 45	Pencil beam scanning delivery system. [70].....	67
Figure 46	Look Up Tables, LUT, of protons in water. [71].....	68
Figure 47	Beam delivery line. [72]	69
Figure 48	Simulation of Monte Carlo Method.	70
Figure 49	Isodose distribution in 3 planes and DVH of a proton therapy treatment planning.[73].....	71

Figure 50	DVH obtained thanks to MC GEATN3. [74]	72
Figure 51	Breast phantom structure. [76].....	74
Figure 52	Images of phantom A. [76]	75
Figure 53	Scheme of the online workflow. [78]	75
Figure 54	VERT [81]	76
Figure 55	Number of patients with clinically relevant anxiety. [83]	77
Figure 56	Sequence of patient treatment in VIPER. [84].....	77
Figure 57	Anthropomorphic phantoms of a child of a) 5-year-old and one of b) 10-year-old. [85].....	78
Figure 58	VP 3D structure following the Male Adult mesh directives [86].	79
Figure 59	I-See s. r. l Web Applications. [88]	80
Figure 60	Target 3D Modelling.....	81
Figure 61	Sectioning process representation.....	81
Figure 62	Generation of CT images set. [86].....	82
Figure 63	Case 1 "Brain" - Section 1.	84
Figure 64	Plots of s for each value of γ , with $c=1$. [89]	84
Figure 65	On the left the original section 1, on the right the gamma corrected section 1 ($\gamma=0.45$).....	85
Figure 66	Assembly of original sections.....	85
Figure 67	Assembly of gamma corrected sections ($\gamma=0.45$).....	86
Figure 68	On the left the gamma corrected section 1 ($\gamma=0.45$), on the right the section 1 obtained by the binary file "mat_HU.bin".....	87
Figure 69	Assembly of the sequence of sections obtained by the binary file "mat_HU.bin".	87
Figure 70	Section 1 obtained by the binary file "mat_ID.bin" with gamma correction ($\gamma=3.5$).....	88
Figure 71	Assembly of the sequence of sections obtained by the binary file "mat_ID.bin".....	88
Figure 72	Case 2 "Prostate" - Section 83.	90
Figure 73	On the left the original section 83, on the right the gamma corrected section 83 ($\gamma=0.40$).....	90
Figure 74	Assembly of original sections.....	91
Figure 75	Assembly of gamma corrected sections ($\gamma=0.40$).....	91

Figure 76	On the left the gamma corrected section 83 ($\gamma=0.40$), on the right the section 83 obtained by the binary file “mat_HU.bin”.....	92
Figure 77	Assembly of the sequence of sections obtained by the binary file “mat_HU.bin”.....	92
Figure 78	Section 83 obtained by the binary file “mat_ID.bin”.....	93
Figure 79	Assembly of the sequence of sections obtained by the binary file “mat_ID.bin”.....	93
Figure 80	Case 3 "Left Lung" - Section 54.....	95
Figure 81	On the left the original section 54, on the right the gamma corrected section 54 ($\gamma=0.50$).....	95
Figure 82	Assembly of original sections.....	96
Figure 83	Assembly of gamma corrected sections ($\gamma=0.50$).....	96
Figure 84	On the left the gamma corrected section 54 ($\gamma=0.50$), on the right the section 54 obtained by the binary file “mat_HU.bin”.....	97
Figure 85	Assembly of the sequence of sections obtained by the binary file “mat_HU.bin”.....	97
Figure 86	Section 54 obtained by the binary file “mat_ID.bin”.....	98
Figure 87	Assembly of the sequence of sections obtained by the binary file “mat_ID.bin”.....	98
Figure 88	Contouring of OARs.....	100
Figure 89	4SeePlan GUI.....	100
Figure 90	Contouring of Target 1.....	101
Figure 91	Angles setup.....	102
Figure 92	Axial view, gantry 270°, couch 0°.....	103
Figure 93	Axial view, gantry 169°, couch 0°.....	103
Figure 94	Coronal view, gantry 270°, couch 0°.....	104
Figure 95	Coronal view, gantry 169°, couch 0°.....	104
Figure 96	Sagittal view, gantry 270°, couch 0°.....	105
Figure 97	Sagittal view, gantry 169°, couch 0°.....	105
Figure 98	Ortho view, gantry 270°, couch 0°.....	106
Figure 99	Ortho view, gantry 169°, couch 0°.....	106
Figure 100	DVHs of PTV, brain and skin (external contour) obtained with Fast Optimization and Monte Carlo, for gantry 270°, couch 0°.....	108

Figure 101	DVHs of PTV, brain and skin (external contour) obtained with Fast Optimization and Monte Carlo, for gantry 169°, couch 0°.....	109
Figure 102	DVHs of PTV, brain and skin (external contour) obtained with Fast Optimization, for gantry 270°, couch 0° and gantry 169°, couch 0°....	110
Figure 103	DVHs of PTV, brain and skin (external contour) obtained with Monte Carlo, for gantry 270°, couch 0° and gantry 169°, couch 0°.....	112
Figure 104	Contouring of Target 2.....	114
Figure 105	Fields parameters.....	115
Figure 106	Dose Deposition All Fields yx projection for gantry 1 field technique.	115
Figure 107	Dose Deposition All Fields yx projection for 4 fields technique.....	116
Figure 108	Ortho view, 1 field technique.....	117
Figure 109	Ortho view of 4 fields technique.....	117
Figure 110	DVHs of PTV, brain, left eye, left optical nerve and skin (external contour) obtained with Monte Carlo, for 1 field and 4 fields.....	119

List of Tables

Table 1	Organs, HU and ID. [56].....	55
Table 2	Dose reduction with bismuth and lead shielding. [53]	58
Table 3	Dose constrains for adults and for children concerning the intracranial organs. [75]	72
Table 4	Mass density values and volumes for the constituent of the skeleton of the reference Male and Female. [87]	79
Table 5	Punctual values of the dose absorbed by the 99%, 98%, 50%, 2% and 1% of the volume, for gantry 270°, couch 0°.....	107
Table 6	Punctual values of the dose absorbed by the 99%, 98%, 50%, 2% and 1% of the volume, for gantry 169°, couch 0°.....	109
Table 7	Punctual values of the dose absorbed by the 99%, 98%, 50%, 2% and 1% of the volume, for gantry 270°, couch 0° and gantry 169°, couch 0° calculated with Fast Optimization.	110
Table 8	Punctual values of the dose absorbed by the 99%, 98%, 50%, 2% and 1% of the volume, for gantry 270°, couch 0° and gantry 169°, couch 0° calculated with Monte Carlo method.....	111
Table 9	HI and CI for gantry 270°, couch 0° and gantry 169°, couch 0° calculated with Fast Optimization and Monte Carlo method.....	112
Table 10	Punctual values of the dose absorbed by the 99%, 98%, 50%, 2% and 1% of the volume, for 1 Field.	118
Table 11	Punctual values of the dose absorbed by the 99%, 98%, 50%, 2% and 1% of the volume, for 4 Fields.....	118
Table 12	HI and CI for 1 Field and 4Fields.	119

Introduction

The *International Agency for Research on Cancer* releases each year data regarding cancer statistics worldwide. In 2020 19.3 million of people has been diagnosed cancer and 10 million has died for this cause.

Figure 1 shows the incidence and the mortality depending on the World Area relative to 2020, as we can see the most affected area is China.

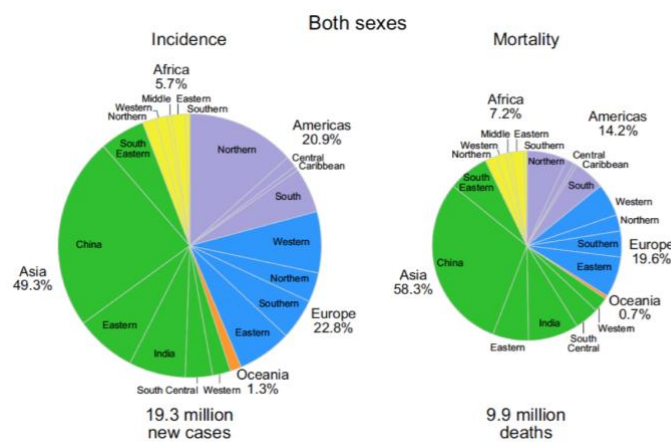


Figure 1 Incidence and mortality depending on the World Area relative to 2020.[1]

Figure 2 shows the incidence and the mortality depending on the type of cancer relative to 2020.

It has been estimated that the most diffused tumour is the female breast cancer, with 2.3 million of new cases. While the tumour with a higher mortality is the lung cancer, with 1.8 million of deaths. [1]

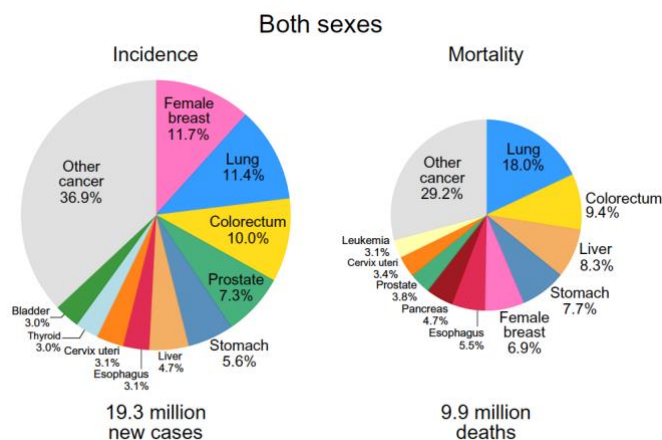


Figure 2 Incidence and the mortality depending on the type of cancer relative to 2020.[1]

The procedures that deal with the cancer treatments are surgery, radiotherapy and chemotherapy.

Radiotherapy is the result of nuclear medicine, as it uses subatomic particles or ions to treat tumours. It is a very efficient technique that is continuously in a development phase. The bases of radiotherapy erect on two areas which seem very different but which marry harmoniously, that are physic of ionizing radiation and radiobiology.

Even if at first thought radiotherapy is a word connected to the medicine world, behind it hides the hard work of physicists and engineers.

Thanks to the cooperation with the *I-See s. r. l.* society it has been possible to deepen the technicalities that give life to the radiotherapy process dedicated to patient care.

Chapter 1

Physics principles of ionizing radiation

The term *radiation* defines the phenomena of transmission of energy in space through particles or waves, which will propagate in the space interacting with matter.

Radiations can be divided in two big groups depending on the way they interact with molecules and atoms, *non-ionizing radiations* which have lower frequencies, and *ionizing radiations* which have higher frequencies.

In nature a radiation is defined ionizing when it is able to ionize atoms, detaching electrons from their structure. So ionizing radiations are able to break chemical bonds in molecules or even in atoms. Ionizing radiations can have corpuscular or electromagnetic nature. The corpuscular radiations can be composed of light particles, i.e. electrons and positrons, and heavy particles, i.e. alpha particles, or neutral particles, i.e. neutrons.

The electromagnetic particles are gamma and X rays.

Ionizing radiations have natural origin in the case they are cosmic rays or if they are produced by particles coming from the cosmos or from the decaying of radioactive substances contained in the Earth's crust. Every year a human is exposed to 2.4 millisievert (mSv) of natural background of radiation.

For example, radon, that is a natural material, is very dangerous for workers that work in underground or in areas with high presence of radon. Instead if we talk about cosmic rays, they will concern air personnel.

Ionizing radiations can also be artificial, in fact they can be the result of nuclear reactions or of the decaying of artificial radioactive substances, or they can be generated by some electronic devices.

Ionizing radiation can damage the cells or the entire body.

The somatic damage regards the cellular structure, a healthy cell can be killed or transformed in an ill cell, in this last case the patient can start suffering of leukemia or tumour. Leukemia is a rapid cancer while tumour employs more years to develop. The sensibility to radiation depends obviously from the kind of organ, in fact bone marrow and thyroid are the most attacked.

The cancer risk increases with the intensity of the radiation dose and for weak people, like children or ill people.

The genetic damage regards the gene structure and so the reproductive organs, causing miscarriages or altering the genetic chromosome, giving rise to disease.[2]

Non-ionizing radiations are not able to ionize atoms, the only effect they can have is to make atoms and molecules oscillating and producing heat.

Non-ionizing radiations can be divided in Extremely Low Frequency, ELF, and Radiofrequency and microwaves.

- The fields at very low frequency are generated at home or work in correspondence of electrical equipment or cables, or in correspondence of high voltage lines or transformers.

The problem regards the fact that these fields generates inside the body electric currents that overlap the natural one and can generate nervous and muscular overexcitations. The magnetic field at very low frequency are more difficult to shield respect to the electric one. There could be some possible correlation between the onset of leukemia in children leaving near high voltage lines.

- Radiofrequency are generated in telecommunication, like transmitters or mobile telephony, while microwaves are for example generated in microwave ovens. The fields generated by the high frequency are given by the combination of electric and magnetic field, they generate the electromagnetic fields, that are easy to shield. The exposition to short but intense field only generate thermic effects, like the heating of tissues. The Specific Absorption Rate, SAR, represent the quantity of energy absorbed by the body per unit mass, W/kg. When the absorption overcome 10 W/kg the effect they get worse causing serious damage. The more sensitive organs are the less vascularized one because they have a poor blood circulation and they heat faster. [3]

1.1 Classification of ionizing radiations

Radiological physics is the study of the interaction of ionizing radiations with matter and the exchange of energy that this entails. Radiological physics began with the discovery of radium by Marie and Pierre Curie and of the X-rays by Wilhelm Röntgen in the 1890s. It was shortly before these two discoveries made their way into the world of medicine, first with the first X-ray photograph made by the same Röntgen in 1895 and lately with the with the use of X-rays in radiography.[5]

Ionizing radiations in the interactions give part of their energy to matter, producing *excitement* and *ionization*.

In the first case, if the radiation has not enough energy to ionize the atom, the electron will move to a higher energy level. To come back to its original state the electron can emit a photon, whose energy is equal to the differences of the two energy levels, or can give energy to another electron that will live the atom, this last phenomenon is called *Auger effect*.

In the second case, radiation has enough energy to ionize atoms or molecules of matter in a direct or indirect way. The *International Commission on Radiation Units, ICRU*, first has established the differences between *Directly ionizing radiations* and *Indirectly ionizing radiations*.

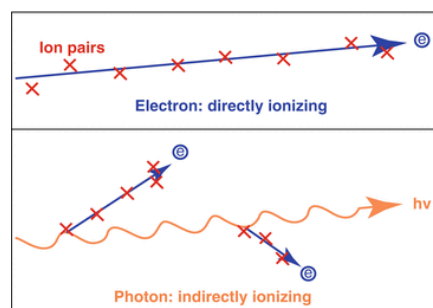


Figure 3 Directly and Indirectly ionizing radiation. [4]

The *Directly ionizing radiations* is composed of fast charged particles, i.e. electrons and protons, that deposit their energy into matter thanks to Coulomb collisions. In this case the radiation delivers its energy to orbital electrons, belonging to atoms, whose releasing kinetic energy will be equal to the difference of the energy of the radiation and the binding energy. If these electrons have enough energy to ionize other atoms are called *secondary electrons*.

The loss of energy of the radiation depends on the “*impact parameter*” b , that represents the minimum distance of the radiation’s particle from the nucleus.

Considering “ a ” equal to the ray of the atoms:

1. If $b > a$ it's possible to have *Soft collisions*. The particle will give only a small part of its energy to the orbital electrons. This phenomenon can take to ionization of the atom through the releasing of an electron with very small energy or excitation of an orbital electron.

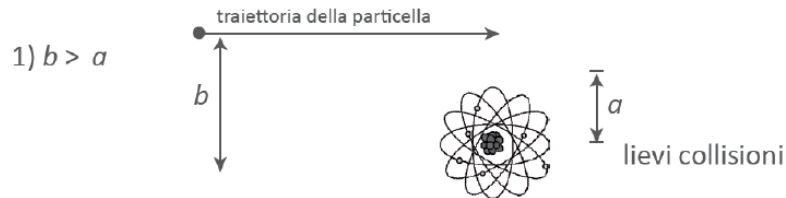


Figure 4 Impact parameter for charged particles through a medium, *Soft Collisions*. [5]

2. If $b \sim a$ it's possible to have *Hard collisions*. The particle of the radiation in this case can interact directly with an orbital electron releasing more energy. Electrons released from hard collision are called *Delta ray*, δ .

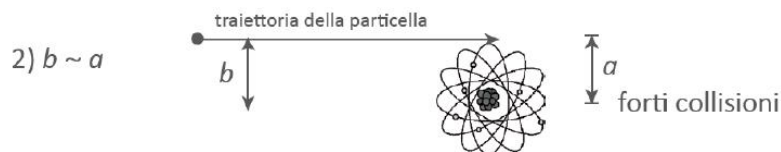


Figure 5 Impact parameter for charged particles through a medium, *Hard Collisions*. [5]

3. If $b \ll a$ it's possible to have *Bremsstrahlung* phenomenon. The charged particle, usually an electron, that passes near the nucleus of an atom, will decelerate and its trajectory will be deflected due to the electric field around the atomic nucleus.

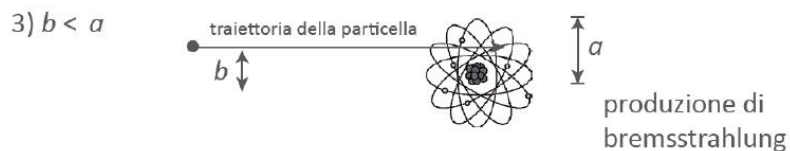


Figure 6 Impact parameter for charged particles through a medium, *Bremsstrahlung*. [5]

For the conservation of kinetic energy, the particle will emit photons.



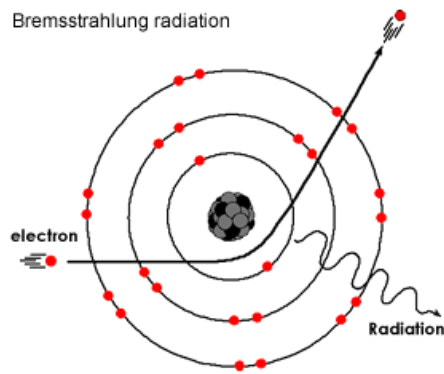


Figure 7 Bremsstrahlung radiation. [6]

The *Indirectly ionizing radiations* are generated by uncharged particles, i.e. photons and neutrons or X and γ rays, which have two impacts on matter. First of all, uncharged particles will give their energy to matter, freeing charged particles of atoms, or nucleus, that in a second phase will propagate and ionize matter.

The possible phenomena generated by interaction of photons and matter are:

- *Photoelectric effect*, the photon gives all its energy to an orbital electron that will be ejected from its orbit with an energy equal to the difference between the energy of the photon and the binding energy;

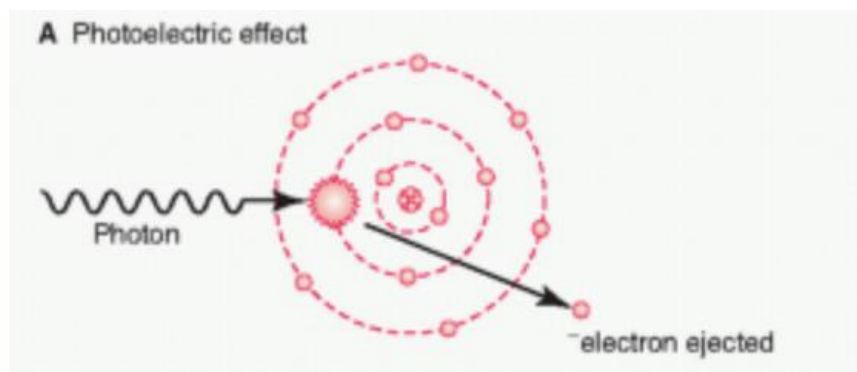
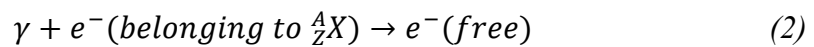
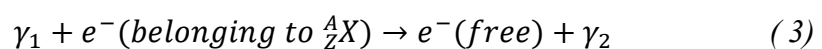


Figure 8 Photoelectric effect. [7]

- In *Compton scattering* the photon gives only part of its energy to eject the atom's electron from its orbit and the remaining energy is emitted through a secondary photon.



Where: $h\nu_1 > h\nu_2$.

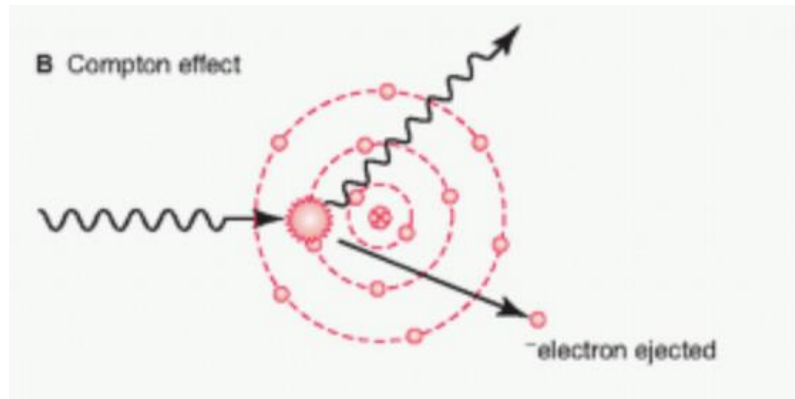


Figure 9 Compton scattering. [7]

- *Pair production* happens when the photon hits the nucleus of an atom, giving birth to an electron and a positron. The atom remains unchanged.

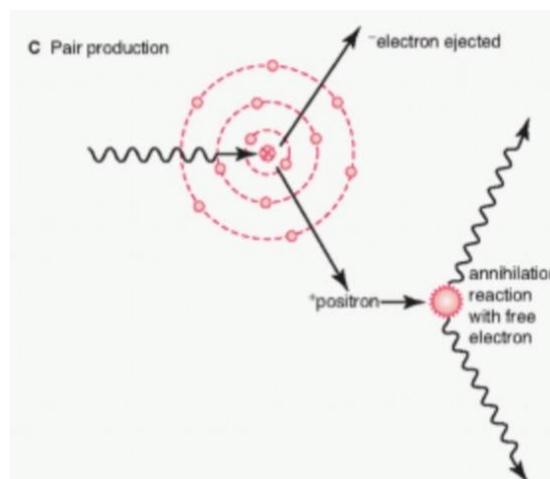


Figure 10 Pair production. [7]

The pair production can be generated also through the interaction of a photon with an electron, “*triplet emission*”.



Successively the positron can interact with another electron producing two photons in the process called *annihilation*.



The possible phenomena generated by interaction of neutrons and matter are multiple:

- Production of γ -rays (n, γ)
- Production of charged particles (n, p), (n, α), ...

- Production of other neutrons (n, n'), (n,2n'), ...
- Production of fission fragment (n, f)
- Spallation reaction, that consists in a shower of secondary particle due to the interaction of high energy neutrons with a nucleus

The quantities of energy given to matter through *excitement* and *ionization* are almost the same. Ionization has a lower probability to happen but it involves the transfer of bigger amount of energy, in the order of keV. Contrarily, excitement has a higher probability to happen but it involves the transfer of lower amount of energy, the difference of energy between the ground state and the excite state is in the order of 1-100 eV.

1.2 Ionizing radiation field

The *ionizing radiation field* is the region of the space crossed by the radiation. There are different quantities to describe and treat the radiation field.

A way to describe the *radiation field* is to count the particles passing through a sphere, with center in P and ray r , sufficiently small, in an interval of time $[t_0, t_1]$.

The geometry taken into consideration is a sphere because it presents the same target area to rays incident in all the directions. The sphere should be small but finite if we are taking into consideration stochastic quantities and infinitesimal, with a volume dV , if we are taking into consideration non-stochastic quantities. The system treated in this case is non-stochastic.

The quantity of rays detected per measurement will in general follow Poisson distribution, but for a large number of measurement it can be approximated to Gaussian distribution.

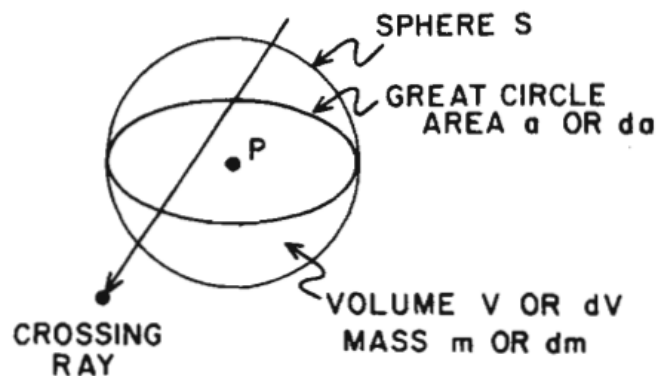


Figure 11 Characterizing radiation field at a point P in terms of the radiation traversing the spherical surface S. [5]

Fluence

The *fluence* is defined as the relation between the number of particles that cross the finite sphere in a time interval, dN , and the great circle area, dA .

$$\Phi(t_0, t_1) = \frac{dN}{dA} \quad (7)$$

The unit of measure of fluence is $[m^{-2}]$.

Fluence rate

The *fluence rate* is defined as the derivative of the fluence in time.

$$\varphi = \frac{d\Phi}{dt} = \frac{d}{dt} \frac{dN}{dA} \quad (8)$$

The *fluence rate* represents the number of particles that cross the spherical surface S in the unit of time. The unit of measure of fluence rate is $[m^{-2}s^{-1}]$.

Energy fluence

The *energy fluence* is the total amount of energy, transported by the particles, that cross the sphere S. Considering monoenergetic particles with energy E, the energy fluence is defined as:

$$\Psi = E \frac{dN}{dA} = E\Phi \quad (9)$$

The unit of measure of energy fluence is $[J m^{-2}]$.

Energy fluence rate

The *energy fluence rate* represents the amount of energy that cross the spherical surface S in the unit of time. The *energy fluence rate* is obtained deriving the energy fluence.

$$\psi = \frac{d\Psi}{dt} = E \frac{d\Phi}{dt} = E\varphi \quad (10)$$

The unit of measure of energy fluence is $[J m^{-2}s^{-1}]$.

1.3 Dosimetric quantities

The dosimetry of ionizing radiation studies the transfer of energy into matter and the dosimetric quantities describe the different phases which rule the process of transferring of energy. [8] The 3 non-stochastic quantities that are at the bases of radiological physics are the *kerma*, the *absorbed dose* and the *exposure*. The *energy transferred* and the *energy imparted* are the the columns on which the previous ones stand.

Energy transferred

In the case of indirectly ionizing radiation the *energy transferred* is associated to the first phase, in which the interaction of radiation with matter gives birth to the charged particle that will ionize and excite matter.

$$\epsilon_{tr} = \mathcal{E}_{\gamma,in} - \mathcal{E}_{\gamma,out} - \Delta m \cdot c^2 \quad (11)$$

Where:

- $\mathcal{E}_{\gamma,in}$ is the total energy of the ionizing radiation entering the volume V;
- $\mathcal{E}_{\gamma,out}$ is the total energy of the photons exiting the volume V, except for the photons originated from radiative losses of charged particles in V. For this reason $\mathcal{E}_{\gamma,out}$ does not include the energy due to the bremsstrahlung, the energy of photons generated by annihilation and the energy of photons of fluorescence;
- $\Delta m \cdot c^2$ is the change of mass and of rest energy of all the particles involved in the interaction, associated to phenomena of pair creation and annihilation.

Kerma

The *kerma*, K , is the quantity of energy transferred to charged particle per unit mass, including radiative loss of energy and excluding the energy passed from one charged particle to another. Kerma is the acronym of “*kinetic energy released in matter*” and it is referred only to the indirectly ionizing radiation. In particular to the first step of indirectly ionizing radiation, that regards the energy transferred to charged particles.

$$K = \frac{\epsilon_{tr}}{m} \quad (12)$$

The units of measure of kerma are Gray and rad.

Where: $1 \text{ Gy} = 1 \text{ J/kg}$ and $1 \text{ Gy} = 100 \text{ rad}$.

The kerma for X and γ rays is the energy transferred per unit mass of the medium to electrons and positrons. The kinetic energy of electrons can be spent in the Coulomb force

interactions with atomic electrons generating ionization and excitation. The kinetic energy of positrons is lost in annihilation processes.

It's possible to divide the total kerma in two contributions, the collision kerma and the radiative kerma.

Energy imparted

The *energy imparted* is the amount of energy deposited inside the matter of mass m and volume V . This energy is associated to kinetic energy due to the multiple interactions that the particles have with matter.

$$\epsilon = \mathcal{E}_{\gamma,in} + \mathcal{E}_{charged,in} - \mathcal{E}_{\gamma,out} - \mathcal{E}_{charged,out} - \Delta m \cdot c^2 \quad (13)$$

Where:

- $\mathcal{E}_{\gamma,in}$ is the energy of the photons entering the volume V ;
- $\mathcal{E}_{charged,in}$ is the energy of the charged particles entering the volume V ;
- $\mathcal{E}_{\gamma,out}$ is the energy of the photons exiting the volume V ;
- $\mathcal{E}_{charged,out}$ is the energy of the charged particles exiting the volume V ;
- $\Delta m \cdot c^2$ is the change of mass and of rest energy of all the particles involved in the interactions, associated to phenomena of pair creation and annihilation.

The unit of measure of energy imparted is [J].

Dose

The *absorbed dose*, D , is the energy delivered by the radiation inside the volume V per unit mass and it is linked to any type of ionizing radiation. In the case of indirectly ionizing radiation the dose is associated to the secondary particle generated by the primary radiation.

$$D = \frac{\epsilon}{m} \quad (14)$$

The unit of measure of dose is Gray.

Where: $1 \text{ Gy} = 1 \text{ J/kg}$.

The absorbed dose is the fraction of energy that remains in the matter and produce the effect correlate to radiation. So if D is equal to 0 the effect of the dose on the body are null.

Exposure

The *exposure*, X , is the capability of a photon beam to ionize air. The exposure defines the relationship between the absolute value of the total charge of the ions produced in the air when all the electrons and positrons liberated by photons in air of mass dm are stopped in air:[5]

$$X = \frac{dQ}{dm} \quad (15)$$

The energy necessary to produce dQ is equal to the net energy transferred to charged particles in air.

The unit of measure of the exposure is the Roentgen.

Where: $1 R = 2.580 \cdot 10^{-4} C/kg$.

1.4 Coefficients of interactions of radiations with matter

Interaction between ionizing radiation and matter depends on the nature of the radiation and of the matter and on the energy of the radiation.

For this reason an interaction coefficient has been introduced for each kind of interaction linked to the capacity of matter to stop radiation.[8]

1. Interaction of charged particle with matter

The most important coefficient for the interaction of charged particles with matter is the *Stopping power*. It represents the loss of kinetic energy of charged particles inside matter.

Considering a beam of charged particles that lose an energy dE going through a medium of length dl , the stopping power is:

$$S = -\frac{dE}{dl} \quad (16)$$

The unit of measure of the stopping power is $[J/m]$ or $[MeV/cm]$.

In particular, for protons the stopping power is given by the *Bethe-Block Formula*: [9]

$$-\frac{dE}{dl} = 2 \pi N_A r_e^2 m_e c^2 \rho \frac{Z}{A} \frac{z^2}{\beta^2} \left[\ln \frac{2 m_e c^2 \gamma^2 \beta^2 W_{max}}{I^2} - 2 \beta^2 - \delta - 2 \frac{C}{Z} \right] \quad (17)$$

with:

- I is the “Average potential for excitation”
- Z, A, ρ represent the characteristics of the medium

- z, β, γ represent the characteristics of the incident particle
- W_{max} is the maximum energy transferred in one collision
- r_e is the classical electron ray
- m_e is the electron mass
- N_A is the Avogadro number
- C represents the shell correction
- δ represents the density effect
- c is the light speed

Instead for electrons the stopping power will be: [9]

$$S = \left(-\frac{dE}{dl}\right)_{coll} + \left(-\frac{dE}{dl}\right)_{rad} \quad (18)$$

where:

- $\left(-\frac{dE}{dl}\right)_{coll}$ represents the energy loss due to collision
- $\left(-\frac{dE}{dl}\right)_{rad}$ represents the energy loss due to radiation

Practical applications involve the use of mass stopping power, that is given from the relation of the stopping power and the density of the medium.

The unit of measure of S/ρ is [MeV cm³ / g].

Knowing the initial kinetic energy of the radiation and stopping power is possible to calculate the *penetration length* in the medium.

2. Interaction of neutrons with matter

Neutron particles have a lower probability of interaction with matter, they could be absorbed or go through the medium without interacting.

The coefficient that represents this phenomenon is the *attenuation coefficient*, that measures the probability of a neutron to have an interaction in a medium.

Considering a neutron beam hitting a target of thickness dl with an intensity I , the *attenuation coefficient* is defined as:

$$\mu = -\frac{1}{I} \frac{dI}{dl} \quad (19)$$

Integrating along a medium of thickness L it's possible to obtain an intensity that decreases exponentially along the target.

$$I(L) = I_0 e^{-\mu L} \quad (20)$$

The *attenuation coefficient* is connected to the cross section with the relationship

$$\mu = \sigma \cdot n_T \quad (21)$$

where n_T is the nuclei's density of the target.

In general:

$$\mu = \sum_j \sigma_j \cdot n_j \quad (22)$$

If we take into consideration a target with a non-homogeneous *attenuation coefficient* the intensity will be equal to:

$$I(L) = I_0 e^{-\int_0^L \mu dx} \quad (23)$$

3. Interaction of photons with matter

Photons, like neutrons, have a non-zero probability to pass through a medium without interacting. The characteristic coefficient also in this case is the *attenuation coefficient*.

If we are in presence of non-monochromatic beam the total intensity will be equal to:

$$I(L) = \int I_0(\mathcal{E}_\gamma) \cdot e^{-\int_0^L \mu(\mathcal{E}_\gamma) dx} d\mathcal{E}_\gamma \quad (24)$$

The attenuation coefficient is equal to the sum of the μ of Compton scattering, pair production and photoelectric effect.

$$\mu_{tot} = \mu_{photoelectric} + \mu_{Compton} + \mu_{pp} \quad (25)$$

Chapter 2

Radiobiology

All started in 1895 with the discovery of X-rays, to which followed at the end of 1890 the discoveries of radioactivity from Henry Becquerel, of the electron from J.J. Thompson and of polonium and radium.

Following these events, the first testimonies of damages due to ionizing radiations began to emerge.

In 1896 a constructor of vacuum tubes showed injury to hands' skin, now called subacute X-ray dermatitis. In 1901 Becquerel, that used to take a glass vial containing radium salts in the pocket of the gown, had a skin rash.

In the early 1900s some studies showed that exposition to X-rays caused sterility in animals and started to be reported the first cases of tumours and leukemia due always to X-rays. In 1922, 100 deaths of radiologists were recorded due to presumably radiation-induced cancer.

The geneticist and biologist Thomas Hunt Morgan, professor at Columbia University of New York, did some experiments on the fruit fly submitting it to X and γ rays. The results were surprising, as they showed genetic mutations in the flies that were also transmitted to subsequent generations.

In the 50' the spouses Russell showed the damages of radiations on embryonic and fetal development until the seventy-fifth day after the conception. Thanks to their studies was discovered that pregnant women need a radioprotection also for low doses of radiations. During the years of World War II and subsequent years, in which various nuclear weapons were used, the populations were exposed to an unusual amount of radiations, just think to Hiroshima and Nagasaki bombing.[10]

The effects that radiations have on humans immediately attracted the attention of experts, who created real scientific associations, like the *United Nations Scientific Committee on the Effects of Atomic Radiation*, UNSCEAR, created in 1955 or the *Committee on the Biological Effects of Ionizing Radiations*, BEIR. These structures published several papers on the multitude of aspects that govern Radiobiology.[12]

So, a new branch of science at the base of radiotherapy born, that treats basic principles of physics and biology concerning the use of ionizing radiation on biological tissues. [11] Radiobiology studies all the biological events that follow the interaction between the ionizing radiation and tissue. The phases that follow one another are five: the physical phase, the chemical phase, the biochemical phase, the biological phase and the clinical phase.

But before going into the details of these phases is necessary to give a general framework on the basic element on which human biology is founded.

Biological tissues are formed by cells, which have the capacity of replicating themselves through the process of mitosis. The time gap between successive divisions is called “cell cycle time”; human liver cells may live from six months to a year before being replaced. When cells proliferate rapidly and in an uncontrolled way can generate a benign or malign tumours, also called cancer. The malign tumours spread to the other organs through a process called metastasis. [14]

2.1 Hints of cell biology

2.1.1 Cell structure and function

The cell is the fundamental unit of human body, it can have different shapes and functions, with a size varying between $10\ \mu\text{m}$ and $50\ \mu\text{m}$. It is composed of four parts: the *cell membrane*, the *nucleus*, the *nucleolus* and the *cytoplasm*.

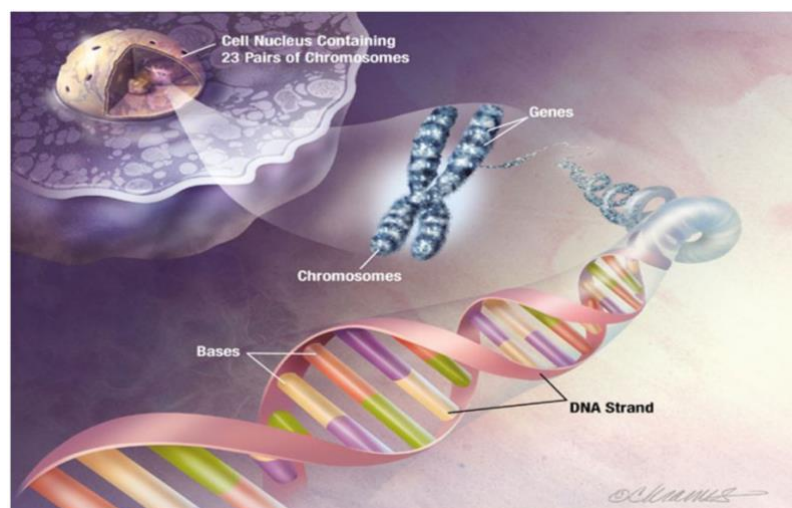


Figure 12 Cell nucleus, Chromosomes and DNA.

The *cell membrane*, also called *plasma membrane*, is a double layer of phospholipid molecules and its function is to divide extracellular material from intracellular one. The

other important function is to rule the passage of substances from outside to inside of the cell and vice versa.

The *nucleus* is composed of a fluid nucleoplasm surrounded by a nuclear membrane. The cell nucleus contains 23 pairs of Chromosomes, that are composed of multiple linear DNA (deoxyribonucleic acid) molecules. [15] The DNA contains the genetic code, unique for each living creature. Its aim is to control and rule cellular activity.

The DNA of a cell is a polymer composed of 4 types of nitrogen bases held together by weak chemical bounds: *Adenine*, *Guanine*, *Thymine* and *Cytosine*. DNA is composed of two filaments, long almost 2 meters, wrapped helically. [16]

The *nucleolus* occupies the central part of the cells and its main function is to synthesize RNA, ribonucleic acid.

The *cytoplasm* is composed by organelles immersed in a fluid matrix, called cytosol. The main activities of cellular life take place in the *cytoplasm*, *i.e.* cell expansion, growth and replication. [15]

2.1.2 Cell life cycle

The cell life cycle is divided in two phases. The *interphase* is the phase in which the cell performs its vital functions and where it spends most of its life, at some point it will be ready to divide and it will undergo *mitosis*. Mitosis is a short process by which the nucleus turns into two nuclei. [16]

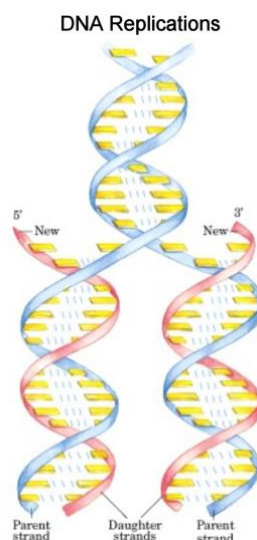


Figure 13 DNA Replication. [16]

The *interphase* is divided in three phases:

- Phase G1 is the phase in which the cell grows;
- Phase S the cell duplicates and synthesizes the DNA;

The DNA replication is based on the creation of two other DNA molecules, each of which composed of a father DNA filament and a new one, daughter DNA filament.

- In Phase G2 the cell synthesizes proteins necessary for cellular division.

At the end of Phase G2 the cell is ready to go through mitosis, the mother cell divides in two daughter cells. [16]

2.2 Radiobiological phases

2.2.1 Physical phase

The Physical phase lasts from 10^{-16} to 10^{-18} seconds and it regards the interaction of the ionizing radiation with the atoms belonging to the tissues. The effect that can verify depends on the type of ionizing radiation, even if at the end the final processes are excitation and ionization.

If the ionizing radiation has a corpuscular nature it would generate always ionization, instead if it has an electromagnetic nature the effects that can provoke are: the photoelectric effect, the Compton effect, the pair production and the nuclear photodisintegration. Obviously, the type of effect depends also from the energy that radiation has and from the atomic number of the absorber. In medicine the only effects that can be induced are the photoelectric effect, the Compton effect and the pair production.[17]

If the electrons freed, because of ionization, have enough energy they could interact with other atoms and generate a chain reaction.

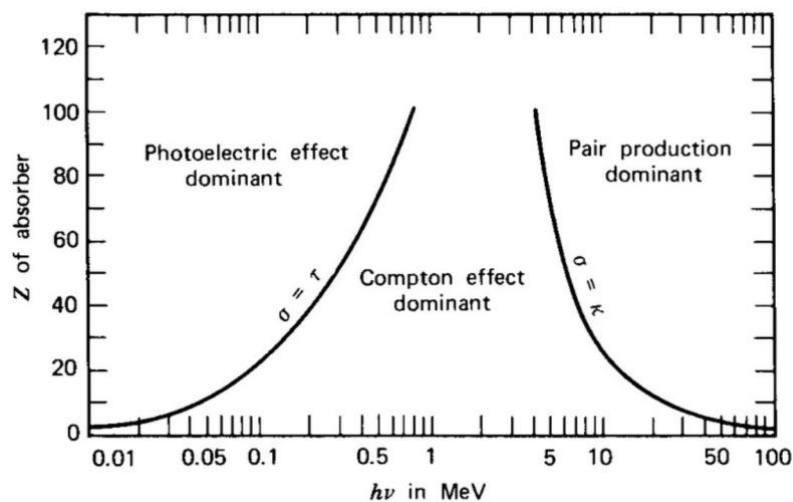


Figure 14 Energetic domains of photoelectric effect, Compton effect and pair production in function of the energy of the radiation and of the atomic number of the absorber. [13]

In this phase are defined two important quantities: the *Linear Energy Transfer* and the *Relative Biological Effectiveness*.

- The *LET, Linear Energy Transfer* represents the quantity of energy deposited per unit length in the medium crossed by ionizing particles.

$$(LET)_{\Delta} = \left(\frac{dE}{dl}\right)_{\Delta} \quad (26)$$

Where dE is the energy deposited in a length dl , considering only collisions with an energy transfer smaller than Δ . [8] The unit of measure of the LET is [keV/ μm].

LET is inversely proportional to radiation velocity and directly proportional to the ionizing particle's charge elevated at two.

The *LET* and the *Stopping Power* are equal in case we consider all the events related to the energy transfer.

It's possible to distinguish two kind of radiations in terms of local deposition of energy:

- The radiation with low LET are composed of photons and electrons;
- The radiation with high LET are composed of protons, neutrons and ions.

At the macroscopic level the radiation with low LET have a major probability to penetrate in the tissues. And at the microscopic level the probability of hitting the target, cell, is higher for radiation with high LET.[24]

A radiation with high LET will lead to a major biological damage with a minimum penetration length because it will lose most of its energy in a short path.

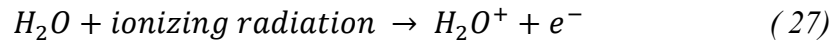
The LET is not able to differs the effect of radiations with ions with different Z. [25]

- The *Relative Biological Effectiveness* defines the biologic effect that a radiation can have referring to a determinate physic dose. This quantity is strictly connected to LET's definition. In fact, initially it is proportional to the LET and then it increases with the growth of it. The RBE of radiation with low LET is equal to 1. For the rest of radiations the RBE is the ratio between the equivalent dose and dose of radiation "R". The RBE of radiation with high LET is 3 for neutrons and over 8 for alfa particles.

2.2.2 Chemical and biochemical phase

The chemical phase, that lasts around 10^{-3} seconds, describes how the atoms or molecules, that has been excited or ionized, start reacting with other cellular components.

The human body is composed for the major part of water, for this reason ionizing radiation react mostly with molecules of water, radicalizing them.



The water ion will then generate radicals, responsible for the biological damage of the DNA.[17]

Hydroxyl Radical:



Hydrogen Radical:



The biochemical phase treats the effect that radiation can cause to cells. Even if biological damage can interest different areas of the cell, like the cell or the mitochondrial membrane, the worst damage is on the DNA, that is the most sensible target and the more difficult to repair.

When radiation interact with DNA, it breaks the DNA strands. The DNA is able to repair itself if only one filament is broken, *Single-strand break*, but it need a certain time. If both filaments are broken, *Double-strand break*, the DNA cannot be repaired.

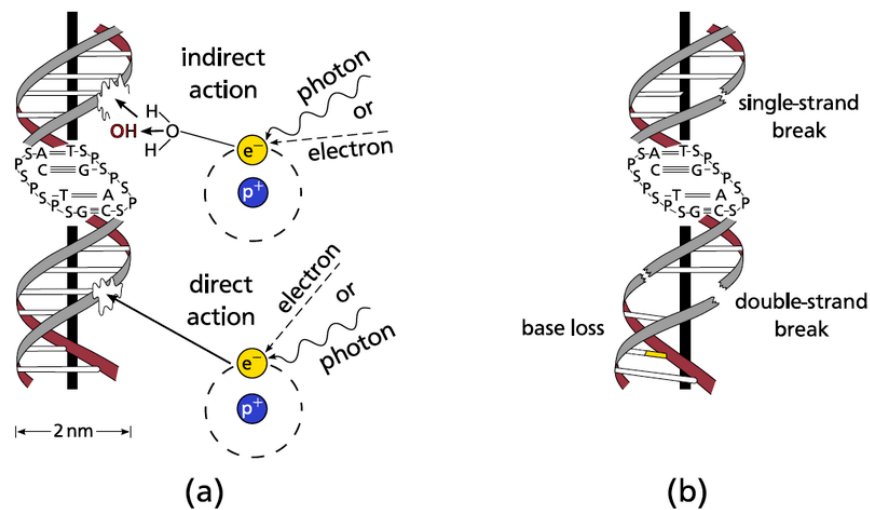


Figure 15 (a) Direct and Indirect radiation damage to the DNA. (b) Cell DNA damage due to radiation. [26]

Giving up energy the radiation can direct or indirect damages.

- In the *Direct damage* the radiation ionizes the DNA contained inside the cell. The cells have the ability to repair themselves if the damage is not to complex. If the cell

does not manage to repair itself it will die. The direct damage is principally provoked by the radiation with corpuscular nature.

- In the *Indirect damage* the radiation will ionize or excite water components of the cell generating free radicals, that will damage DNA. Also in this case if the cell does not manage to repair it will die. The indirect damage is principally caused by photons.

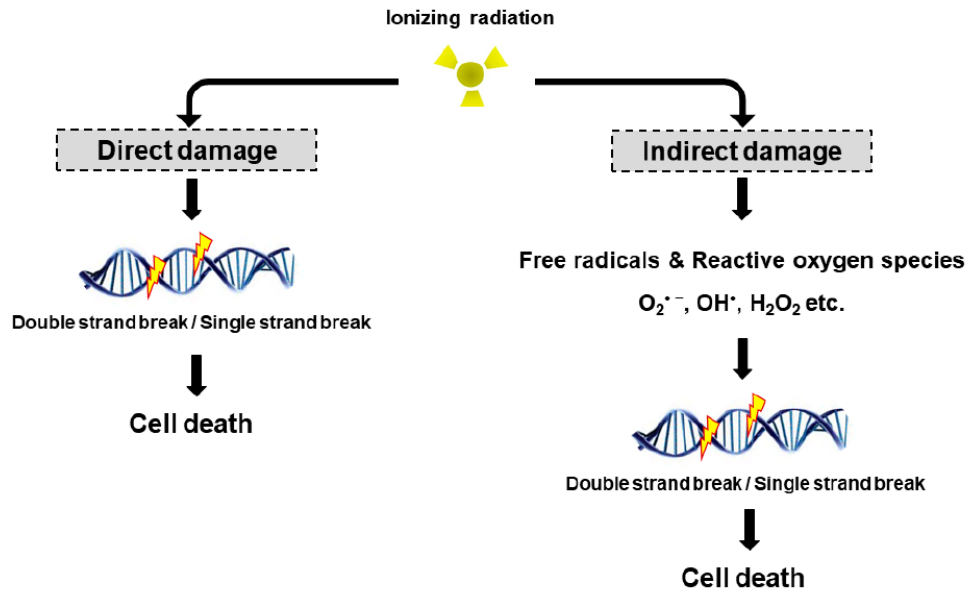


Figure 16 Direct and Indirect DNA damage due to ionizing radiation. [18]

If the molecular damage is non repairable that means that the cell will die, in the molecular damage is repairable we can have two cases. The first case is the potentially lethal damage, where the enzymatic systems are able to heat the cell, the second case is the sub-lethal damage, where to kill the cell is necessary more than one of this damage in the near areas. [19]

2.2.3 Biologic phase

The Biologic phase is about the effects that DNA damage can took to. These effects on cells have long time expansion, from days to years.

- The *instantaneous death*, also called interphase death, is due to exposition to high dose and it causes the disintegration of the cell in few hours, that can lead to the deterioration of the organ to which they belong. This event regards lymphocytes, oocytes and nerve cells;
- The *reproductive death*, in which the cell, unmodified in form and function, will not be able anymore to reproduce. The cell that usually have a reproductive death are

intestinal epithelial cells and spermatogonia. This kind of cell death is the most common in the medical treatment;[17]

- The *genetic death* is due to the alteration of cell's genes;
- The *apoptosis*, that is a biological process that plan the death of the ill cell;
- *Genetic mutation* of the DNA.
- The initiation of *carcinogenesis process*, due to long term exposure to radiation.

To describe the effect of radiation is necessary to define the *total dose* of a radiation and the *equivalent dose*.

- The *total dose* is the quantity of energy absorbed by tissues after an exposure to radiation per unit of mass. It is measured in Gray.
- The *equivalent dose*, D_X , is the dose of X rays of 200 keV producing the same biological effect of the dose D_R of radiation "R". The *equivalent dose* depends on the type of radiation and cells. The unit of measure of the *equivalent dose* is the *Sievert* or *rem*.

Where $1 \text{ Sv} = 1 \text{ J/kg}$ and $100 \text{ rem} = 1 \text{ Sv}$.

Cell survival depends on:

- the dose. For example, high LET radiations generate a damage mostly irreversible, because they have a high ionization density;
- on the presence of oxygen. When a cell is hit by a low LET radiation in presence of oxygen is 3 times more sensible. The probability to die for a cell is strictly connected to the oxygen tension. Another positive aspect of having low quantity of oxygen is that the free radicals produced are less and so the direct damage are reduced;
- the type of cell. In fact, different eukaryotic cells have a different capacity of repair themselves, or different radio sensibility;
- on the fractioning of the radiation. In fact, if we submit a cell to the same dose but fractionated in time the damage will be reduced.[17]

The fractioning of the dose give birth to the 4R of the Biology:

1. *Repair* of the molecular damage;
2. *Resettlement* of the cell, that reduce the damage in healthy tissues. But unfortunately it is a phenomenon that regards also tumour cells, lengthening treatment time;
3. *Redistribution*, generate a synchronization of cell phases;
4. *Re-oxygenation*, the fractioning reduces hypoxia inside the tumour tissues, increasing radiosensitivity of tumour cells.

Repair and resettlement make tissues more radio resistant, while redistribution and re-oxygenation make tissues more radiosensitive.[17]

2.2.4 Clinical phase

In the clinical phase are studied the late and acute effects of radiation on human tissues. First, let's distinguish the damages in *somatic*, that refers to the individual that has been subjected directly to the ionizing radiation, and *genetic*, that refers to his progeny.

Furthermore, the damages can be deterministic and stochastic.

The *deterministic* damages are present only after a certain limit dose is exceeded and their gravity is function of the quantity of the dose. Some somatic example could be infertility, cataract or skin irradiation syndrome.

In the *stochastic* damage the probability of occurrence is function of the dose. In fact, for low dose it's very improbable to have a stochastic damage.[18]

The worst effect of somatic stochastic damages is the onset of tumours and leukemia.

It's possible to distinguish the clinical manifestation times of damage on tissues in:

- *Acute* responses that show themselves during the treatment. Tissue that have these response time are skin, bone marrow and mucosa. The clinical manifestation follow an order as the dose released increases: erythema, epitheliolysis, ulceration, necrosis. The damage is repaired by the stem and proliferative cells, who survived to the radiations. If this does not happen, the repair is implemented through a healing process.
- *Sub-acute* responses that have a time scale of 2-3 months after the therapy. They are reversible and depend on the dose and on the volume of the involved tissue. The possible effects can be: subacute actinic pneumonia, subacute encephalopathy and Lhermitte's syndrome.
- *Late* responses that have a time scale of months or years after the therapy. They regard fibroblasts, endothelial cells, osteoblasts, chondroblasts, oligodendrocytes and Schwann cells. The clinical damage depends on the dose, it is difficult to recover and it can be anticipated by trauma and infections. [19]

So an uncontrolled exposition to ionizing radiation can took to a series of negative effect, but things change in using them properly. In fact, the ionizing radiation can be used in radiotherapy to kill malign cells.

Chapter 3

Radiotherapy

The use of ionizing radiation made its way in medicine in 1896, with the studies of a French doctor, Victor Despeignes, who was one of the first to treat tumour with X-rays. The results he obtained broadly reflect what a radiotherapy treatment today leads to, that is a decreasing of pain and of the tumour dimension. Unfortunately, his studies were considered unreliable because his patient was undergoing several treatments at the same time.

In the same year doctor L. Freund used radiation to treat moles that were present on the neck and on the back of his patient, a 4-year-old girl. The problem is that the only thing that caused her were deep ulcers. Fortunately following this failure, doctor Freund in collaboration with doctor Schiff had a successful applied treatment on a lupus vulgaris case, on which they write a paper.

In 1898 the dermatologist William Pusey wrote about positive effect that radiation could have on acne and hypertrichosis.

Even if the first tumour treatment with radiation date back to 1896, the first real success was obtained by Emil Grubbe, who underwent radiotherapy a patient with breast cancer with positive results.

In 1899, Tor Stenbeck published the results regarding the treatment of a malignant tumour through X-rays. Little by little more and more cases were sign in, even if the real physical and biological reasons, for which this type of treatment was successful in treating cancer, were not known. Since then until now the techniques of using radiation have evolved and differentiated.[20]

Nowadays, radiotherapy is known as the technique used to treat malignant tumours, through the use of radiations.

Radiotherapy can have different aims:

- *Curative radiotherapy* is used to eliminate the tumour;
- *Preoperative radiotherapy* is used before the surgery, to reduce the dimension of the tumour and to avoid that ill cells could diffuse;
- *Postoperative radiotherapy* is used after the surgery, to ensure total elimination of tumour cells;
- *Intraoperative radiotherapy* consists in the injection of a dose of radiation in the patient during the surgery;
- *Palliative radiotherapy* is used to stop the grown of the tumour and to decrease the pain;
- *Total body radiotherapy* is used in the case in which the tumour is diffused in the lymphatic system or between the blood cells. In this case all the body will be irradiated;
- *Ablative radiotherapy* consists in the use of high dose radiation for the cure of small tumours.

Radiations can be administered in the body from outside or from inside.

- *External radiotherapy* consists in the use of hitting the patient with X-ray beams or particles beams, composed of protons or carbon ions.
- *Internal radiotherapy* is a procedure that request the insertion in the patient and the positioning near the tumour mass of a radioactive body that emit radiations. The radiative sources are sealed, to prevent them from entering the bloodstream.[21]

3.1 Bragg's peak

Each type of radiation has different penetration depth in cells, for example X-rays lose energy in the first part of their path while protons and carbon ions dissipate higher energy in depth.

So, if we need to treat deep tumours is more efficient using protons and carbon ions, the form of radiotherapy that uses these particles is called *hadrontherapy*.

In Figure 17 is represented the radiation absorbed in function of the thickness of the tissue for X-rays, protons and carbon ions.

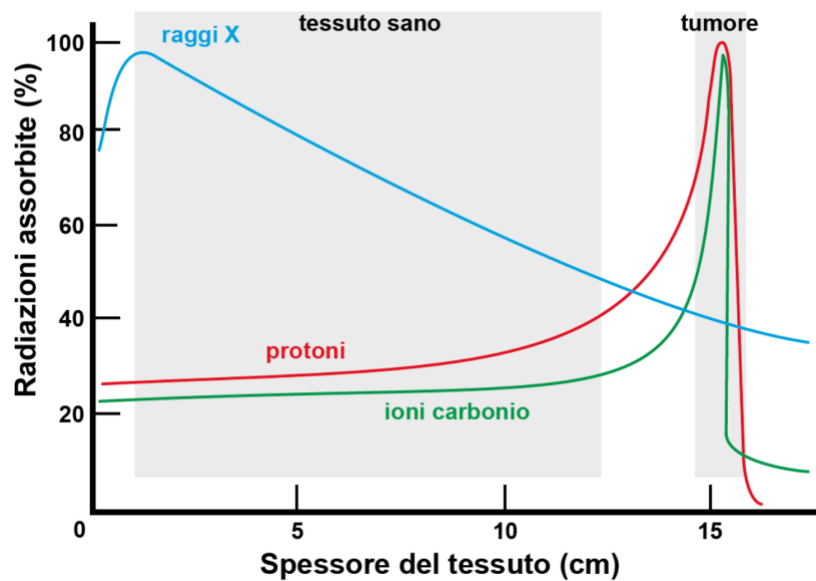


Figure 17 Absorbed radiation in function of the thickness of the tissue for X-rays, protons and carbon ions. [27]

X-rays absorbed dose decreases exponentially with increasing depth. Instead for carbon ions and protons the absorbed dose increases with the increasing depth, until it reaches the dose peak, called *Bragg's peak*, in the deep of the tissue, where the tumour is localized. Overcome the Bragg's peak the absorbed dose decreases instantaneously to zero for protons and to values close to zero for carbon ions.

The ions' curve does not reach zero because the primary ions, through fragmentation, will produce nuclei which have a velocity near to the primary ions and for this reason they can go deeper. [8]

The Bragg's peak of carbon ions is more restricted than the protons one because the effect of the loss of energy is higher.

The positive thing in using *hadrontherapy* is that the healthy tissue is less damaged.

In the following Figure 18 is shown a comparison between the use of protons, carbon ions and photons to treat brain, lung and rectum intestine tumours.

The dose, that is the quantity of radiation deposited in the tissue, is represented by the color scale going from the lowest dose, blue, to the highest dose, red. It's possible to notice that the use of hadrons, that are protons and carbon ions, is preferable first of all because the area affected by the beam is less spread and second because the part with the highest dose correspond to the tumour area. [27]

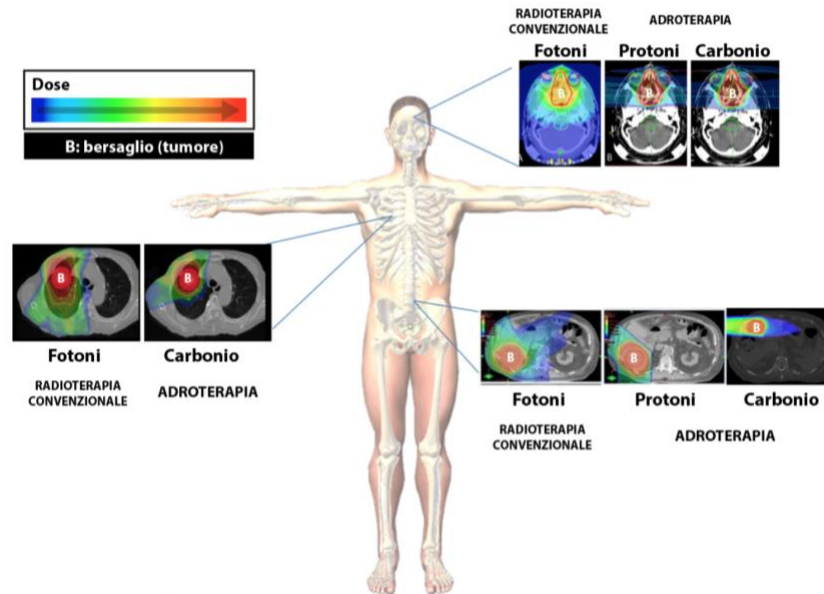


Figure 18 Comparison between the use of protons, carbon ions and photons to treat brain tumours, lung and rectum intestine tumour. [27]

In Figure 19 are shown the dose distribution for a photons radiation with 10 windows of access, *Intensity Modulated Radiation Therapy*, and protons radiation with 3 windows of access, *Intensity Modulated Proton Therapy*. It's possible to notice that in IMRT the diffusion of the radiation in the spinal cord is higher and that in the IMPT is possible to have a more controlled radiation space. [28]

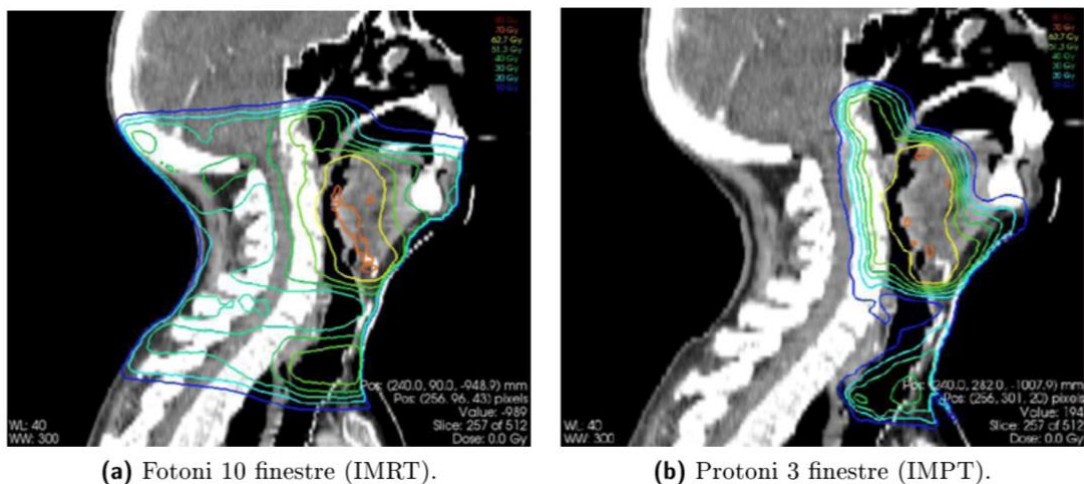


Figure 19 Dose distribution for a photons radiation with 10 windows of access and protons radiation with 3 windows of access. [28]

If it's necessary to treat spread areas hadrontherapy treatment provides for use multiple particles beams with different energy, corresponding to different position of Bragg's peak. The *Spread-Out Bragg Peak*, showed in Figure 20, represents the set of curves of protons or of carbon ions beam having different energy. [28]

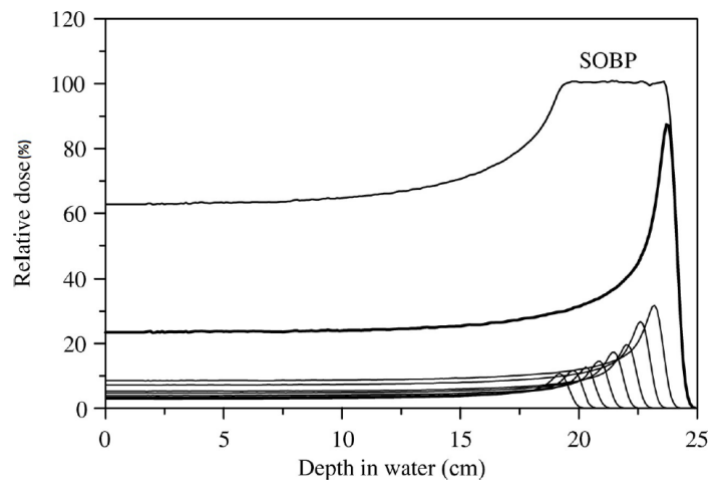


Figure 20 Spread-Out Bragg Peak. [28]

3.2 Radiotherapy Center

The use of radiotherapy is indicated for the 60 % of patients with a tumour, in particular for breast, lung, prostate, colon tumours.

Unfortunately, as shown in Figure 21, the radiotherapy machines are not present in all the countries, most of all in Africa. For example, in Ethiopia there is only one radiotherapy center for all the population. [29]

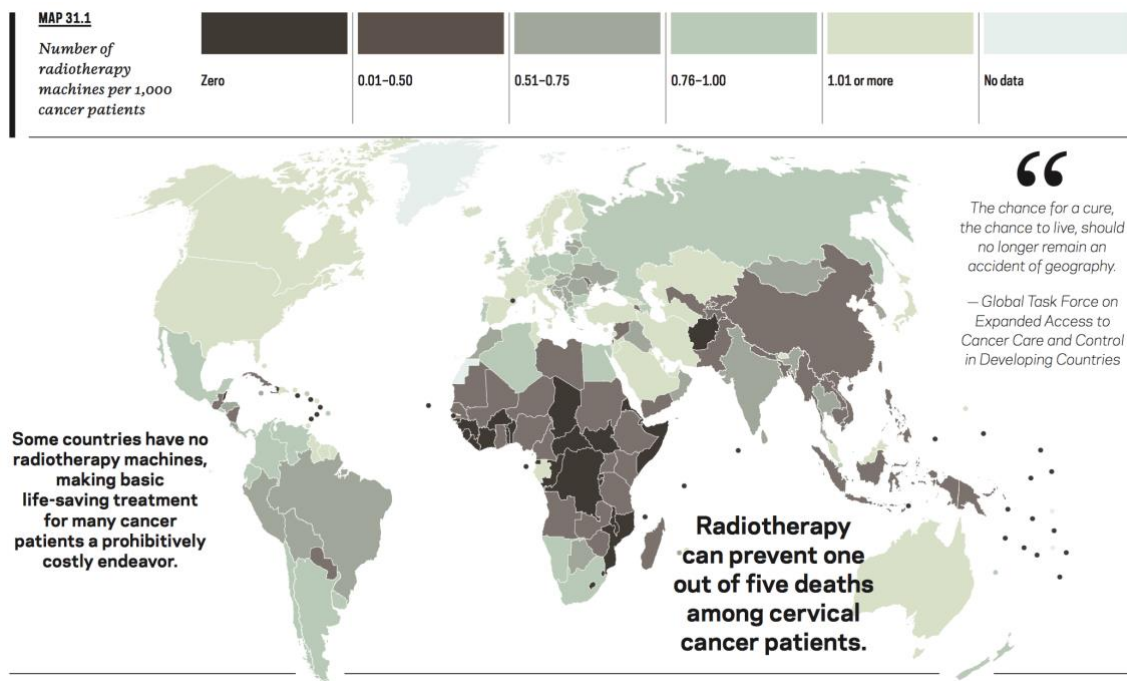


Figure 21 Number of radiotherapy machines per 1000 cancer patients. [29]

The tumours that are difficult to export surgically and that are radio resistant, that are able to repair themselves after radiotherapy, can be more efficiently treated thanks to hadrontherapy.

The tumours that are difficult to operate are tumours located in the spine or inside the brain, positioned near sensible organs like spinal cord, eyes, optical nerves or brain tissue. Instead, the more common radio resistant tumours are the prostate tumour, the ocular melanoma, salivary gland tumours and so on. [30]

The hadrontherapy centers in Italy are:

- *Centro Nazionale di Adroterapia Oncologica*, CNAO, located in Pavia. This is the only center in Italy able to generate protons and carbon ions beams. The accelerator is a synchrotron created thanks to the collaboration with the National Institute of Nuclear Physics, INFN, the CERN and the GSI.
- *Centro di AdroTerapia ed Applicazioni Nucleari Avanzate*, CATANA, located in Catania. It treats only eye tumours through a cyclotron able to accelerate protons beam to the kinetic energy of 60 MeV. It opened in 2002 thanks to the collaboration with the Sud National Laboratories, LNS, in Catania, and it's operative only some weeks a year.
- *Centro di Protonterapia*, located in Trento. Also this center uses a cyclotron, combined with the use of two rotating rooms that allows to adjust the angle of entry of the beam into the patient.[31]

A radiotherapy centre is composed of a particle accelerator, transmission lines and a treatment room.

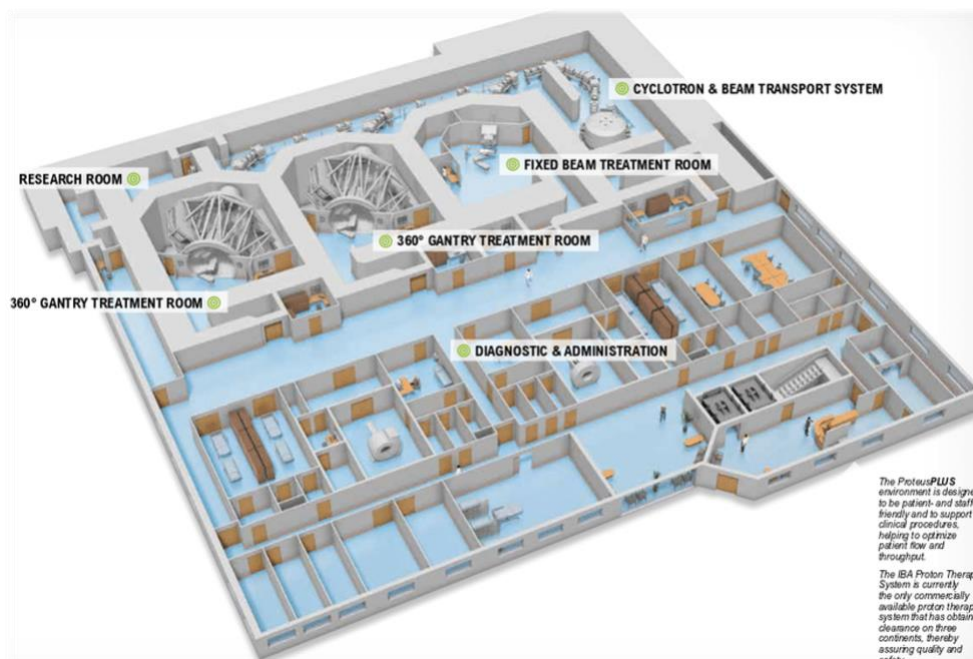


Figure 22 Scheme of a hadrontherapy centre. [32]

3.2.1 Particles accelerator

The first accelerator particles was built in 1931 by Robert Van de Graaff, it was composed of electric fields that accelerated ions using voltage between 10 and 20 MV. [33]

Nowadays, particles accelerators are used to accelerate particles at high energy, the machines used in hadrontherapy can be circular, like cyclotrons and synchrotrons, and linear, like LINAC.

3.2.1.1 Cyclotron

Cyclotron was invented in 1929-1930 by Ernest O. Lawrence and it is used to accelerate protons. The Cyclotron is composed of two electrodes, among which is established a radio frequency alternate voltage that generate a varying electrical field, posed inside two electromagnets that generate a static magnetic field.

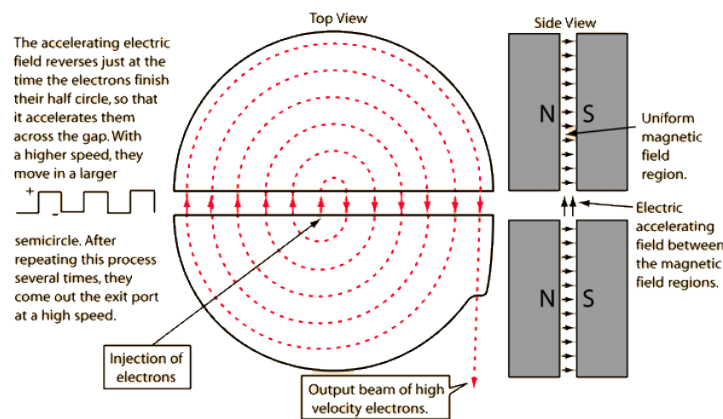


Figure 23 Scheme of a cyclotron. [34]

The magnetic field make the particle assume a helical trajectory, while the electric field accelerate them. The particles are inserted from the centre and at each turn they are accelerated, obviously the electric field has to vary because it has always to be opposed to the motion of the particles. The frequency of particles has to be equal to the radio frequency: $\omega_c = \omega_{RF}$.

If we consider having particles with charge q and mass m , a magnetic field B and a cyclotron ray R_{out} , the kinetic energy of the particle at the exit of the cyclotron, if particles have a velocity equal $v \ll c$, is equal to:

$$\mathcal{E}_{k,out} = \frac{q^2 B^2}{2m} R_{out}^2 \quad (31)$$

If particles have not a velocity $v \ll c$ there are two options:

- The first one is to change ω_{RF} , maintaining constant the magnetic field. In this case cyclotron is called Synchrocyclotron. The problem is that it's possible to insert in the machine only one group at a time, because the radiofrequency will be synchronized to the first group of particles, so it's necessary to wait that it will exit.

$$\omega_{RF}(v) = \frac{qB}{m} \frac{1}{\sqrt{1 - \left(\frac{\omega_{RF} r}{c}\right)^2}} \quad (32)$$

- The second one is to change the magnetic field in function of the cyclotron ray, maintaining constant the ω_{RF} . In this case cyclotron is called Isochronous cyclotron.

$$B(r) = \frac{\omega_{RF} m}{q} \sqrt{1 - \left(\frac{v}{c}\right)^2} \quad (33)$$

3.2.1.2 Synchrotron

Synchrotron is a toroidal particle accelerator and it is used to accelerate protons and carbon ions. It was invented by the two scientists E. M. McMillan and V. Veksler in 1945. The machine is composed of a deflector zone, whose aim is to define the direction of the particles, and an acceleration zone, where the particles are accelerated.

Particles are accelerated varying electric field and deflected by the magnetic field, generated by a magnet.

If we consider a particles' beam of charge "e" and relativistic momentum p and R the ray of the Synchrotron, the magnetic field is equal to:

$$B(r) = \frac{p}{eR} \quad (34)$$

Considering the fact that the ray of the Synchrotron, R , and the charge of the particles, e , remain constant, the magnetic field, B , will be proportional to the relativistic momentum.

The Synchrotron belonging to CNAO is the only one in Italy able to extract from the atom the carbon ions. The Synchrotron has a ray of 25 meters and a total circumference long 80 meters. It is situated in a bunker with concrete walls 2 to 6 meters thick, whose aim is to protect workers from radiations.

In the Synchrotron room are situated two sources from which are take the particles beam. The protons and carbon ions are separated from the atoms thanks to the use of the magnetic fields and radiofrequencies. The particles beam is pre-accelerated and sent to the Synchrotron where the protons reach kinetic energy of 250 MeV while the carbon

ions reach the kinetic energy of 4800 MeV. After exiting the Synchrotron the particles are sent into the treatment room.[35]

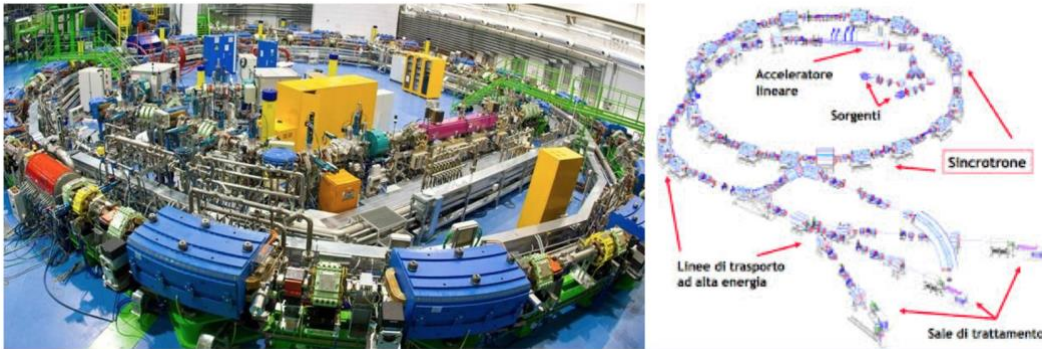


Figure 24 Picture and scheme of Synchrotron situated in CNAO. [35]

3.2.1.3 LINAC

The *linear particle accelerator, LINAC*, is composed of a vacuum chamber, that contains an injector source and a series of drift tubes separated by gaps, and a RF oscillator.

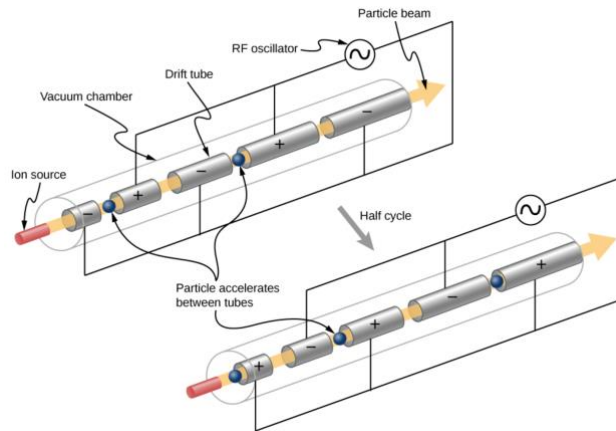


Figure 25 LINAC [36]

The aim of the vacuum chamber is to avoid the contact with other particles.

The *injector* produces particles packages, in the case of protons beams they can reach for example energy of 7 MeV, protons can be released through impulses of 5-10 μs each of which with a frequency of 100-200 Hz. [37]

The *RF oscillator* generates an AC voltage, ΔV , between the *gaps*, Δx , that generates an electric field.

$$E = \frac{\Delta V}{\Delta x} \quad (35)$$

The particle will be accelerated in the gaps, where it will be submitted to the electric field, and it will maintain constant its velocity inside the tube, that will protect the particles from decelerating.

In the gap the increasing of particle kinetic energy will be:

$$\Delta \mathcal{E}_k = q \Delta V \quad (36)$$

where q is the charge of the particle.

The length of the drift tubes increases so that velocity of the particles can increase too.

$$l = v \cdot T \quad (37)$$

where:

- T is the period of the oscillating field;
- l is the distance between two gaps;
- v is the velocity of the particle

3.2.2 Transmission lines

The beam has to be conducted to the treatment rooms through the transmission lines. It's necessary to preserve the velocity and the energy of the beam during the path and the directional deviations.

To transport the beam is necessary a vacuum tube and to direction it is are used magnetic element, called *deflectors*.

The terminal part of the transmission line can be connected to a rotating mechanical piece, called *gantry*, that allows to hit the target from different directions. This treatment method permits to treat more complex tumour volume and so to optimize the process.

The *gantry* had to direction the beam through magnetic devices that are big and expensive, for example protons to follow a curvature ray of 1 meter have to be subjected to a magnetic field of 1.8 T, that is a huge one.

Moreover, the distance between the exit of the beam and the patient has to be at least of some meters, so we need a passive expansion system.[38]

The gantry can be *isocentric* or *eccentric*, the first one expect the patient to be positioned on the axis of rotation of the gantry itself, while in the second one will be the patient to be moved. [39]

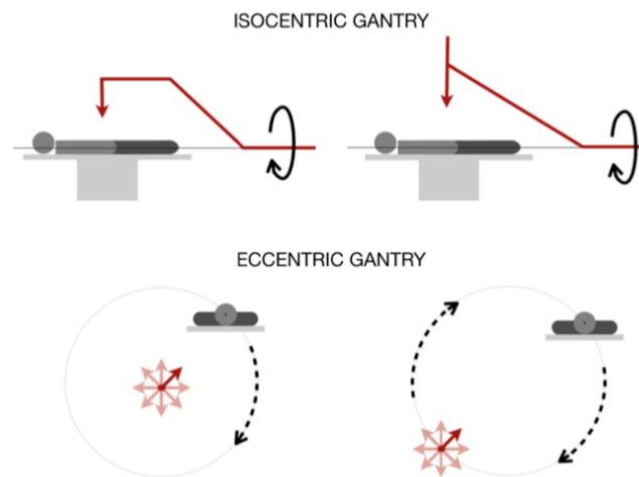


Figure 26 Isocentric and eccentric gantry. [39]

3.2.3 Treatment room

The treatment room has different components according to the kind of tumour that has to be treated. The following examples are based on the techniques applied by CNAO.[40]

Head and neck cancers

The treatment room is composed of the *Patient Positioning System*, the *Optical Tracking System* and the *Patient Verification System*.

The *Patient Positioning System* is constituted of a carbon fiber bed, where the patient will be placed, that can be moved by a robotic arm.[40]



Figure 27 Patient Positioning System. [40]

Afterwards, the patient will be immobilized through a mask, custom built for each patient. The *Optical Tracking System* is a system of three infrared camera able to capture the positions of the optoelectronic markers positioned on the mask. This system is used to guarantee the correct position of the patient before and during the treatment.[40]

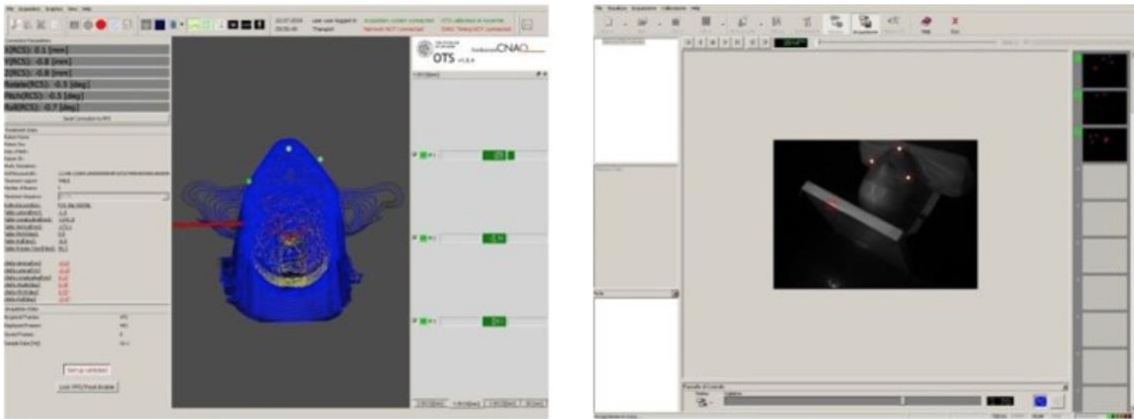


Figure 28 Optical Tracking System. [40]

The *Patient Verification System* is able to take two X-rays images that will be compared with the initial simulation images. This comparison permits us to position the patient in the correct place to start the treatment.

The treatment is based on a certain number of sessions. [40]

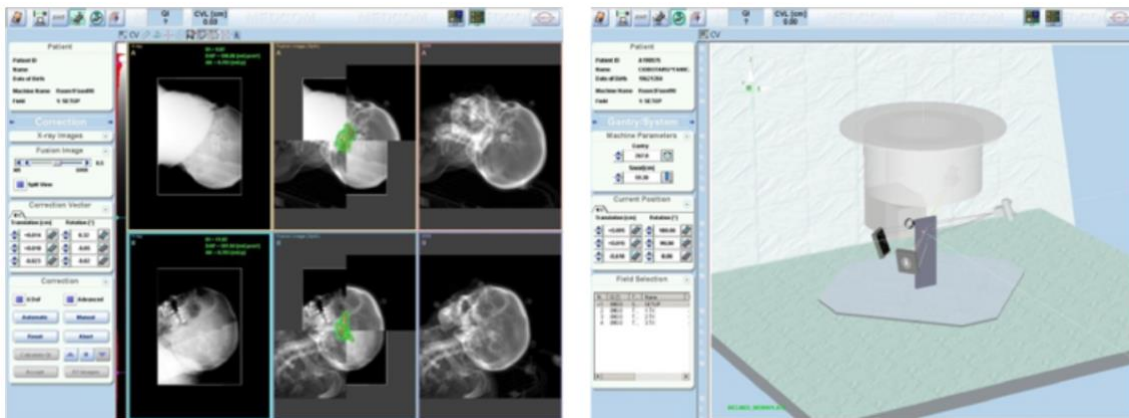


Figure 29 Patient Verification System. [40]

Pelvic and abdominal tumours

For the pelvic and abdominal tumours treatment, in addition to the treatment room, is used another room where the patient is positioned in the correct way on the carbon fiber bed through a series of laser, CAPH room (Computer Aided Positioning in Hadrontherapy). [40]



Figure 30 Carbon fiber bed in CAPH room. Error! Reference source not found.

The use of the *Patient Positioning System* and of the *Patient Verification System* remains the same. Moreover through the *Patient Verification System* is captured a 3D image of the internal organs.

After making sure that the patient is well positioned the treatment session can take place.[40]

Eye cancers

In the treatment room is situated a machine composed of a chair, where the patient has to sit, that is moved by a robotic arm.

The correct position of the patient is controlled by the *Patient Verification System*, that controls the position of the surgical clips situated by an eye surgeon before the simulation.[40]



Figure 31 Patient Positioning System. [40]

To guarantee the correct positioning of the sight is necessary to use a new system, *Eye Tracking System*, that follows the movement of the eye, so it's possible to give instruction to the patient to reposition his sight.[40]

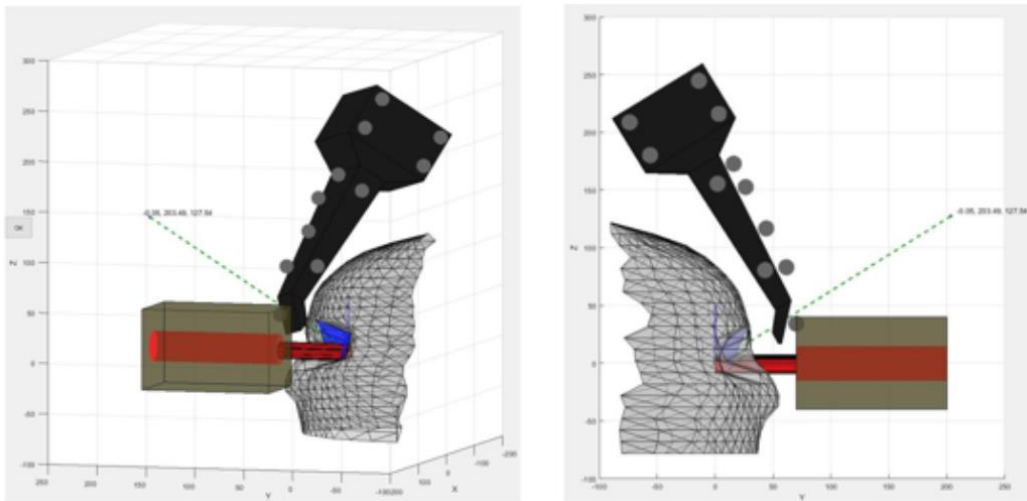


Figure 32 Eye Tracking System. [40]

Chapter 4

Treatment planning

Radiotherapy treatment provides for the succession of several phases.

The first phase regards the prescription of the radiotherapy treatment by the doctor. During the first visit the doctor will evaluate if the patient is suitable for the treatment and if necessary will ask for other specialist examinations.

The second important passage is the signature of the informative consent, that contains all the information about the descriptions of the tumour, of the treatment proposed and of the collateral effects that could arise.

In the third phase the patient will be subjected to a computed tomography, CT, or if necessary also to a magnetic resonance, that will allow the doctor to localize with high precision the tumour. To simplify the vision of the tumour could be necessary to inject into the patient of a contrast medium. The patient is positioned on the CT cot through immobilizers or through frameless devices.

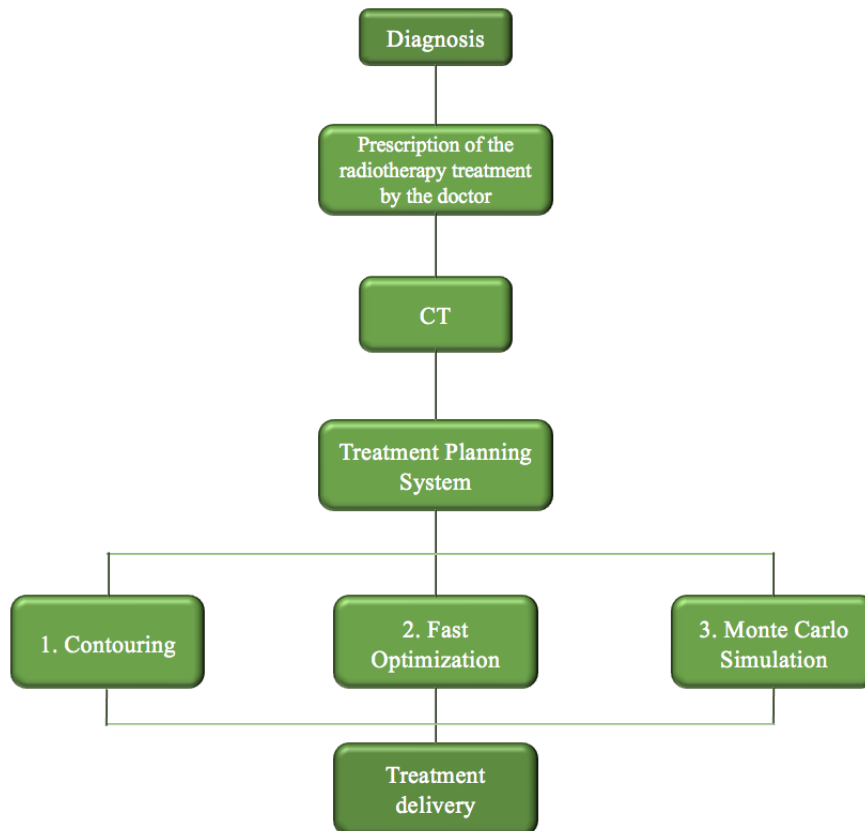
The fourth phase provides for the use of the *Treatment Planning System*, a software that will receive the CT images data.

The first step is contouring of the *Volume Of Interests*, *VOI*, and the second one is to optimize and simulate the radiotherapy treatment plan.

Doctors and physicals can now plan the therapy, stabilizing the exact distribution of the doses, that is how many radiations can hit which points and where are the organs at risk not to be affected.

At the end of these passages the treatment plan can be delivered to the patient.

Treatment with protons consists on average of 35 sessions, each of which will last maximum 30 minutes, for 5 times a week, for 7 weeks. Medical checks are carried out during and after the treatment. During the treatment the patient is controlled by the medical staff, that is able to communicate whit him. [42]



The proton therapy is also the best chosen for treating children, thanks to the low collateral effects on their organism and also because it is very precise and painless. [43]

4.1 Computed Tomography

The *Computer Tomography*, CT, is a procedure that allows to obtain 2D images of the body that are used to reconstruct the 3D structure.

In 1967, the engineer Godfrey Hounsfield and the physicist Allan Cormack projected the first machinery able to perform a brain Computed Axial Tomography, for which they won the Nobel prize for medicine in 1979. The first Computed Axial Tomography was done in the Atkinson Morley Hospital in Wimbledon, London, to a patient suffering from brain cysts. Hounsfield was the first scientist to combine an X-ray machine and a computer.

The examination expected the instrument to turn by 180° around the cranium, generating 160 images for each degree and in total 28800 images. The total time taken by the machine could go from a minimum of 5 minutes to a maximum of 10 minutes. Then a computer spent 2 hours and a half to process all the information and generate the images. In 1974 in Italy was installed the first CT, at the Bellaria Hospital in Bologna.

Thanks to further studies carried out by the professor Ralph Alfidi and Hounsfield, in 1975 was constructed a Computed Axial Tomography machinery able to reproduce images of the chest.

The first CT for all the body was the Automatic Computerized Transversal Axial, ACTA, projected by Robert Ledley at the Georgetown University.

Nowadays, the system of CT are more precise and complex thanks to the development of new the machinery and computer.

The CT tomograph is composed of a X-ray tube, at high intensity, detectors and a computer with a dedicated software.

4.1.1 X-ray tube

The X-ray tube is a glass bulb, inside which the vacuum has been made, that contains a negative electrode, the cathode, and a positive electrode, a copper anode, among which has been established a voltage. Inside the cathode is placed a tungsten filament that will be crossed by an electric current, this process will generate the photoelectric emission for which a beam of conduction electrons is released. The electrons will be accelerated and moved towards the anode by an electrostatic field, generating an electric current.

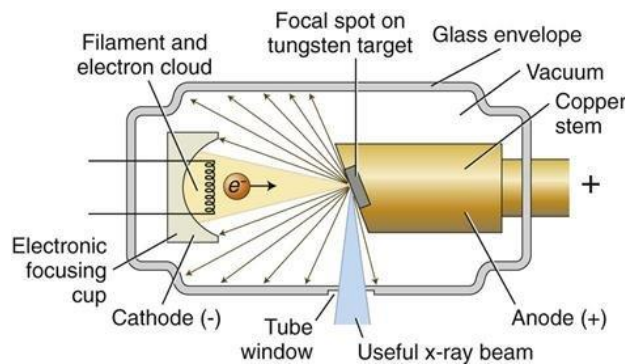


Figure 33 X-ray tube scheme. [45]

The force applied to each electron is:

$$\vec{F} = -e\vec{E} \quad (38)$$

where:

- e is the charge of the electron;

- \vec{E} is the electric field.

When the electrons hit the anode, thanks to the *Bremsstrahlung* mechanism or the *characteristic radiation*, the X-rays are produced.

The *characteristic radiation* is generated when an electron hit an orbital electron of the atom, that would leave its position. This gap will be filled by an upper level electron, which will lose part of its energy that will be transformed into X-rays. The *characteristic radiation* produces X-rays with higher energy respect to *Bremsstrahlung*.

The energy given to the anode depends on the characteristic of the electrons:

$$\mathcal{E}_k = e \Delta V \quad (39)$$

where:

- e is the electric charge of the electron;
- ΔV is the potential difference.

X-rays are composed of photons, particles that behave like corpuscle and also like wave but that are massless. The energy of photos depends on the initial energy of the electrons and on the distance between the electrons and the anode and it is equal to:

$$E = h \nu \quad (40)$$

where:

- h is the Planck's constant;
- ν is the frequency of the electromagnetic wave.

X-rays are electromagnetic waves at high frequency with wavelength between 1 nanometers (nm) and 0.001 nanometers (nm) and they are classified as ionizing radiations.

Only 1 % of the electron's energy is transformed in X-rays the remaining part becomes thermal energy, that could increase dangerously the temperature of the anode that could melt, so it is preferable having a rotating anode.

The material used to construct the target is tungsten, first because it is a heavy material and it is able to emit a more intense X-rays and second because it has a high fusion point and it is able to disperse heat efficiently.

Changing the voltage at the ends of the tungsten filaments it's possible to change the current that cross it, its temperature and so also the quantity of conduction electrons freed and of the X-rays. The temperature of the tungsten filament must overcome 2200 °C to have electronic emission and must not go over 2500 °C because it could verify evaporation.

The target is tilted 20° respect to the perpendicular direction to the electron beam, because in this way electrons will hit a bigger surface and the intensity of X-rays will be higher.

The material chosen to wrap the target is copper because it is a good conductor of electricity and heat and for these reasons it is used to avoid that the target could melt. Furthermore, changing the voltage, V , it's possible to change the maximum energy of the electrons and consequently of the X-rays.

The X-rays to go out from the vacuum chamber through a window, whose aim is to filter low energy radiation, which are not able to cross the patient. So, the window is characterized by an aluminium filter.

Another important element is the collimator, that permit to modify the form of the X-rays beam. The collimator is composed of a series of foils, a mirror and a light. These tools delete the diffusion radiations and enhances the quality of the images.[44]

4.1.2 CT Detectors

X-rays, generated by the source, will be directed towards the body, that has different densities, so X-rays will be attenuated at different levels.

For example, in the case of lungs, air has a lower attenuation and so a higher number of X-rays will arrive on the detector, creating a darker image.

Detectors receive the X-rays, measure them and send the data to a computer, that will process the information reconstructing first the 2D images and then the volume.

In practice, the detectors transform the intensity of X-rays into electric signals.

The material of the detector also called, *direct conversion material*, need to have high *efficiency* in detecting the X-ray quanta, around 80%, and high *sensitivity*. [46]

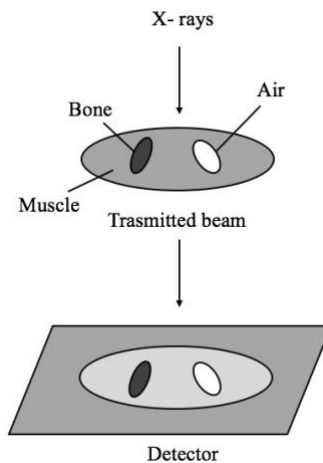


Figure 34 Detector

Detectors could be solid or gaseous:

- One model of solid detector element could be composed of a scintillator, a photodiode and a substrate. The photons will hit the first layer and will be transformed into optical photons, visible light, whose intensity is related to the energy of the photons. Then

the optical photons will be transformed into electric signals by the photodiode. And at the end, the substrate will transfer the information to the electronic channels. The material used for the scintillator is crystals or polycrystalline ceramic, for the photodiode is crystalline silicon. [48]

- The gaseous detector is composed of a chamber containing a gas, like Xenon, and a pair of electrodes, one cathode and one anode. When the X-rays enters in contact with the gas, they ionize hit, and due to an electric field, electrons will move from the cathode to the anode. At this point the electric charged collected on the anode will be transformed into electric signal. Xenon is a less expensive gas and it can remain stable under pressure. [49]

4.1.3 Attenuation coefficient

The intensity of the X-Ray change when the beam crosses the target, and its variation depend on the kind of beam and of target that are present. The attenuation coefficient defines the probability to interact per unit length, its unit of measure is [cm^{-1}].

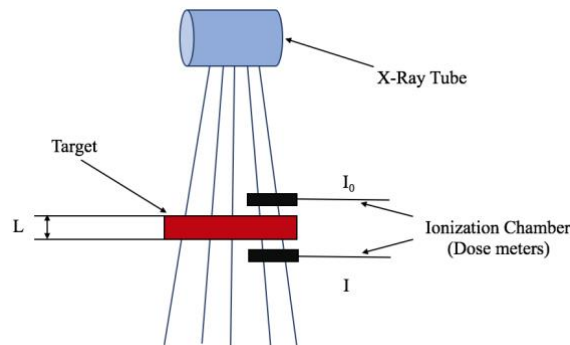


Figure 35 Scheme of interaction between the X-Ray beam and the target.

- If I have a *monochromatic beam* and a *homogeneous target*, the total intensity at the exit of the target will decreases exponentially according to Beer Lambert's law.

$$I(L) = I_0 e^{-\mu(\epsilon_\gamma)L} \quad (41)$$

where:

- I_0 is the initial intensity;
- L is the target thickness;
- ϵ_γ is the photon energy;
- μ is the attenuation coefficient, in general defined by the relation[54]:

$$\mu = \frac{4\pi}{\lambda} \beta \quad (42)$$

with:

β represent the absorption property of the tissue;
 λ is the X-ray wavelength.

- If I have a *non monochromatic beam* and an *homogeneous target*, the intensity will be the integral of (41) in $d\mathcal{E}_\gamma$.

$$I(x) = \int I_0(\mathcal{E}_\gamma) e^{-\mu(\mathcal{E}_\gamma)x} d\mathcal{E}_\gamma \quad (43)$$

Then it's necessary to sum for each sub-interval:

$$I(x) = \sum_{n=1}^N I_0(\mathcal{E}_\gamma, n) e^{-\mu(\mathcal{E}_\gamma, n)x} \Delta\mathcal{E}_\gamma \quad (44)$$

- If I have a *monochromatic beam* and a *non homogeneous target*, the attenuation coefficient will change in space and the total intensity will be:

$$I(L) = I_0 e^{-\int_0^L \mu(\mathcal{E}_\gamma) dx} \quad (45)$$

4.1.4 Hounsfield units

The CT images are generated thanks to the attenuation coefficient. The values of the attenuation coefficients are disposed in a bi-dimensional matrix and then converted in the Hounsfield Units.

The linear attenuation coefficient depending on energy, E, is:

$$\mu(E) = \rho N_A \sum_{i=1}^n \left(\frac{\omega_i}{A_i} \sigma_i(E) \right) \quad (46)$$

where:

- ρ is the mass density $\left[\frac{g}{cm^3} \right]$;
- N_A is the Avogadro constant $\left[\frac{1}{mol^{-1}} \right]$;
- ω_i is the element weight and it is a dimensionless number;
- A_i is the atomic mass of the i^{th} element $\left[\frac{g}{mol} \right]$;
- σ_i is the total cross section $\left[\frac{barn}{atom} \right]$.

To define the value of the attenuation coefficient respect to the position is necessary to calculate the mean value with respect to the spectral function $f(E)$:

$$\tilde{\mu}(s) = \frac{\int f(E) \mu(E,s) dE}{\int f(E) dE} \quad (47)$$

The mean value of the attenuation coefficient is then converted into the Hounsfield Units according to the relation:

$$H = \left(\frac{\tilde{\mu}}{\tilde{\mu}_{H_2O}} - 1 \right) 1000 \quad (48)$$

The values of HU can oscillate from -1000 to +1600, according to the different value of mass density, Figure 36. [55]

In this thesis, the water value of H is set at 0 and the air value at -1000.

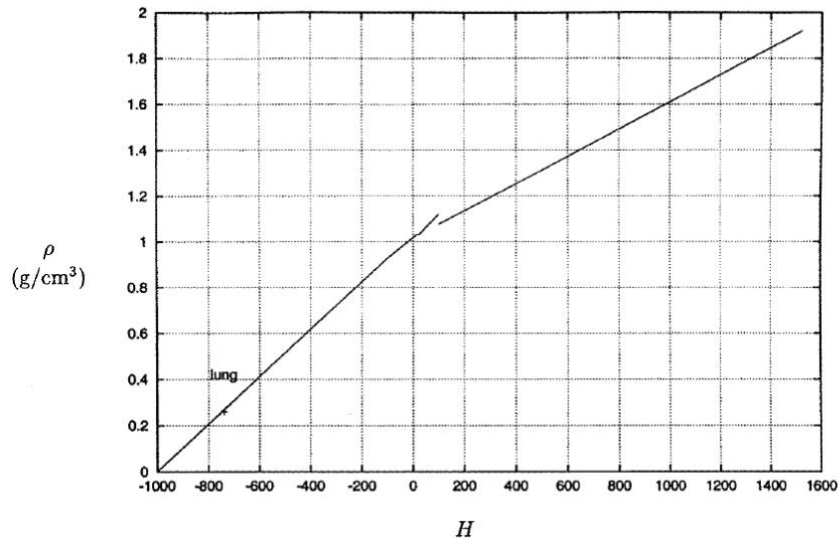


Figure 36 Value of the HU according to the mass density. [55]

The spectral function $f(E)$ is not known a priori so it's not possible to calculate directly the total cross section. In the specific case, in which energy has fixed values in radio diagnostic field, the cross section can be approximated to:

$$\sigma_i(E) = Z_i(K(E))^{KN} + Z_i^{2.86}(K(E))^{sca} + Z_i^{4.62}(K(E))^{ph} \quad (49)$$

where:

- K^{KN} is the Klein-Nishina coefficient;
- K^{sca} represents the coherent and incoherent scattering;

- K^{ph} represents the photoelectric absorption.

In this case the mean value of the attenuation coefficient will be:

$$\mu(E) = \rho N_A \sum_{i=1}^n \left(\frac{\omega_i}{A_i} (Z_i \tilde{K}^{KN} + Z_i^{2.86} \tilde{K}^{sca} + Z_i^{4.62} \tilde{K}^{ph}) \right) \quad (50)$$

where \tilde{K}^{KN} , \tilde{K}^{sca} end \tilde{K}^{ph} are the mean values with respect to the spectral function.

So considering the water attenuation coefficient the relationship $\frac{\tilde{\mu}}{\tilde{\mu}_{H_2O}}$ will be:

$$\frac{\tilde{\mu}}{\tilde{\mu}_{H_2O}} = \frac{\rho N_A \sum_{i=1}^n \left(\frac{\omega_i}{A_i} (Z_i + Z_i^{2.86} k_1 + Z_i^{4.62} k_2) \right)}{\rho_{H_2O} N_A \left(\frac{\omega_H}{A_H} (1 + k_1 + k_2) + \frac{\omega_O}{A_O} (8 + 8^{2.86} k_1 + 8^{4.62} k_2) \right)} \quad (51)$$

where:

- $k_1 = \frac{\tilde{K}^{sca}}{\tilde{K}^{KN}}$
- $k_2 = \frac{\tilde{K}^{ph}}{\tilde{K}^{KN}}$

Substituting (87) in (84) it's possible to evaluate the HU for each tissue.

Taking into account anatomic region with only two different materials it's possible to define a relation between the HU and their physical properties, $(\rho_1, \omega_{i_1}, H_1)$ and $(\rho_2, \omega_{i_2}, H_2)$ with $H_1 < H_2$. Imposing W_1 as the quantity of tissue 1 and $W_2 = 1 - W_1$ as the quantity of tissue 2, ρ and ω_i will be:

$$\omega_i = W_1 \omega_{i_1} + W_2 \omega_{i_2} = W_1 (\omega_{i_1} - \omega_{i_2}) + \omega_{i_2} \quad (52)$$

$$\rho = \frac{m}{\frac{m_1}{\rho_1} + \frac{m_2}{\rho_2}} = \frac{\rho_1 \rho_2}{W_1 (\rho_1 - \rho_2) + \rho_1} \quad (53)$$

Substituting (88) and (89) in (82):

$$\mu(E) = \frac{\rho_1 \rho_2}{W_1 (\rho_1 - \rho_2) + \rho_1} N_A \left[W_1 \sum_{i=1}^n \left(\frac{\omega_{i_1} - \omega_{i_2}}{A_i} \tilde{\sigma}_i(E) \right) + \sum_{i=1}^n \left(\frac{\omega_{i_2}}{A_i} \tilde{\sigma}_i(E) \right) \right] = \frac{\rho_1 \rho_2}{W_1 (\rho_1 - \rho_2) + \rho_1} \left[W_1 \left(\frac{\tilde{\mu}_1}{\rho_1} - \frac{\tilde{\mu}_2}{\rho_2} \right) + \frac{\tilde{\mu}_2}{\rho_2} \right] \quad (54)$$

Using (90) and (84):

$$W_1 = \frac{\rho_1 (H_2 - H)}{(\rho_1 H_2 - \rho_2 H_1) + (\rho_2 - \rho_1)H}$$

Consequently:

$$\omega_i = \frac{\rho_1 (H_2 - H)}{(\rho_1 H_2 - \rho_2 H_1) + (\rho_2 - \rho_1)H} (\omega_{i_1} - \omega_{i_2}) + \omega_{i_2} \quad (55)$$

$$\rho = \frac{\rho_1 H_2 - \rho_2 H_1 + (\rho_2 - \rho_1)H}{H_2 - H_1} \quad (56)$$

With $H_1 \leq H \leq H_2$.

Even if tissues are often more complex, containing more than two materials, the (92) can be used for all tissues. [55]

At each body component is then associated an ID cardinal number. In the following table is shown the association 1:1 of organs, HU and ID numbers.

Organ/Tissue	ID	H	Organ/Tissue	ID	H
Adipose abdominal	1	-98	Linfa 04	44	29
Adipose breast	2	-77	Liver	45	43
Adrenals	3	14	Lumbar spine	46	34
Bladder	4	26	Lung left	47	-741
Bladder content	5	23	Lung right	48	-741
Blood	6	56	Mandible	49	1524
Blood center	7	56	Muscle diaphragm	50	44
Bones feet	8	1524	Muscles face	51	44
Bones hands	9	1524	Muscle feet	52	44
Brain	10	40	Muscle hands	53	44
Cartilage chest	11	102	Muscle legs	54	44
Cartilage clavicole	12	102	Muscle neck	55	44
Cartilage ear	13	102	Muscle thorax	56	44
Cartilage hands	14	102	Nasal cavity	57	-1000
Cartilage humerus	15	102	Oral cavity	58	14
Cartilage legs	16	102	Pancreas	59	32
Cartilage maxilla	17	102	Parotid gland	60	14
Cartilage nose	18	102	Patella	61	1524
Cartilage pelvis	19	102	Pelvis	62	1524
Cartilage spine 1	20	102	Penis	63	36
Cartilage spine 2	21	102	Pharynx	64	54
Cartilage thyroid	22	102	Prostate	65	36
Cervical spine	23	34	Ribs	66	1524
Clavicle	24	1524	Sacrum	67	1524
Colon	25	23	Scapula	68	1524
Colon content	26	0	Skin	69	73
Connective tissues	27	40	Small intestine	70	23
Cranium	28	1524	Small intestine content	71	0
Esophagus	29	54	Spine	72	34
Eyes	30	49	Spleen	73	54
Femur	31	1524	Sternum	74	1524
Fibula and Tibia	32	1524	Stomach	75	41
Gall bladder	33	27	Stomach content	76	0
Glandular breasts	34	14	Sublingual gland	77	14
Heart	35	43	Submandibular gland	78	14
Heart Blood	36	56	Teeth	79	1524
Humerus	37	1524	Testicles	80	36
Hyoid	38	1524	Thimus	82	54
Kidneys	39	43	Thoracic spine	81	34
Lens	40	49	Thyroid	83	42
Linfa 01	41	29	Tongue	84	43
Linfa 02	42	29	Trachea	85	54
Linfa 03	43	29	Ulna and Radius	86	1524

Table 1 Organs, HU and ID. [56]

4.1.5 CT machinery

The CT machineries provide principally the positioning of the patient on a cot, inserted in a X-rays source, but they differ from each other for the motion of their component, for this reason they are divided in generations.

1. The *first generation* is composed of a single detector, that will translate and rotate of one degree together with the source for 180 times to obtain a rotation around the patient of 180°. The time taken per slice is very high, around 5 minutes.[58]
2. The first CT of *second generation* was put into action in 1974 in the Cleveland Clinic. It represented a big progress because of the new use of multiple detectors, but also because the time taken per slice is remarkably reduced to 5-90 seconds. In this case the beam will have an amplitude of 20°-30°, that permitted to eliminate the translate motion, leaving the rotation. [57]

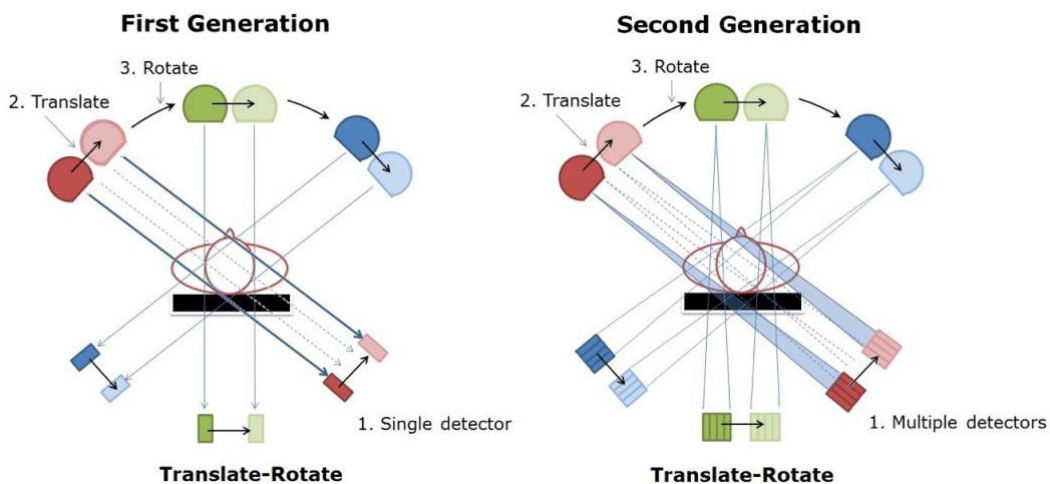


Figure 37 First and second CT generation. [58]

3. In 1975 the nowadays most common CT used was introduced, the *third generation* of CT. The amplitude of the beam was expanded into 30°-50°, allowing to hit all the body of the patient, also the number of detectors was increased. These updates permitted to spend 0.3 seconds to recover one slice.[57]
4. The *fourth generation* involves the use of a fixed ring of detectors, while the source is rotating around the patient. In this case the elimination of the connection cables permits to maintaining the tube in a continuous rotation, eliminating any acceleration or deceleration. [58]

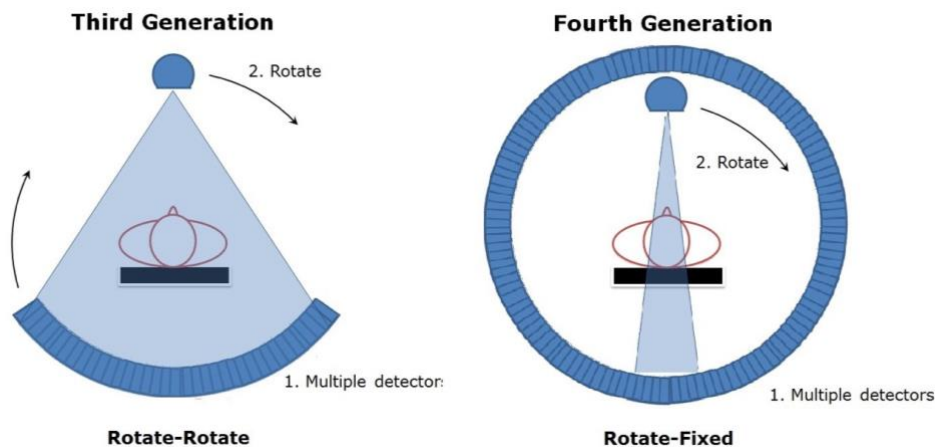


Figure 38 Third and fourth CT generation. [58]

5. At last, the *fifth generation* has no moving parts, it is composed of an electron source that will generate a beam deviated by a magnetic system into the anode, circular crown placed around the patient, that will generate a rotating X-rays beam. The system is highly efficient and it will permit to have high standard images.[59]

4.1.6 CT treatment

The patient is positioned on the cot, lying down, then the CT can start. The cot will move inside the CT scanner and the procedure is controlled by the operator in the control room, who can be in audio contact with the patient. The time of exposure to ionizing radiation is very short, about 35-40 seconds.

The CT examination requires the patient to remain still for about 10/20 minutes, this could be difficult mostly if it's about children. In this case it's possible to inject a sedative to help the patient to relax.

To distinguish solid organs and blood vessels can be helpful using the intravenous infusion of contrast medium, but it's not necessary for all the body parts, for example bones and lungs are by themselves distinguishable thanks to the fact that they contain air. The contraindications of the use of contrast medium regards the predisposition to allergic reactions and kidney failure. Some patients after the injection for few minutes have noticed a feeling of heat diffuses, a strong necessity of urinating, rarely a metallic taste in the mouth and a feeling of nausea. [51] The main pre-indication, in case of the use of contrast medium, is not eating for at least 5 hours before the TC. [50]

The main advice to follow after the CT is to drink abundant water to eliminate faster the contrast medium.

The CT has high radiation dose, so it has to be used with extreme caution and only in cases of necessity. In fact, due to the use of X-rays it could increase the probability of developing tumours or leukemia, mostly in children and young people.[52]

To attenuate the dose is possible using filters. In the following table are shown the average dose measured using bismuth and lead shielding, considering a high voltage standard value, 120 kV_p, a current of 100 mA and an exposure time of 0.1 seconds. The patient dose was measured through an ionisation chamber, in 3 organs of the methylmethacrylate phantom (PMMA). The differences between them is lower than 2-3 %. [53]

120 kV _p	Shielding material	Averaged dose with shielding	Dose reduction (%)
Head	Bismuth	3.02	11.95
	Lead	2.95	13.99
Thyroid	Bismuth	3.00	12.54
	Lead	2.94	14.29
Breast	Bismuth	1.34	12.42
	Lead	1.31	14.38

Table 2 Dose reduction with bismuth and lead shielding. [53]

4.1.7 Imaging acquisition

The reconstruction of a 3D images requires to acquire information on each slices of the tissue. The simplest way to perform the scanning is to rotate the device, moving the source and the detector together and in the same direction.

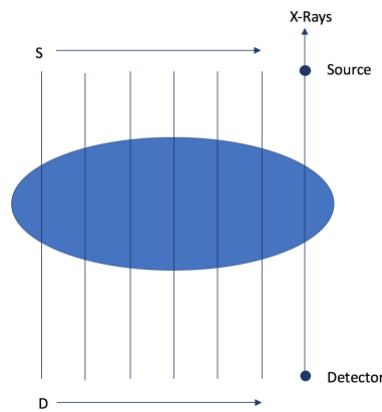


Figure 39 System Source – Detector.[61]

Let's consider the intensity of the radiation produced by the source, I_s , and the intensity of the radiation detected, I_D . The I_s is a known quantity, while the I_D is measured, and the relationship I_D/I_s is smaller than 1 because of the absorption phenomenon.[61]

The variation of the intensity in function of the x axis is:

$$\frac{dI}{dx} = -\mu I \quad (57)$$

Where μ is the *attenuation coefficient*, that represent the facility with which a material is crossed by the X-ray, in this particular case.

If the attenuation coefficient is big means that the material crossed by the X-ray will attenuate the beam largely.

Integrating (35) between the x-coordinate of the source, x_S , and of the detector, x_D :

$$\frac{I_D}{I_S} = e^{-\int_{x_S}^{x_D} \mu(x) dx} \quad (58)$$

This measurement is repeated for each slice, but in this way the total number of measurements will not be enough so, let's consider a two references system:

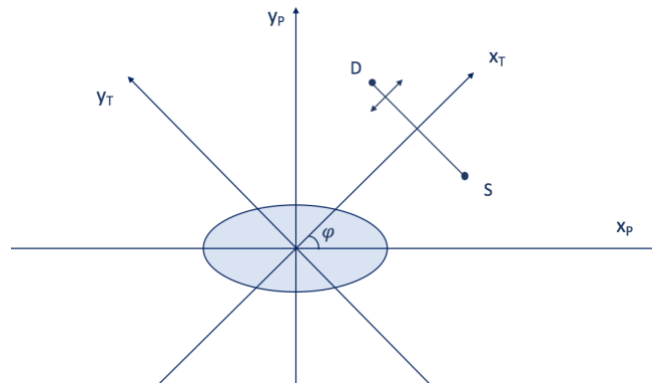


Figure 40 Reference system of the patient and the device. [61]

The reference frame of the patient is fixed and it is represented by the Cartesian plane defined by the axis x_P and y_P .

The reference frame of the device is in motion and it is represented by the Cartesian plane defined by the axis x_T and y_T . Impose φ to be the angle between the two frames.

It's necessary to fix φ and do measurement moving the system, source-detector, along the x_T axis, this procedure is followed for different φ .

Suppose to have a rectangular cross section and to divide it into sub-domains, in which one the attenuation coefficient, μ , is constant. [61]

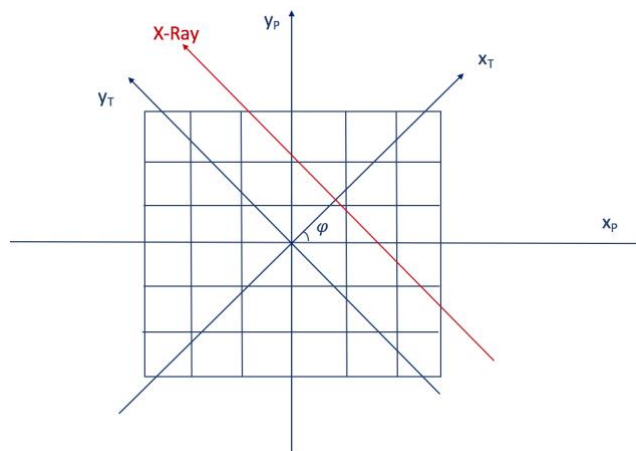


Figure 41 Reference system of the patient, the device and the X-ray. [61]

Let's define the length of the X-ray in the rectangle i for measurement α , $l_{i\alpha}$, where i is the index of each rectangle and α is the index for the measurement count.

The rectangles not crossed by the X-ray will have a $l_{i\alpha}$ equal to 0.

The system of equations is defined by:

$$\lambda_\alpha = \log \left(\frac{I_D}{I_S} \right)_\alpha = \sum_{i=1}^N \mu_i l_{i\alpha} \quad (59)$$

where μ_i are the unknowns.[61]

In reality the source is not a point-like source, it generates a beam with a certain extension, whose center is defined by the x_S axis.

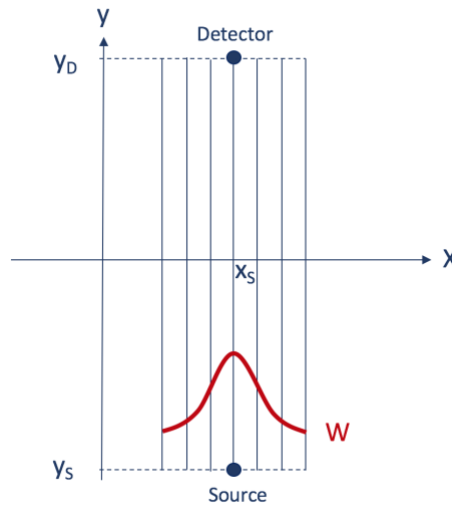


Figure 42 Source shape function. [61]

In this case, the intensity generated by the element source dx is:

$$dI = I_S W (x - x_S) dx \quad (60)$$

where $W (x - x_S)$ is the *shape function*.

While the total intensity of the source, I_S , is known the total intensity arriving to the detector, I_D , depends on the attenuation coefficient of the patient.

$$I_D = \int I_S W (x - x_S) e^{-\int_{y_S}^{y_D} \mu(x,y) dy} dx \quad (61)$$

Let's consider the source not to be too extended:

$$\mu(x,y) = \mu(x_S,y) + \delta\mu(x,y) \quad (62)$$

where $\delta\mu$ is very small.

Proceeding with the calculations it's possible to obtain the Fourier transform of the distribution of the patient attenuation coefficient is:

$$\widetilde{\mu}_P(k_x, k_y) = \frac{\widetilde{\lambda}(k, \varphi)}{\widetilde{W}(\varepsilon)} \quad (63)$$

To calculate μ_P just use the inverse Fourier transform.[61]

4.2 Magnetic Resonance Imaging

A valid substitute o better to the CT is the magnetic resonance, the main difference is based on the physic principles that govern the two machineries.

The concept on which is based the MRI was discovered by two physics Bloch and Purcell in 1946, to which was assigned the Nobel Prize in 1952. Until 1971 the MRI was used only for chemical, physical and molecular analysis and following the studies of Raymond Damadian the MRI started to be used in medicine, to detect tumour tissue.

The first experimental MR tomography was constructed in 1973 by the chemist Paul Lauterbur, who was able to observe tumour tissues in small test tubes. In 1975, the physicist Peter Mansfield began MRI for medical use, developing fast techniques for image reconstruction. And in 1977 the first images of MR was generated, an axial section of a human finger. [62]

The theory on which MRI is based is the *Nuclear Magnetic Resonance*, NMR, that takes advantage of the magnetic moment of spin of the nuclei associated to the movement of the charged particles belonging to the nuclei.

4.2.1 MR machinery

The MR system provides the use of three rooms, the *magnet room*, the *control room* and the *technical room*.

The control room is characterized by the presence of the control console that permits to control the machinery presents in the magnet room without direct contact. There is also a communication device that allows to communicate with the patient. It's also possible to control and modify remotely the temperature, the humidity and the oxygen percentage in the magnet room.

In the technical room there are all the components dedicated to the power supply and the IT management of the RM devices.

The magnet room contains all the MR equipment, like the magnet, the cot where the patient has to be positioned, the RF generator and so on.[64]

The magnet generates an external magnetic field, whose values fluctuates between 0.2 T and 2 T, it's possible to reach value of 7 T only in particular cases.[63]

The type of magnet used in MR are:

- *Permanent Magnets*, which are characterized by blocks of materials that through a strong electric discharge are able to maintain the magnetization acquired for an indefinite interval of time. The materials used to construct these blocks are neodymium-boron-iron alloys, which are able to produce a major density of the Static Magnetic Field. It can reach values of 0.3 T with lower cost. The geometries usually used for this kind of magnets are the "H", the ring, the trapezium and cylinder structures.[65]

- *Resistive Magnets*, which are composed of a series of 4-6 split coils, done of anodized aluminium, surrounded of two circular crown plates within which the cooling water flows. The current will pass in the coils and will generate a Static Magnetic Field, directly proportional to the current and the number of coils. Increasing the number of coils the magnetic field will be stronger but the heat to dissipate will increase to the square. For this reason, the maximum value of SMF obtainable with the resistive magnet is 0.2-0.3 T, which correspond with 200 kW of thermal power to dissipate. If between the coils and the body patient there is air the system will be called *air-core*, if the coils are disposed around an iron structure the system will be called *iron-core*.

The advantages of the air-core system are that it's possible to produce an instant activation and deactivation, to have a metallic shielding and an open geometry. The drawbacks instead are that the coils have a low efficiency and that the installation is critical because of the SMF characteristics.

In the iron-core system, iron's aim is to conduct the magnetic field lines. The installation will be less critical, the secondary field will be reduced and so the efficiency will be higher. Another important advantage of the iron-core is that the rectangular geometry is more comfortable due to the fact that it is more spacious.[63]

- *Superconductive Magnets*, which are composed of superconductive material, whose main characteristic is that under a certain temperature it has a null resistivity. The SMF reached with these magnets is of the order of 0.5 T – 3 T. This new technology was introduced to reach higher magnetic field, because with the resistive magnet was not possible for the high quantity of heat that should be dissipate for Joule effect.

The magnet has a solenoidal structure, composed of a series of split coils that can reach the length of 20 km. The coils are constituted of intertwined threads of Nickel-Titanium and Niobium- Titanium. To maintain the system at low temperature, around 4.2 Kelvin (270 °C), is necessary a cooling system, composed of a copper chamber wet by liquid helium or liquid nitrogen or both.

The advantages are the production of a strong, always active and horizontal SMF, high homogeneity and low weight of the system. Moreover is possible to obtain a

more extended volume of imaging. The disadvantages are that the machinery is very expensive and it has a close gantry that can generate in the patient a claustrophobic reaction.[63]

- *Hybrid Magnets*, which are a mix between the resistive and permanent magnets. They are composed of resistive wires crossed by current and wound around permanent magnets. The advantages and disadvantages are connected to the use of the two different technologies, in fact the hybrid magnets produce vertical field up to 0.5 T with low dispersion. The positive aspect is that it's not necessary the use of a cooling system, while the negative one is that the magnet is sensible to changing of environmental temperature and of current. Hybrid magnets involve the use of an open geometry and the construction of a machine very heavy and that has a high energy consumption. [65]

Inside the magnets are inserted the *Gradients*, coils done of electric wires, whose aim is to generates variations of the magnetic field. The field gradients are 3 and are oriented along the 3 axis of the system of reference, combining the 3 gradients is possible to obtain any section of the body patient. The maximum field variation in the unit space is expressed by the *amplitude*, measured in milliTesla per meter, mT/m . The gradient velocity with high the maximum efficiency is reached is expressed by the *rise time*, measured in milliseconds, $msec$. The relationship between the maximum amplitude and the time necessary for reaching it is called *slew-rate*, measured in $mT/m/msec$.

The Helmholtz coils are used to generate a gradient along the Z axis, they are composed of two coils coaxial with respect to the Z axis. The Golay coils are used to generate a gradient along the X and Y axis and they are composed two pairs of saddle coils. The typical values of the gradients are between 20 mT/m and 100 mT/m. The gradients more intense allow to obtain information about thinner layers.

Another important component of the MR machinery are the Radio Frequency coils, whose aims are to generate the radiofrequency impulses perpendicular to the principal SMF and to detect the return signal generated by the transverse magnetization. The coils are composed of an antenna wrapped up from a copper filament. The principal RF coil is inserted in the SMF magnet and then there are others positioned on the cot. These last one can be receivers and transmitters, receivers only and transmitters only.

The RF coils are of three types: “*saddle*” coils used with magnets that generate a horizontal field; “*solenoidal*” coils used with magnets that generate a vertical field; “*crossed ellipses*” coils used with magnets that generate both horizontal and vertical field. The coils can be:

- *linear conventional*, if they have a saddle geometry. They can be divided in linear conventional coils of volume or surface. The conventional coils of volume have the form of hollow cylinder in which the body patient or part of it, like the head or the chest, can be inserted. The conventional coils of surface have a different form

depending on the zone of the body that has to be examined, they can be flat, circular, enveloping or endocavitary type.

- in *quadrature*, if they are composed of 2 coils perpendicular to each other;
- *phased-array*, if the coils are parallel and each one works separately receiving a different RF signal. The information coming from each coils will be put together to generate a single image. [65]

Others two types of coils are presents inside the MR machinery.

The *shimming coils* are coils inserted in the magnet and their aim is to generate small field to counteract any non-homogeneity of the magnet.

The *shielding coils*, often positioned inside the magnet, weaken the effects of the magnetic field outside it.

Another important element is the *Faraday Cage* that isolates the machinery from external interferences.

The structure that surround the cot can be closed or open.

The *Open Magnetic Resonance* does not surround completely the patient, for this reason it is indicated for claustrophobic patient. The machine use a low magnetic field, of the order 0.2-0.3 Tesla, and it is suitable for the studies of musculoskeletal pathologies.

The main disadvantages of this kind of MR is that it permits to obtain low quality imaging, so it's necessary to widen the thickness of the section under examination that will increase the exposition time. Moreover it is not enough accurate for neurological, cardiological and vascular examinations.

The *Closed Magnetic Resonance* surround completely the patient and so, differently from the open one, it can cause claustrophobic reaction in the patient, maybe it could be necessary the anaesthetization. The machine uses a higher magnetic field, of the order 1-3 Tesla, and it is suitable for the studies of all the part of the human body.

The close MR permits to obtain high quality imaging in very short exposition time. [66]

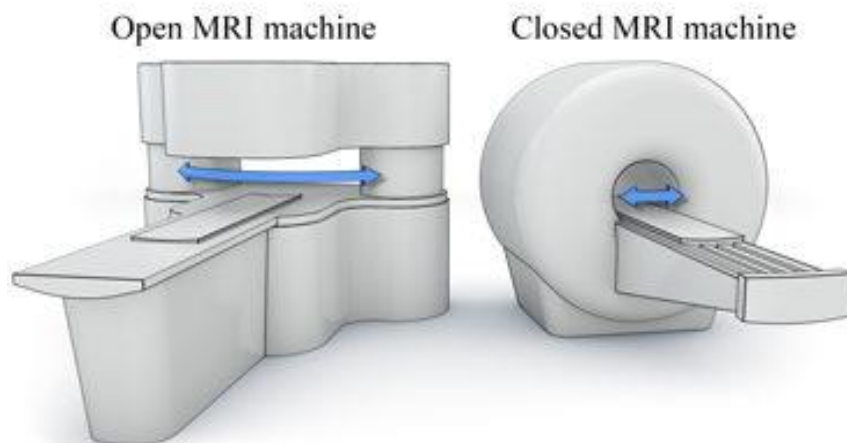


Figure 43 Open and Closed Magnetic Resonance Imaging. [66]

At the end, the computer will process the signal and through software to reconstruct the final image.

The MRI permits to diagnose different pathologies because it is able to visualize both the skeleton, the joints and the internal organs.

4.2.2 MR treatment

The patient subjected to MRI must not wear or have inside his body metal objects of any type, because in the case the objects are outside the body they could interact with the electromagnetic field causing overheating of the surrounding tissue and in the case the objects are inside the body they could be moved by the magnetic field damaging tissues or worse blood vessels.[67] It's not safe having MR with some medical implants, such as pacemaker.[68]

The time necessary for the MR is of about 30-60 minutes, that is longer than the time employed by the CT.[67]

MR scanner are very noisy so probably the patient will wear hear plugs or headphones.

MR permit to find bleeding, brain changes, herniated disc and knee injuries.[68]

Also in this case, as in CT, could be necessary to inject contrast medium in the body, to have clearer image.[68] The medium usually used in this case is the gadolinium, that is a very toxic metal, treated with a water solution. The gadolinium is injected in the patient through veins and followed by a small quantity of physiological solution.[69]

4.3 DICOM

The standard DICOM, *Digital Image COmunication in Medicine*, is an international standard used to manage medical images, so that images produced by different machine can be interchanged between the different hospital wards. Beyond images DICOM is able to store other information about the patient, the hospital, the machine's producer, the type of exam and the treatment plan. The files DICOM contains strictly personal data that must be protected.

4.4 Contouring

The *Contouring* procedure is performed by the radiotherapist doctor that will define the volume of the target and the surrounding organs. Through the directives of the *International Commission on Radiation Units, ICRU*, it's possible to define the following volumes [41]:

- *Gross Tumour Volume*, GTV, is the volume containing the visible tumour outlined at a macroscopic level;
- *Clinical Target Volume*, CTV, contains the GTV and the areas of the tissue to which the tumour could be extended;
- *Internal Tumour Volume*, ITV, contains the CTV and all the neighbouring areas affected due to natural movements of the organs;
- *Planning Target Volume*, PTV, contains the ITV and all the neighbouring areas affected due to the repositioning of the patient and to machine tolerances;
- *Biological Target Volume*, BTV, is a PTV generated taking into account the target biological heterogeneity;
- *Organ At risk*, OAR, are the healthy organs that could be subjected to radiations;
- *Planning organ-at-risk Volume*, PRV contains the OAR and all the neighbouring areas affected due to the repositioning of the patient or natural movements of the organs;
- *Treated Volume*, TV, is the volume that receive the prescribed dose;
- *Remaining Volume at Risk*, RVP.
- *Irradiated Volume*, IV, is include the TV and the areas which receive lower dose.

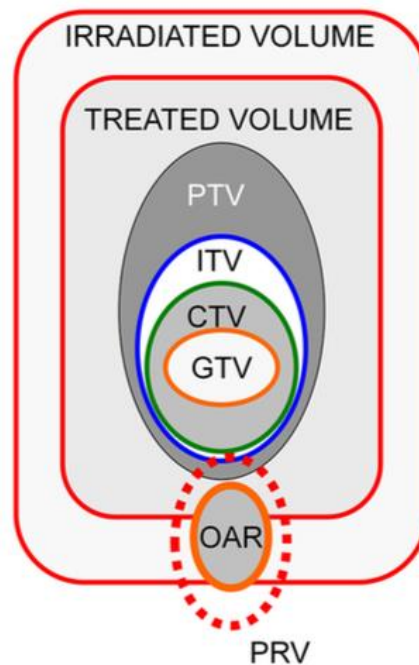


Figure 44 Volume defined in Radiotherapy by ICRU 50/62/83. [41]

During contouring is necessary to take into account a margin linked to the uncertainty deriving from the movement of the organs.

Nowadays new techniques of auto-contouring are being tested in order to optimize this process and to reduce response time.

4.5 Treatment Planning

The simulation of the treatment planning can be inverse or direct:

- The *inverse planning* plans the treatment on the basis of the dose distribution defined by the doctor and it optimizes the process maximizing the dose received by the target and minimizing that one received by the healthy tissues.
- The aim of the *forward planning* is to obtain the best dose distribution for the treatment of the target, this process is defined through a series of simulations that are based on the variation of the main parameters of the beam, as the initial kinetic energy, the direction and the fluence.

4.5.1 Fast Optimization

The Fast Optimization is an Analytical method based on the inverse planning. It starts from the target and according to the dose needed to treat it calculate the beam density. The first step is dividing the target in iso-energy layers and each section is irradiated with a high precision due to the utilisation of very thin proton beams, called *pencil beams*.

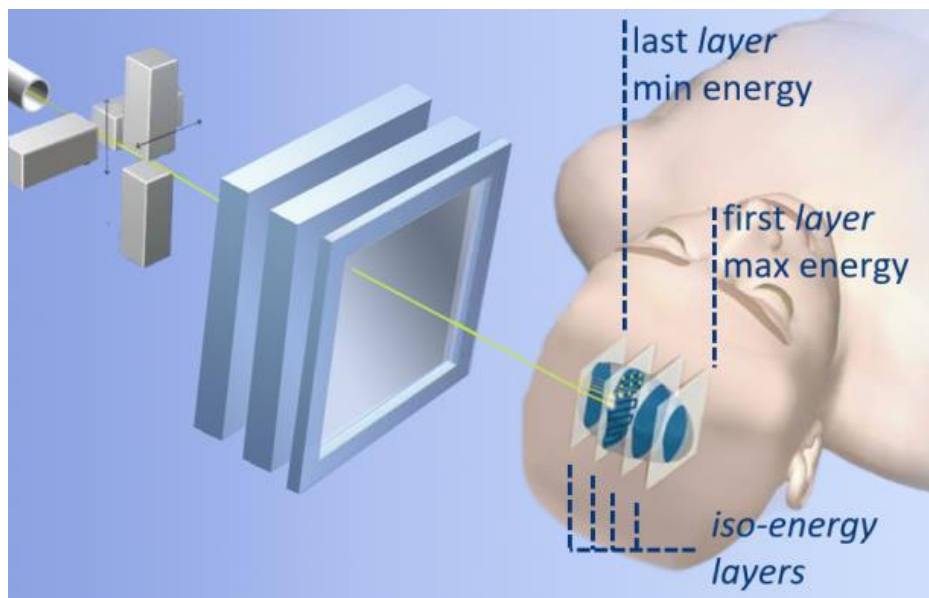


Figure 45 Pencil beam scanning delivery system. [70]

The Fast Optimization involves the use of the Water Equivalent Path Length, WEPL, in which the CT of the phantom are remapped in water equivalent taking into account the tissues densities.

Subsequently the optimization algorithm analyses the Look Up Tables showing the profiles of the deposited energy in water for protons. In Figure 46 are represented the trends of the energy loss in depth in function of the depth in water for protons with different fixed energies.

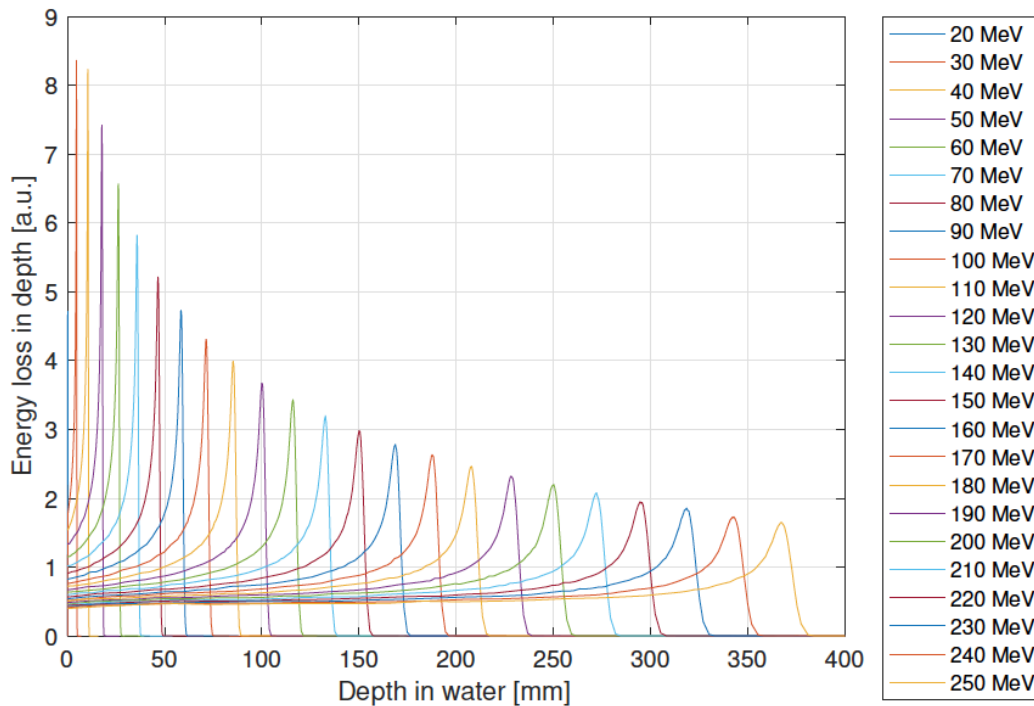


Figure 46 Look Up Tables, LUT, of protons in water. [71]

The last process is the optimization, regards the calculation of the fluence weights necessary to determine the *Spread-Out Bragg Peak*, composed of a set of elementary beams, called *spot*.

The Fast Optimization allow to obtain the kinetic energy, fluence and direction of the set of pencil beams, that generate the Treatment Plan.

The input data required by the Fast Optimization are:

- Total target dose prescribed by the doctor
- LUT
- Irradiation angle
- Contouring of the target

The output data obtained are:

- Treatment plan parameters
 - Kinetic energy
 - Fluence
 - Direction
- Dose matrix
- DVHs

4.5.2 Monte Carlo Simulation

The Monte Carlo Method is based on a probabilistic approach and it follows the forward planning. It takes as input the treatment planning generated and optimized by the Fast Optimization and then simulates the protons tracking from the last part of the beam extraction line into the patient. The beam comes out from the exit window and particles start scattering with air. The quality of the primary beam is affected by the materials used for the exit window and the layers, for this reason a lot of studies have been carried on increasing their efficiency.

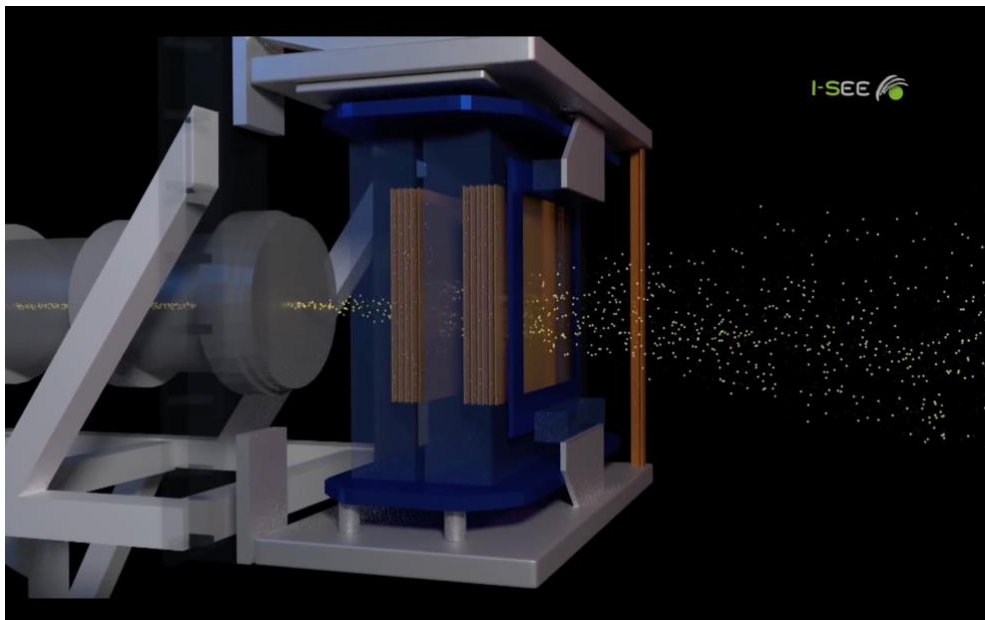


Figure 47 Beam delivery line. [72]

The most critical part is that one including the beam delivery line because it is the phase in which the direction of the beam is set in millimeters order.

The reconstruction of the matrix of original densities of the patient is defined through the dose-to-tissue distribution. The Monte Carlo Simulation takes into account the different attenuation coefficients for each organ improving the quality of the results. The Monte Carlo Simulation has the aim of validating the analytical calculation.

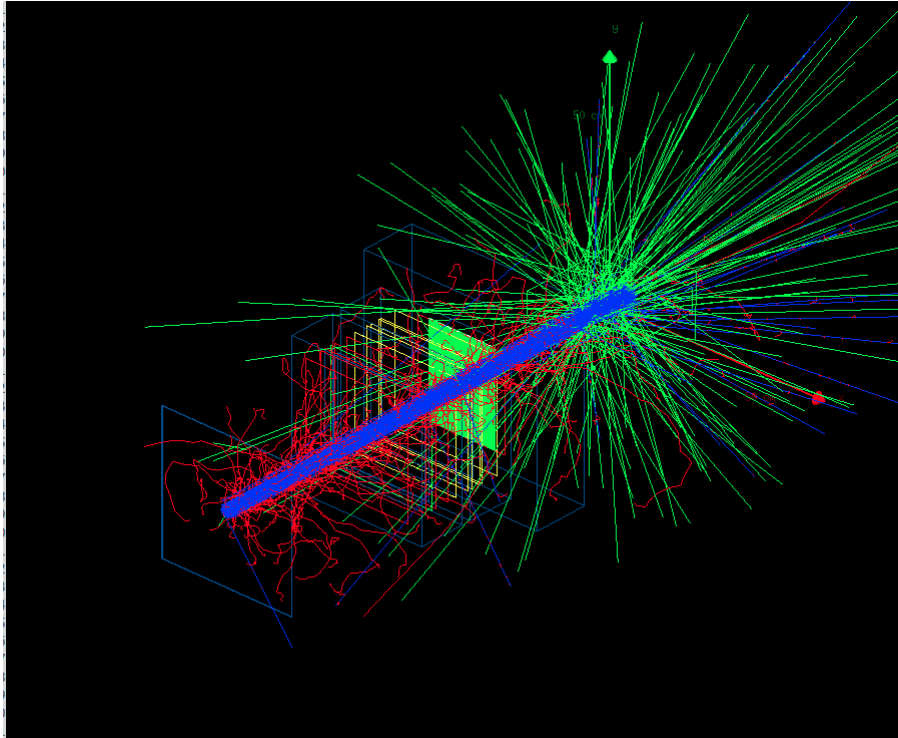


Figure 48 Simulation of Monte Carlo Method.

The input data required by Monte Carlo Simulation are:

- GEANT4 (GEometry ANd Tracking) results simulation, that are the beam line geometry and the Pencil Beam Scanning. GEANT4 is a Monte Carlo code, developed at CERN (*Conseil Européen pour la Recherche Nucléaire*), that simulate the particle transport.
- Fast Optimization plan

The output data obtained are:

- Dose-to-tissue distribution
- Radiobiological computation
- DVHs

4.5.3 Treatment Planning Output

The information obtained by the Fast Optimization and the Monte Carlo Simulation define the goodness of the treatment plan.

The elements that allow to judge the plan efficiency are the following:

1. Isodose chart

The isodose chart represent the isodose curves whose points are characterized by the same dose value. Through the isodose curves is possible to notice at glance if a treatment planning can be reasonably effective. The most desirable case expects that the highest irradiated zone is the target one, while the OAR should have low dose values.

In Figure 49 one example of isodose distribution regarding a periorbital sinonasal squamous cell carcinoma is reported.

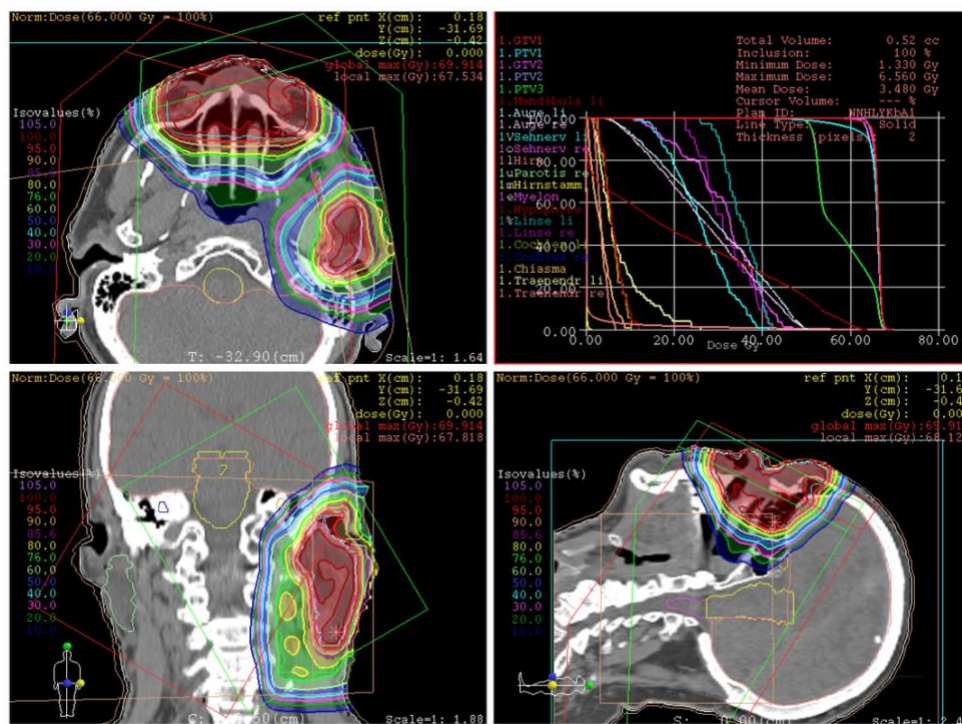


Figure 49 Isodose distribution in 3 planes and DVH of a proton therapy treatment planning.[73]

2. DVHs

The DVHs are the Dose Volume Histograms, that are graphical representation of the dose received by the percentage of the volume of the organ.

The values shown on the ordinates represent the percentage of volume that receives a dose greater than or equal to the value present in the abscissa.

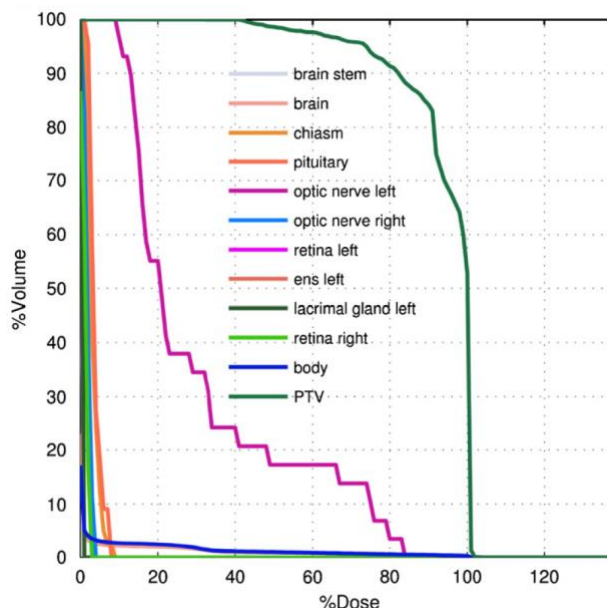


Figure 50 DVH obtained thanks to MC GEATN3. [74]

In theory the target trend should have a shape nearer to a rectangular one, that would mean that the target will absorb the maximum of the dose. Instead the other organs trend should be as lower as possible, in the way that their absorbed dose is the lowest. Each organ obviously has medical limit that cannot be overcome, principally for the most sensible organs.

In the following table, is possible to watch the dose constrains for adults and for children concerning the intracranial organs, calculated with two different criteria.

OAR	Constraints for adults		Constraints for children (if different from the ones reported for adult patients)
	Primary criteria	Secondary criteria	
Optic chiasma	$D_{max} < 54$ [10,11] $D_{max} < 55$ [12]	$D_{max} < 60$ [10]	
Cochlea	$D_{mean} \leq 45$ Gy [13,14] $D_{mean} < 50$ Gy [10]		$D_{mean} < 35$ Gy [16]
Hippocampus	Hippocampus $D_{max} \leq 6$ Gy and $V_3 Gy \leq 20\%$ Hippocampal avoidance volume $D_{max} < 25.2$ Gy and $V_{20 Gy} \leq 20\%$ [21,22] $D_{max} < 12$ Gy [23] $V_{7.2 Gy} < 40\%$ [25] $D_{mean} < 30$ Gy [24] $D_{max} < 54$ Gy [10,29]		
Brainstem		$D_{max} < 60$ Gy [10] $D_{39 Gy} < 10$ cc [29]	
Pituitary gland	$D_{max} < 50$ Gy [34] $D_{max} < 60$ Gy [10]		$D_{mean} < 25$ or 30 Gy [32] $D_{max} < 42$ Gy [35]
Retina	$D_{max} < 45$ Gy [10, Yamazaki] $D_{max} < 50$ Gy [Shaffer]		
Lacrimal gland	$V_{30 Gy} < 50\%$ [Sreeraman] $D_{max} < 40$ Gy [Jeganathan]		
Lens	$D_{max} < 6$ Gy [Piroth] $D_{max} < 10$ Gy [10, Yamazaki]		

Table 3 Dose constrains for adults and for children concerning the intracranial organs. [75]

3. Homogeneity and Conformity indices

The Homogeneity Index (HI) is a coefficient, that represent the homogeneity of the dose distribution in the region of interest. The HI is defined, in ICRU n. 83, as the relationship between the difference of the near-minimum dose $D_{2\%}$ and the near-maximum dose $D_{98\%}$ and the dose $D_{50\%}$. From the practical point of view the value of HI represents the quantity of peaks in the dose distribution and the value of maximum homogeneity is 0.

$$HI = \frac{D_{2\%} - D_{98\%}}{D_{50\%}} \quad (64)$$

The Conformity Index (CI) is a coefficient, that represent the conformity of the region of interest. The CI is defined as the relationship between the tumour volume covered by the 95% isodose and the planned target volume. The ideal value of CI is 1, if $CI > 1$ it means that the region irradiated is bigger that the target volume and if $CI < 1$ it means that the tumour is partially irradiated. A value of CI between 1 and 2 indicate that the procedure is correct, otherwise there will be deviation from the protocol that must be in place. From the practical point of view the value of CI represents the delineation of the contouring of the dose.

$$CI = \frac{TV_{prescr}}{PTV_{vol}} \quad (65)$$

Chapter 5

VPatient3D

5.1 Anthropomorphic Phantom

Nowadays, the use of Anthropomorphic Phantom in the science community is increasing, helping the world of medicine, physics and engineering to do research without putting at risk patient's health.

Physics and engineering in this particular case are at the service of medicine, they have to develop new techniques to cure human diseases. *Computed Tomography* (CT) and *Magnetic Resonance* (RM) are only some examples that depict this cooperation through a detailed reconstruction of human anatomic structure.

The Anthropomorphic Phantom can be physical or virtual.

The physical reconstruction of human body can have different aims in medicine, for example it can be used to test medical machines. Just think about the experiment done from the researches Ruvio et al on the use of a new machine, the Microwave Imaging (MWI), to improve the diagnoses of the breast tumour. They compared the imaging efficiency detection of this new technology with the ones used until now, that are the Magnetic Resonance Imaging (MRI), the Ultrasound (US), the mammography and the Computed Tomography (CT). The phantoms created in this test are two, phantom A and phantom B, that has a more complex structure.

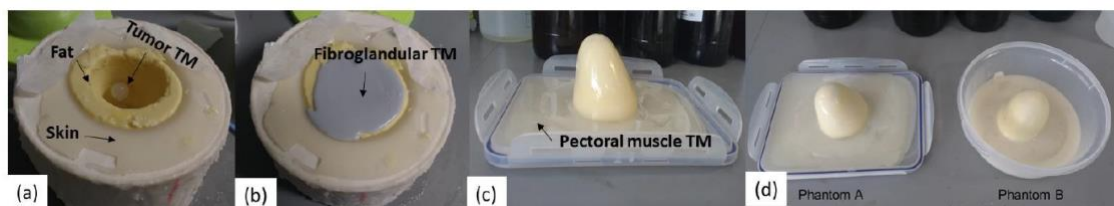


Figure 51 Breast phantom structure. [76]

The images generated from the different machines about the phantom A are shown in the following figure.[76]

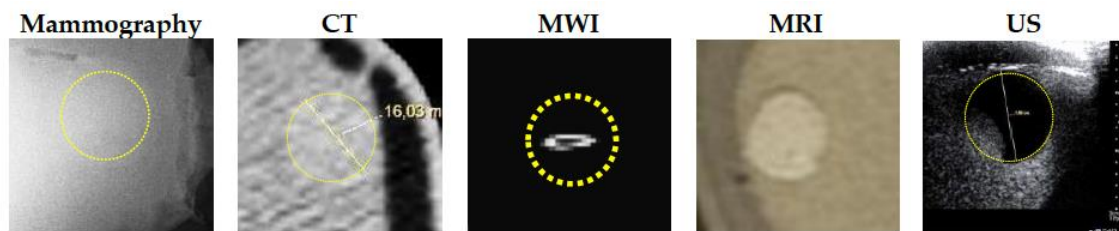


Figure 52 Images of phantom A. [76]

Another aim of the Anthropomorphic Phantom can be the implementation of the images quality of MRI and CT. It's possible to calibrate the machine, for example the CT, with different value of voltage, current, scan time and pitch to reduce the volumetric CT dose index maintaining an image quality equal to the standard one. [77]

The general positive aspects of using an Anthropomorphic Phantom are that it can be subjected to each condition, it permit to have more coherent results and it is easy to find.

The AP can be used also for the implementation of radiotherapy treatment.

In 2019 in “Physics in Medicine & Biology Journal” was published an article regarding the treatment procedure in MR-Linac radiotherapy using a VAP. The MR-Linac is a hybrid machine constituted by a conventional linear accelerator and a Magnetic Resonance machine. The scheme of the online workflow (Figure 53) shows the steps that the program has to execute. First the MR images are acquired from the MR-Linac, these will be used to generate pre-treatment MRI and CT scans. In this way it's possible to create the treatment plan, that will be adapted thanks to the repetition of MRI. [78]

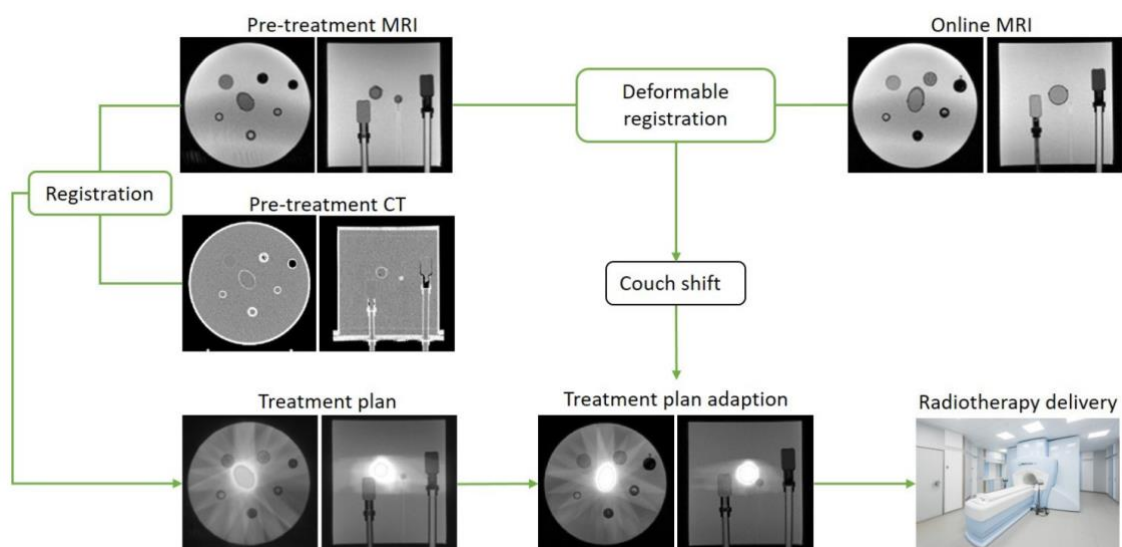


Figure 53 Scheme of the online workflow. [78]

The Virtual Anthropomorphic Phantom can be used for as many positive aims. The interactive platforms created, which foresee the presence of the Virtual Anthropomorphic Phantom, can be used from researchers, from students or from the patients themselves depending on their purpose. Among the most used platforms is INSIMU, an app that gives the possibility to every student all over the world to practice clinical reasoning skills through the use of a virtual patient simulator, born from the collaborations of the *International Federation of medical Students' Associations* and other *Universities*. [79]

One of the most important field in medicine in which the Virtual Anthropomorphic Phantom (VAP) can be used is *Radiotherapy*. Known is the fact that the disadvantage of Radiotherapy is that the radiation, used to kill the tumour cells, can also hit the healthy cells and for this reason is important to optimize the process. *VAP* has assumed an important role in Radiotherapy treatment, because it let us study and practice on virtual patient in a safe environment. [80] In Bellevue College has been improved a 3D simulator of a cancer patient which receives a dose of radiation generated by a linear accelerator, this software is called VERT, *Virtual Environment Radiation Therapy*.

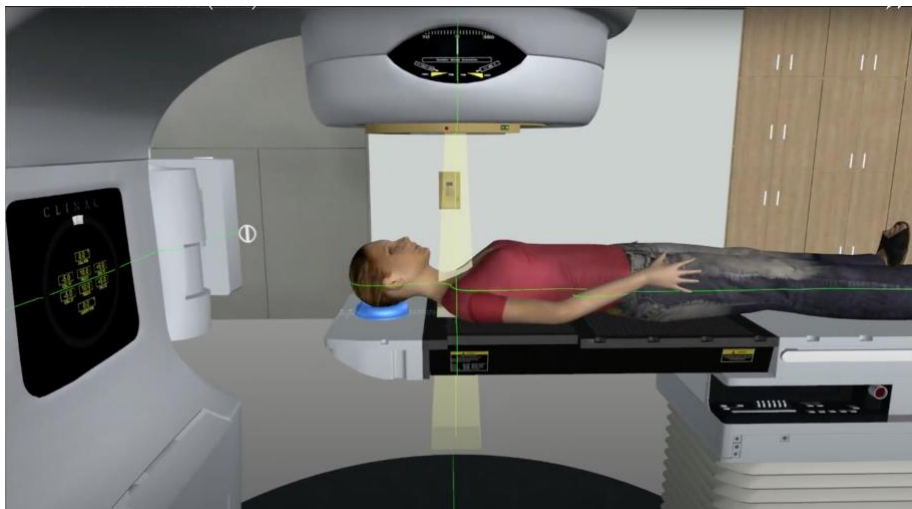


Figure 54 VERT [81]

This simulator can be used by student to develop their skills, by researchers to improve radiotherapy treatment but also for real patient that can experience the radiotherapy treatment without the pressure of the clinic. [82] The theme of anxiety in Radiotherapy is very important most of all for the psychical health of the patient. Studies shows how the radiotherapy treatment generate anxiety in men mostly during the first time, because they have not yet experienced it. It has been conducted a study on the increasing of the number of patients with clinically relevant anxiety during the radiotherapy treatment. [83]

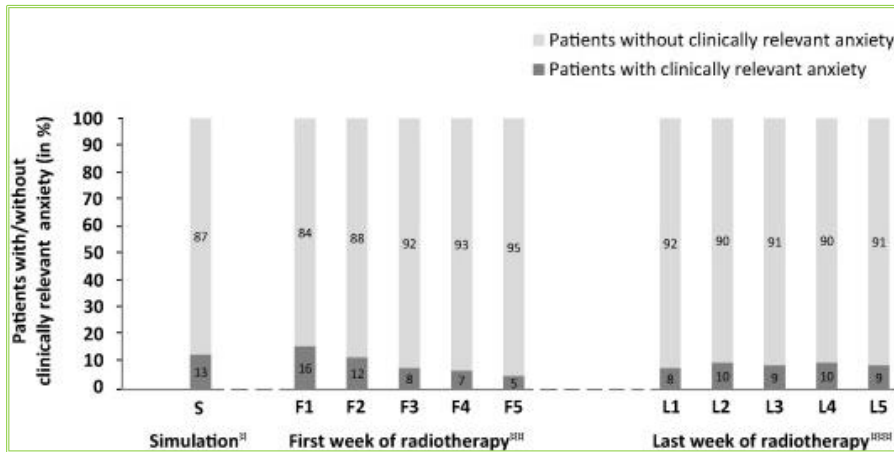


Figure 55 Number of patients with clinically relevant anxiety. [83]

For this reason, is necessary to initiate the patients making them experience virtually the radiotherapy treatment. A good patient education can reduce consistently the anxiety. The *Virtual Patient Education in Radiotherapy, VIPER*, by Alexander Raith, student of the St. Polten University of Applied Sciences, has been developed to reduce anxiety of cancer patients. [84]

The user, through VIPER's phantom, can run through all the sequences that constitute a radiotherapy treatment.

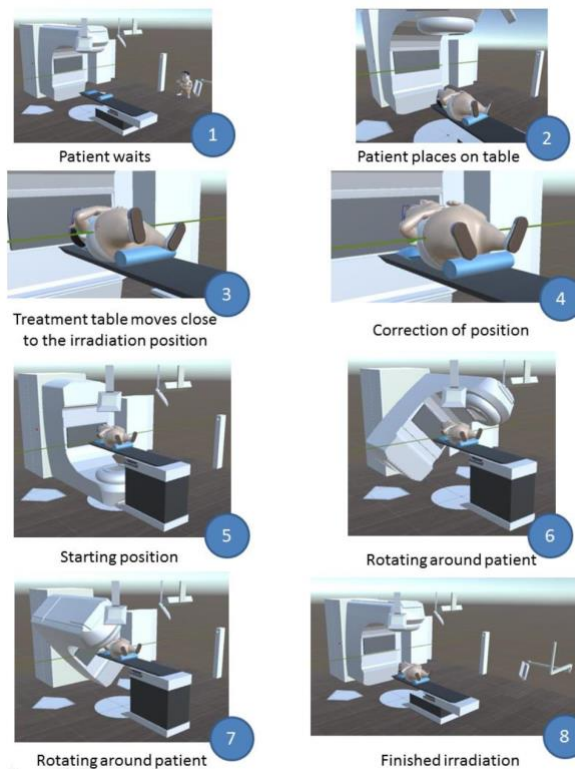


Figure 56 Sequence of patient treatment in VIPER. [84]

The experiment done by the doctors Neves et al is interesting because of the use of two pediatric anthropomorphic phantoms, representing the biological structure of a child of 5-year-old and one of 10-year-old. The scientists wanted to determine the effective and the absorbed dose. From this study, it is denoted that the organs that receives the highest doses are the eye lens, the salivary glands and the thyroid. Moreover, the 5-year-old child registered the highest effective dose. [85]

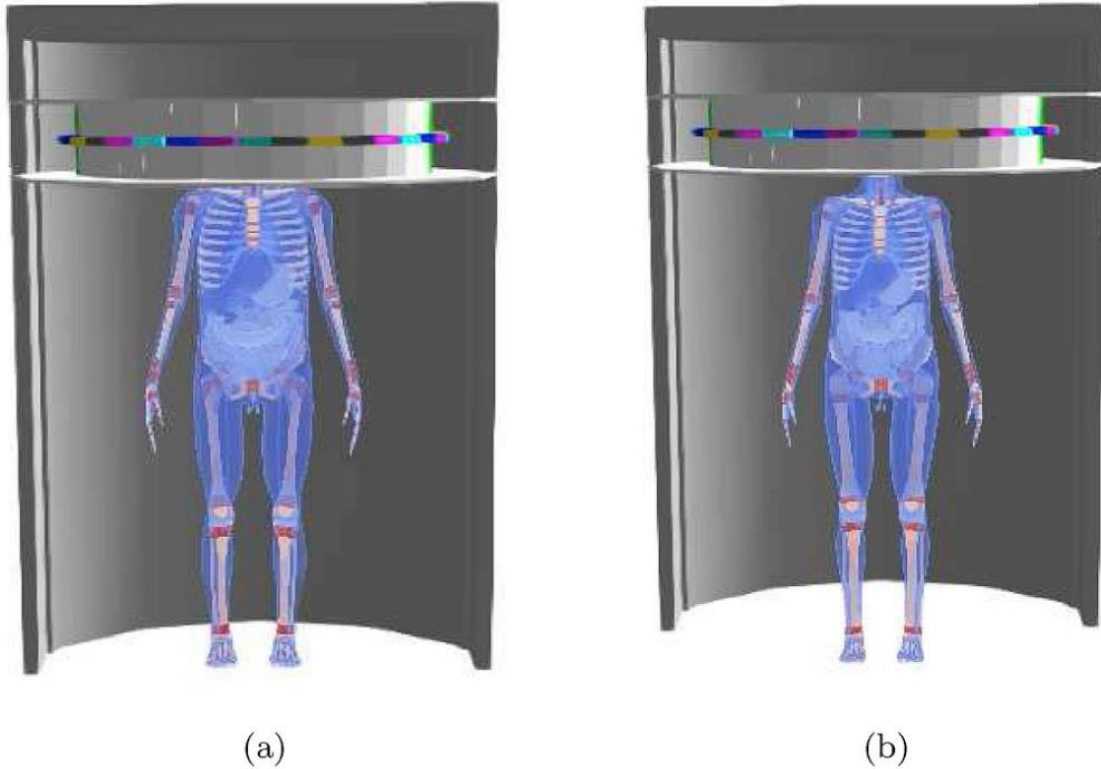


Figure 57 Anthropomorphic phantoms of a child of a) 5-year-old and one of b) 10-year-old. [85]

5.2 Virtual Patient 3D

The *VPatient 3D* is the project carried out in Turin by the spin-off between the *I-See s. r. l.* and the *National Institute of Nuclear Physics*. The VP is a virtual phantom with the form of an average man, shaped on the directives of the MASH, Male Adult meSH, supine model, belonging to the *Caldose* site.

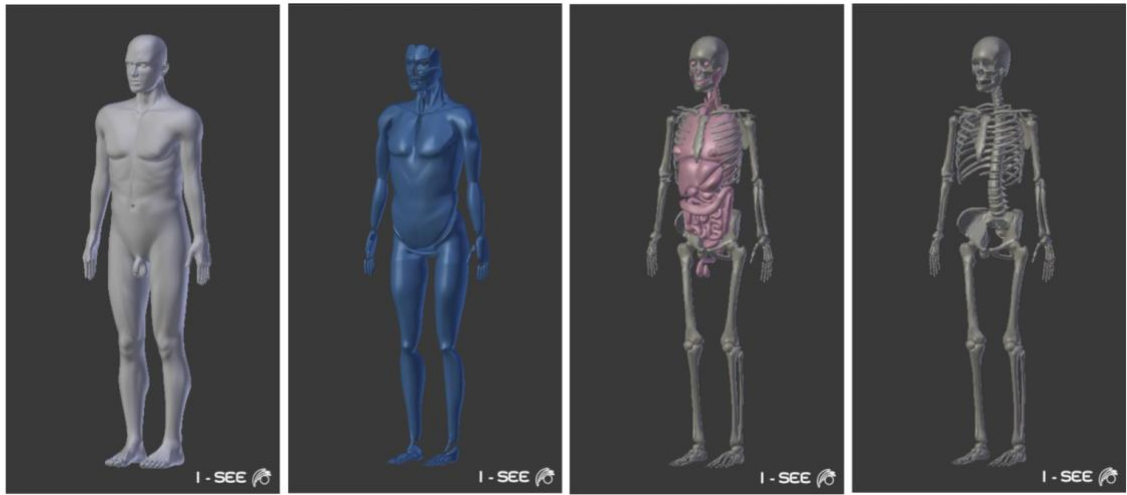


Figure 58 VP 3D structure following the Male Adult mesh directives [86].

The dimension, position and material densities of the organs follow the guidelines of the ICRP human-Adult Male model, described in the *ICRP Report 110*, published in 2009. In the following table, extrapolated from the *ICRP Report 110*, are listed the mass density values for the constituent of the skeleton of the reference Male and Female.

	Mass (g)		Mass density (g/cm ³)	Volume (cm ³)	
	Male	Female		Male	Female
Mineral bone	5500	4000	1.92	2860	2080
Cortical bone	4400	3200		2290	1670
Trabecular bone	1100	800		570	420
Cartilage	1100	900	1.10	1000	820
Active bone marrow	1170	900	1.03	1140	870
Inactive bone marrow	2480	1800	0.98	2530	1840
Miscellaneous	200	160	1.03	190	160
Total	10,450	7760	1.35	7730	5770

Table 4 Mass density values and volumes for the constituent of the skeleton of the reference Male and Female. [87]

The VP can be used for CT generation and in Radiopharmaceutical and TPS simulations. In Radiopharmaceutical field it allows to simulate the passage of the substances through the body and to calculate the deposited dose.

In this master thesis will be deepened the role of VP in generation of CT image and in simulation and optimization of TPS.

The positive aspects of using the virtual patient to create artificial CT images are first of all that CT of real people are not well-defined respect to that one of the phantom and second that the real CT are private and so not easy to obtain.

The artificial CT are used in TPS simulation to optimize the process of detection and treatment of the target and to validate the efficiency of new TPS.

The *I-See s. r. l.* has also developed web applications that allow researchers to do their own simulations.

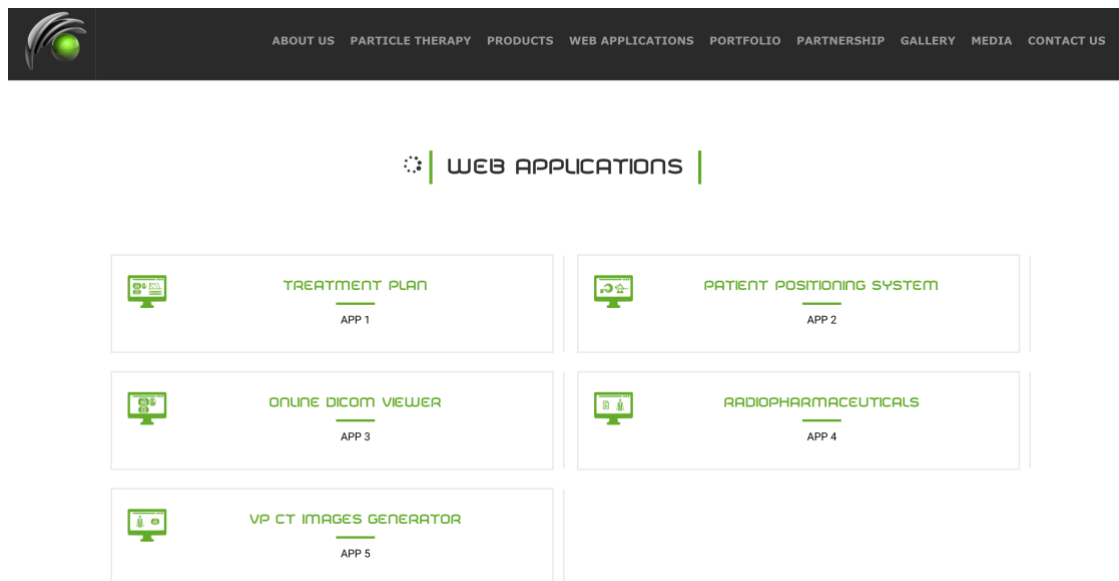


Figure 59 I-See s. r. l Web Applications. [88]

5.3 DICOM CT Generation

The first step for the generation of CT images is the modelling of the 3D target. This process can be realized through the *Virtual Patient Online Interface*, developed by the *I-See*. The user can manage directly a 3D model of the *VPatient* and he has the possibility of shaping and positioning a target.

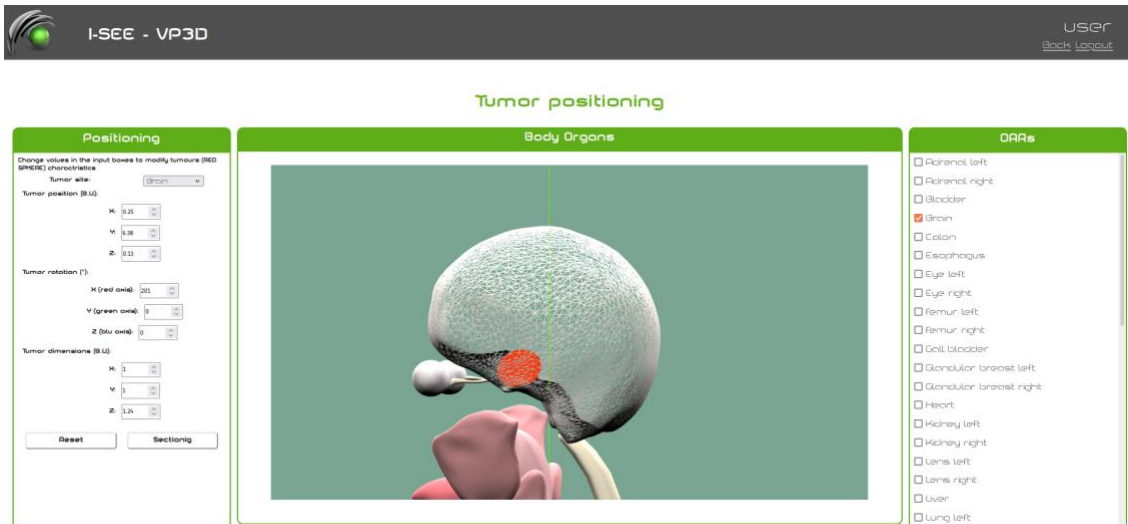


Figure 60 Target 3D Modelling.

The generation of the CT from the Virtual Patient is composed of two principal steps: the *sectioning* and the *compositing*.

The *sectioning process* consists in the positioning of a plan in the target zone, that will slide longitudinally, the results will be the frames for each organ.

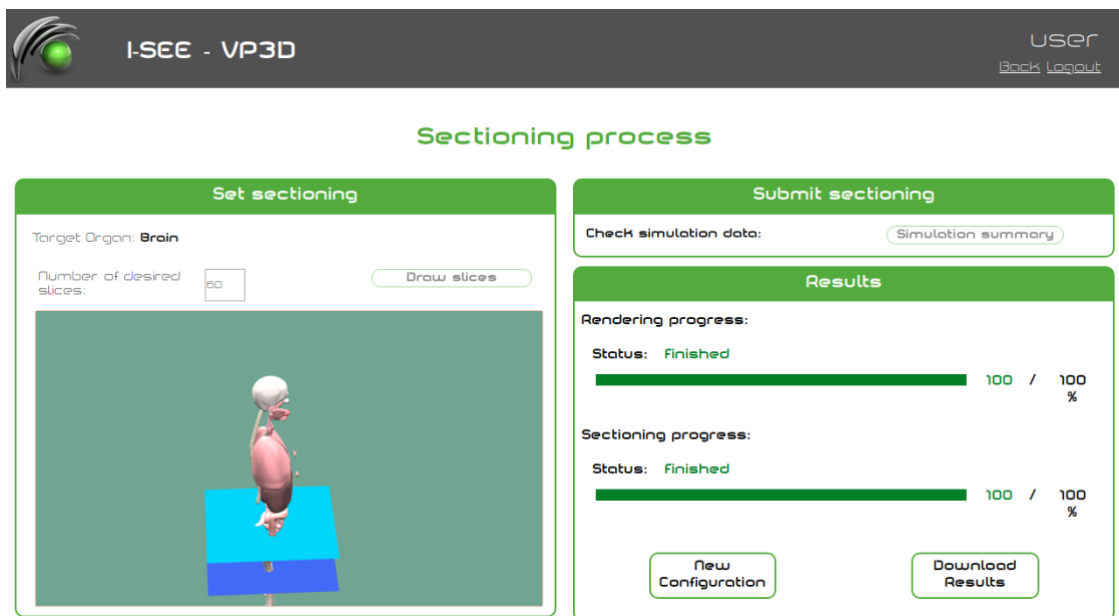


Figure 61 Sectioning process representation.

In the *compositing process* the corresponding frames of each organs are overlapped in one, generating the sections of the interested zone of the patient.

In compositing process the HU and the ID numbers and the colour data are associated to the organs.

As a result of the *compositing process* will be created three matrices, which will contain respectively HU, ID and greyscale data, where 0 corresponds to black and 1 to white.

The 3D matrices containing HU and ID will be converted in binary format, while the colour matrices will be saved in .png images of the sections, which corresponds to the CT image set, downloadable by the user.

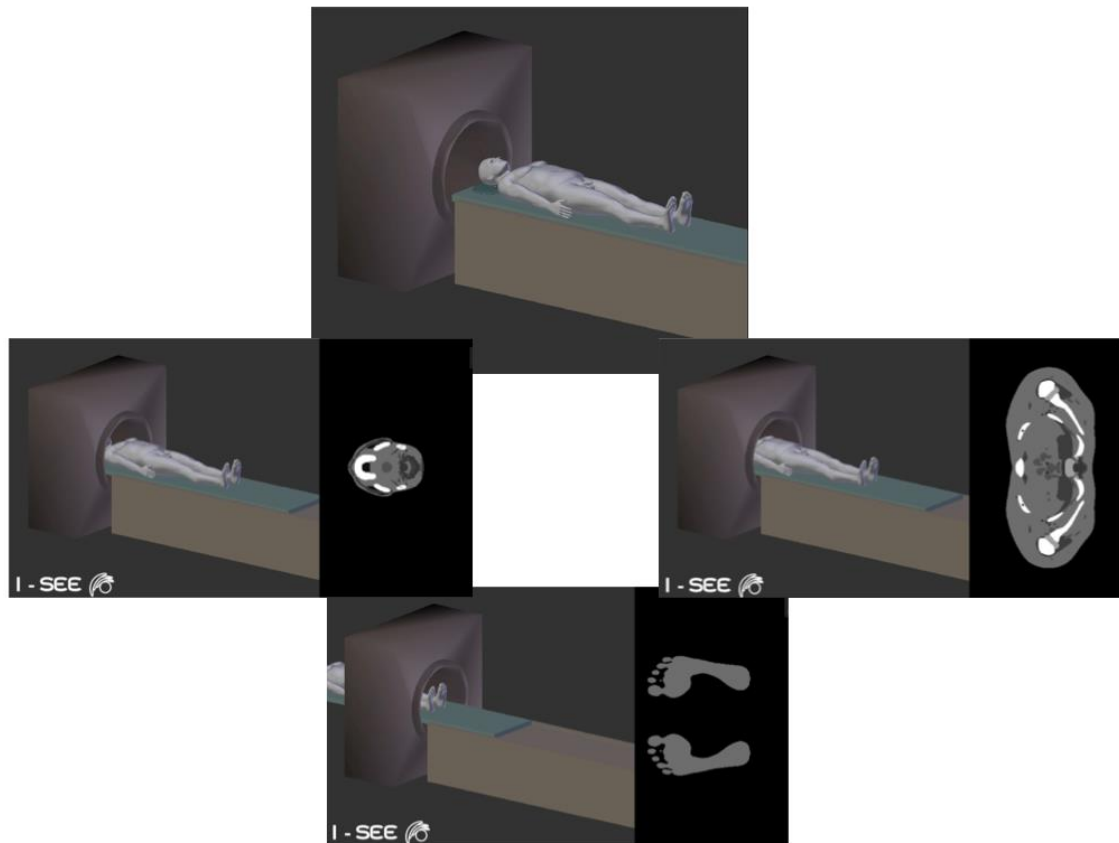


Figure 62 Generation of CT images set. [86]

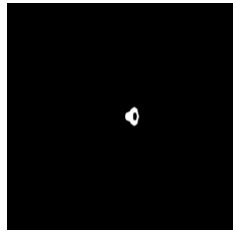
The first part of this master thesis is about:

- Managing of the post processing of the compositing to improve quality of CT images;
- Checking the goodness of the binary matrices.

The targets modelled and analysed are positioned in three different zones of the VP, the brain, the prostate and the left lung.

5.3.2 Case 1: Brain

The frames generated are 64 and are distant one from the other 3 mm. The organs involved in the 1st section are the following:



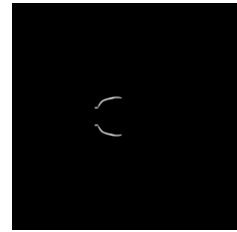
Cervical Spine



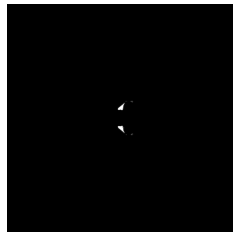
Connective Tissues



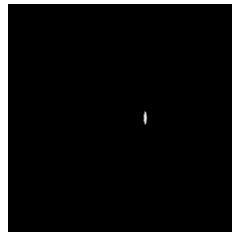
Mandible



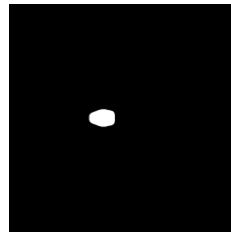
Muscle Face



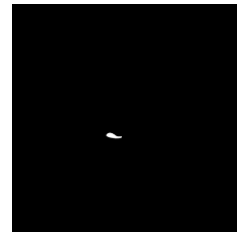
Muscle Neck



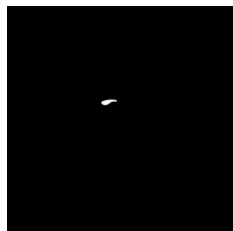
Muscle Torax



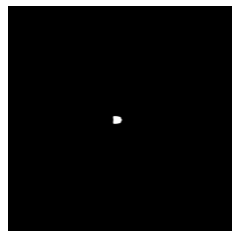
Paranasal Sinuses



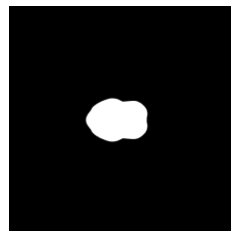
Parotid Gland Left



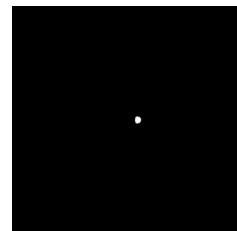
Parotid Gland Right



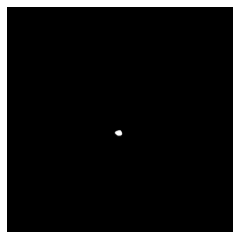
Pharynx



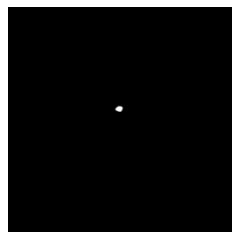
Skin



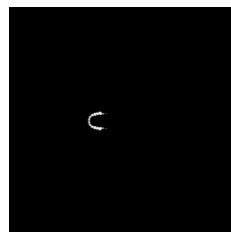
Spine



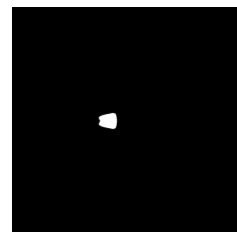
Submandibular
Gland Left



Submandibular
Gland Right



Teeth



Tongue

The section obtained through the use of the MATLAB codes “*vol_conversion*” and “*compositing*” is:

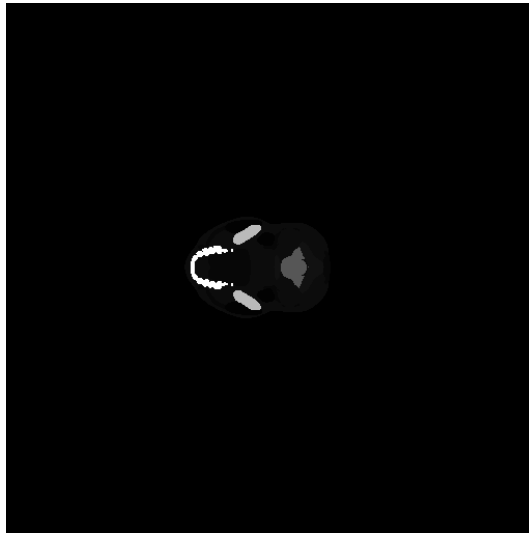


Figure 63 Case 1 "Brain" - Section 1.

The Figure 63 hasn't a good contrast, for this reason it has been necessary to apply the *gamma correction*, in the script “*Filtro_gammalog_brain*”. The mathematical formula used is:

$$s = c * r^\gamma \tag{66}$$

where “*s*” is the initial images, “*r*” is the correct image and “*c*” is a constant equal to 1. In this case γ has been assumed equal to 0.45 thanks to which is possible to obtain a good contrast.

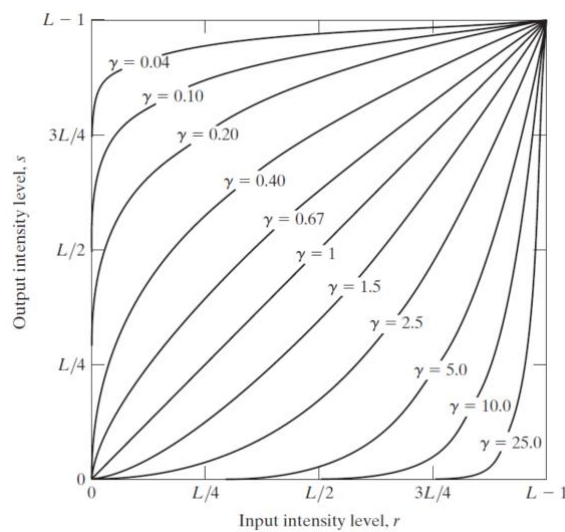


Figure 64 Plots of *s* for each value of γ , with $c=1$. [89]

In Figure 65 is possible to notice the difference between the original picture and the corrected one.

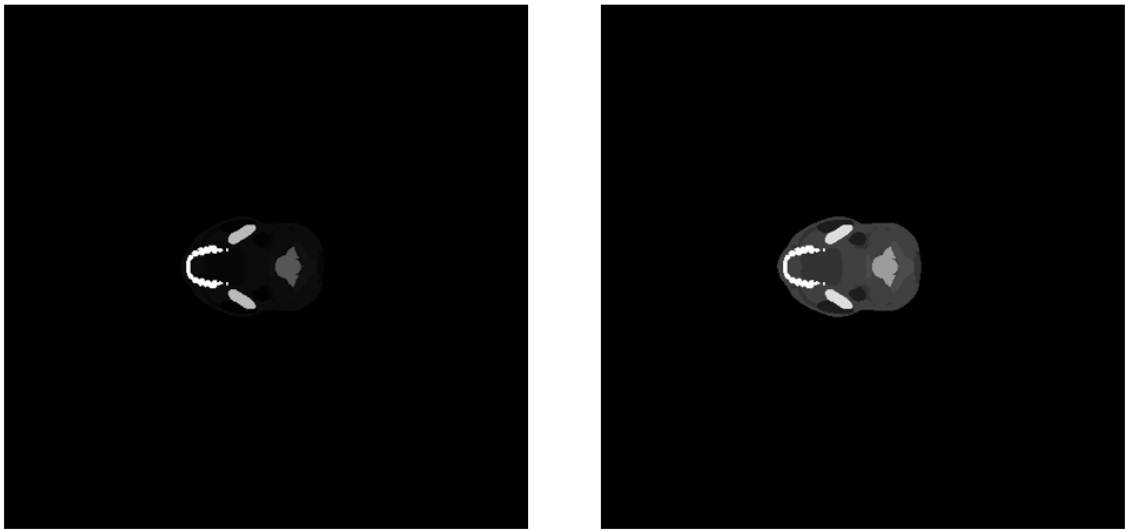


Figure 65 On the left the original section 1, on the right the gamma corrected section 1 ($\gamma=0.45$).

The previous procedure has been reiterated for each section.

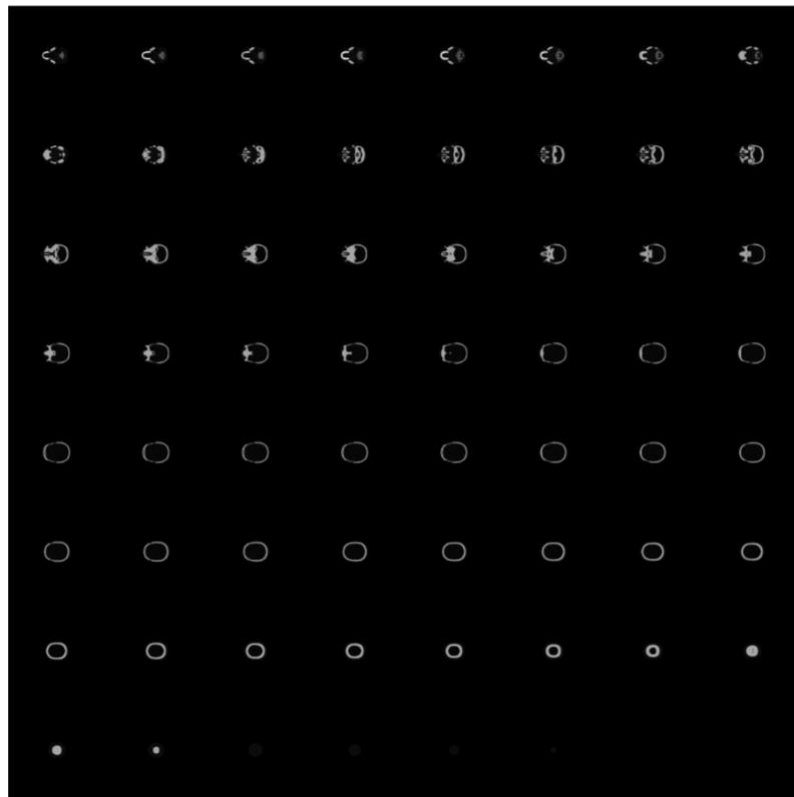


Figure 66 Assembly of original sections.

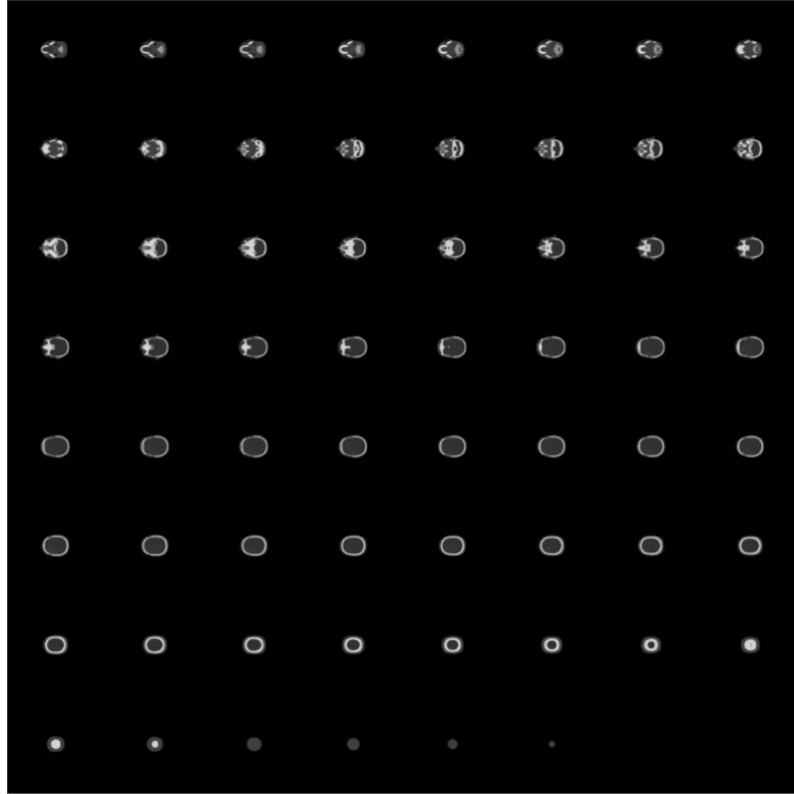


Figure 67 Assembly of gamma corrected sections ($\gamma=0.45$).

The following steps regards the processing of files in binary format “*mat_HU.bin*” and “*mat_ID.bin*”, obtained in “*compositing*” from 3D matrices.

In the MATLAB script “*HU_brain*” it was first memorized the binary file “*mat_HU.bin*” in 64 2D matrices, each of which of the size 512 X 512 pixels. Among all the sections has been chosen the first one to be in line with the previous example.

To make the image come closer to the gamma corrected image in this case is necessary to scale the data by setting a minimum value,0, and a maximum value, 300.

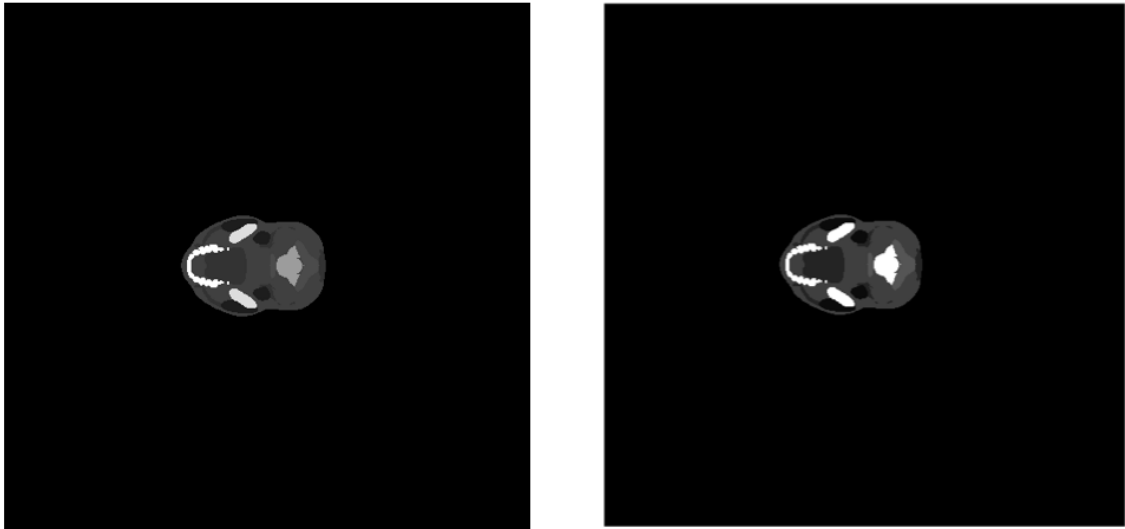


Figure 68 On the left the gamma corrected section 1 ($\gamma=0.45$), on the right the section 1 obtained by the binary file “mat_HU.bin”.

The assembly of the sequence of sections obtained by the binary file “mat_HU.bin” was also performed.

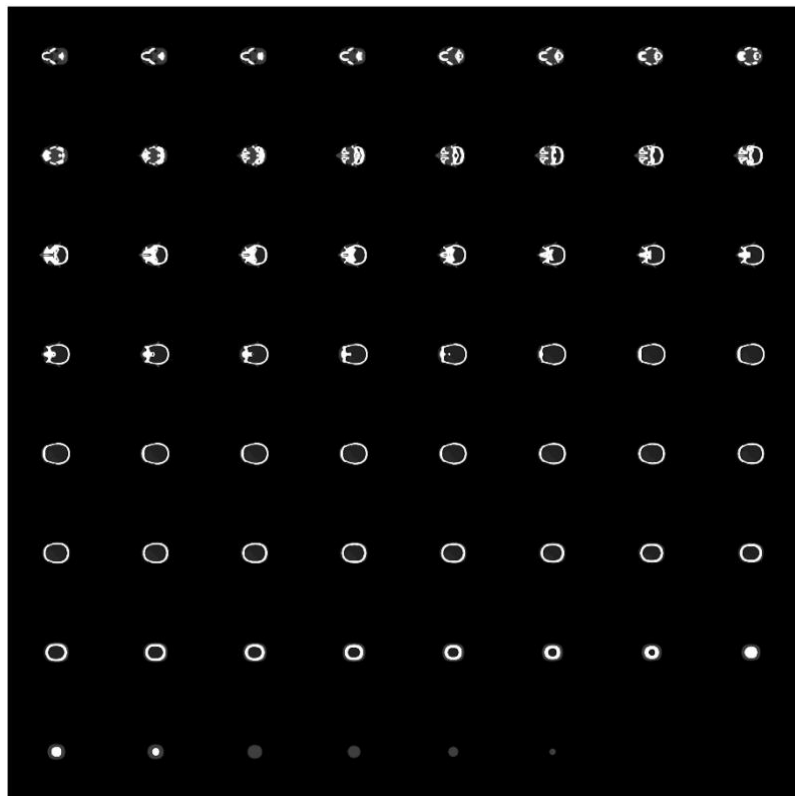


Figure 69 Assembly of the sequence of sections obtained by the binary file “mat_HU.bin”.

For the binary file “mat_ID.bin” has been applied the same procedure and in addition one gamma filter with $\gamma=3.5$ was applied, the reference MATLAB script is “ID_brain”.

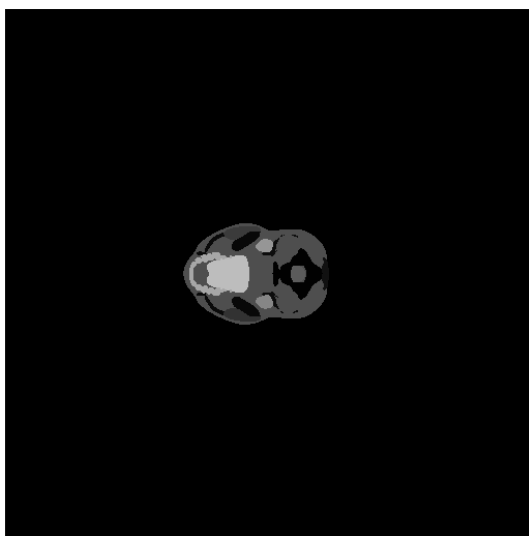


Figure 70 Section Iobtained by the binary file “mat_ID.bin” with gamma correction ($\gamma=3.5$).

Figure 70 is different from Figure 68 because the ID vector assign a cardinal number to each organ.

Subsequently the assembly of the sequence of sections obtained by the binary file “mat_ID.bin” was also performed.

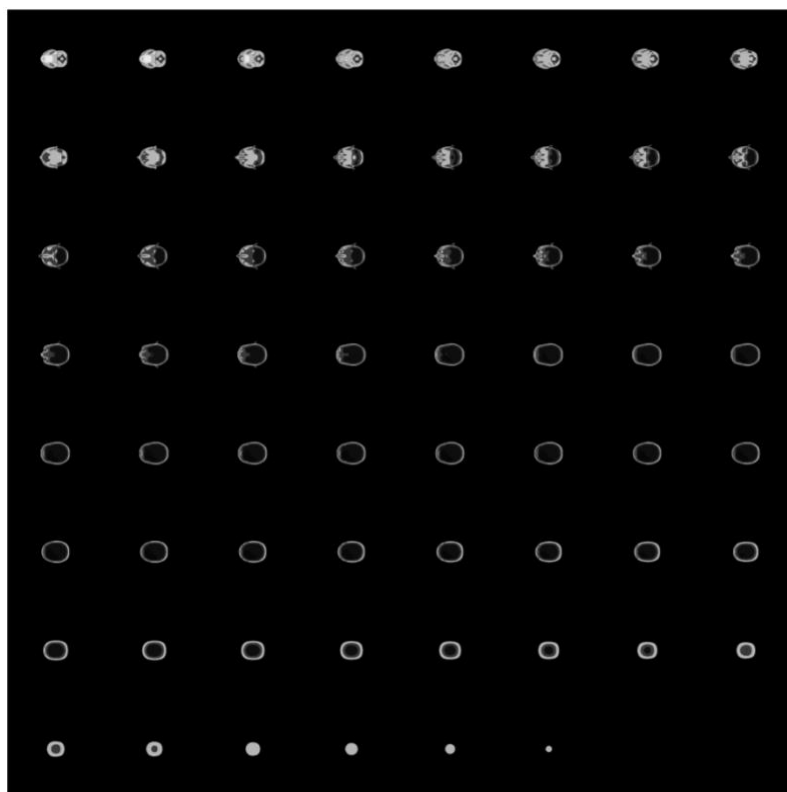
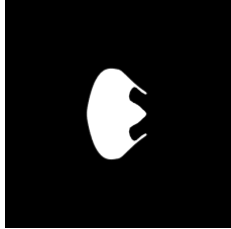


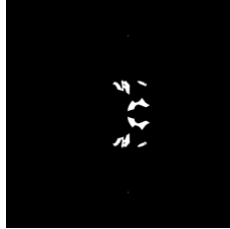
Figure 71 Assembly of the sequence of sections obtained by the binary file “mat_ID.bin”.

5.3.3 Case 2: Prostate

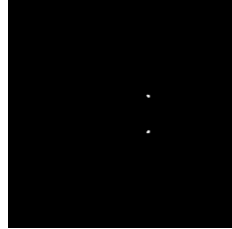
The frames generated are 83 and the organs involved in the last section, that is the 83th, are the following:



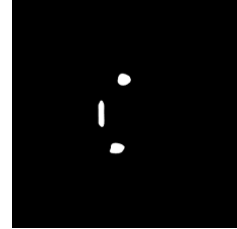
Adipose Abdominal



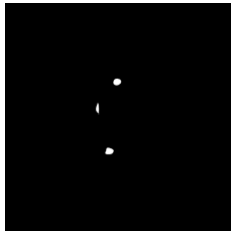
Blood



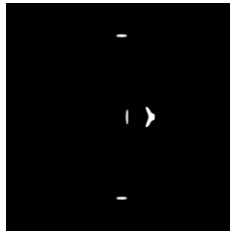
Cartilage Pelvis



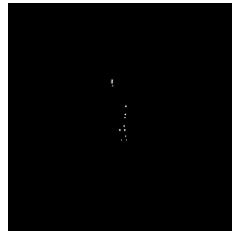
Colon Content



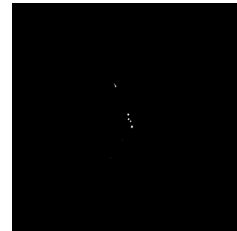
Colon



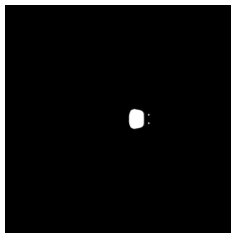
Connective Tissues



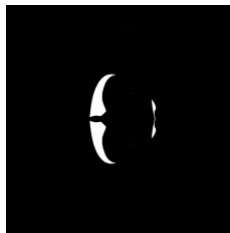
Linfa_02



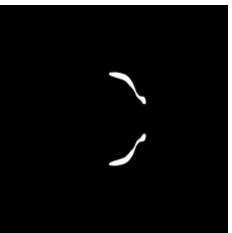
Linfa_03



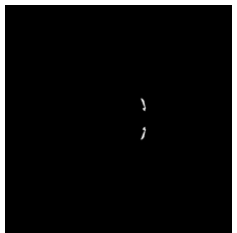
Lumbar Spine



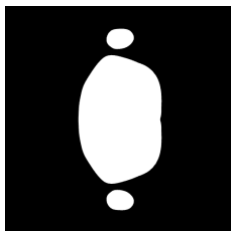
Muscles Torax



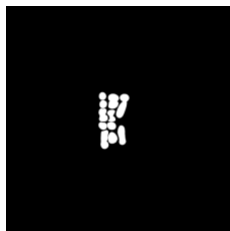
Pelvis



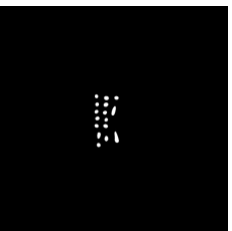
Sacrum



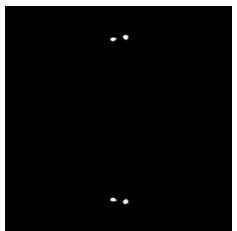
Skin



Small Intestine
Content



Small Intestine



Ulna Radius

The section obtained through the use of the MATLAB codes “*vol_conversion*” and “*compositing*” is:

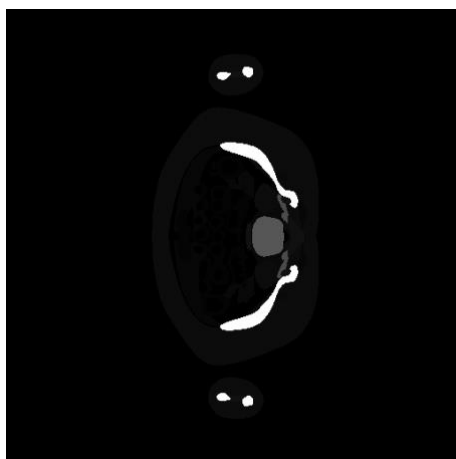


Figure 72 Case 2 "Prostate" - Section 83.

The Figure 72 hasn't a good contrast, for this reason it has been necessary to apply the *gamma correction*, in the script "*Filtro_gammalog_prostate*".

In this case γ has been assumed equal to 0.40 thanks to which is possible to obtain a good contrast.

In the following figure is possible to notice the difference between the original picture and the corrected one.

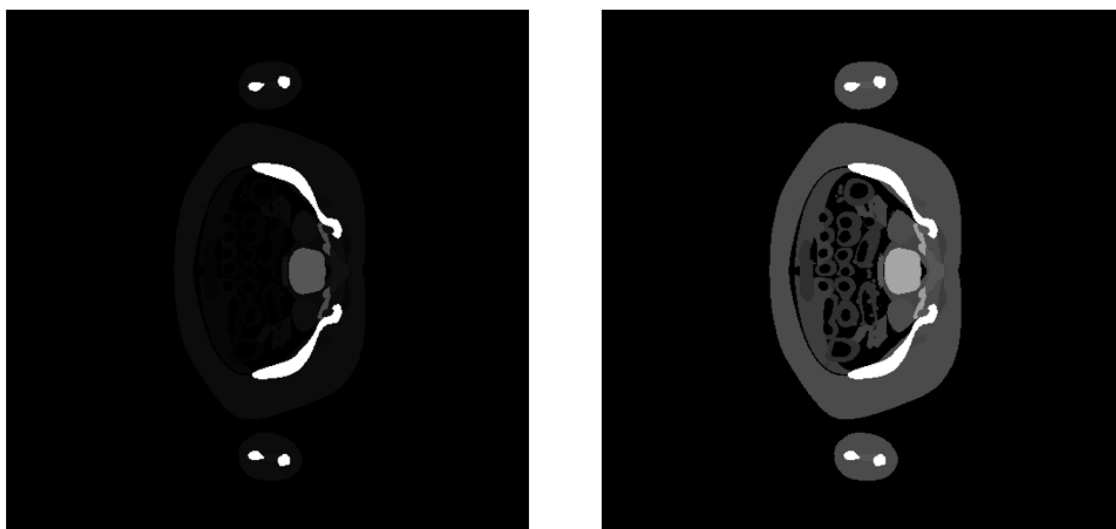


Figure 73 On the left the original section 83, on the right the gamma corrected section 83 ($\gamma=0.40$).

The previous procedure has been reiterated for each section.

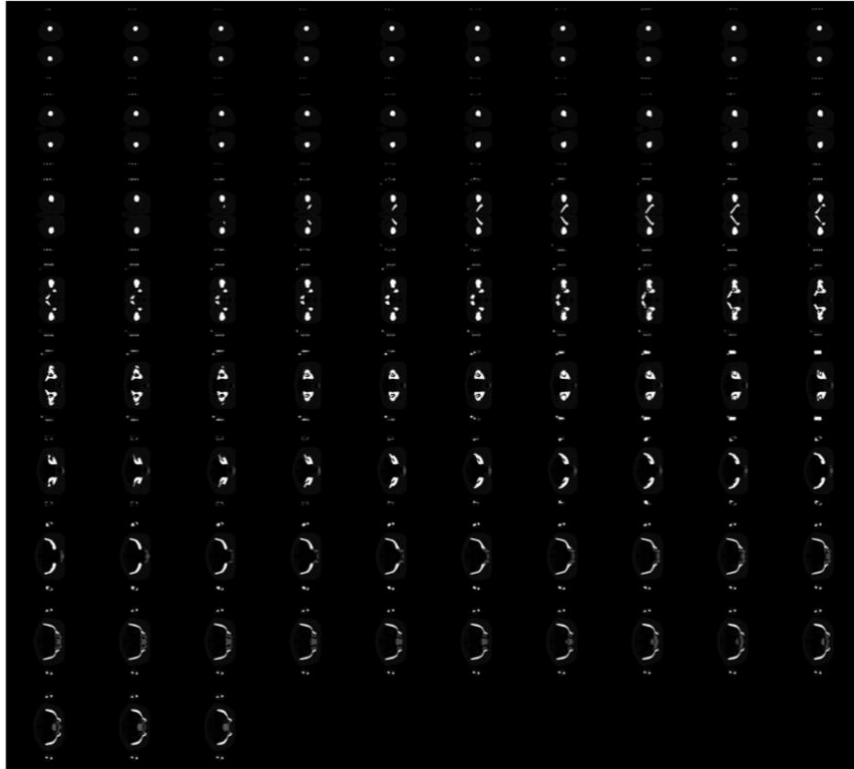


Figure 74 Assembly of original sections.



Figure 75 Assembly of gamma corrected sections ($\gamma=0.40$).

The following steps regards the processing of files in binary format “*mat_HU.bin*” and “*mat_ID.bin*”, obtained in “*compositing*” from 3D matrices.

In the MATLAB script “*HU_prostate*” it was first memorized the binary file “*mat_HU.bin*” in 83 2D matrices, each of which of the size 512 X 512. Among all the section has been chosen the last one to be in line with the previous example.

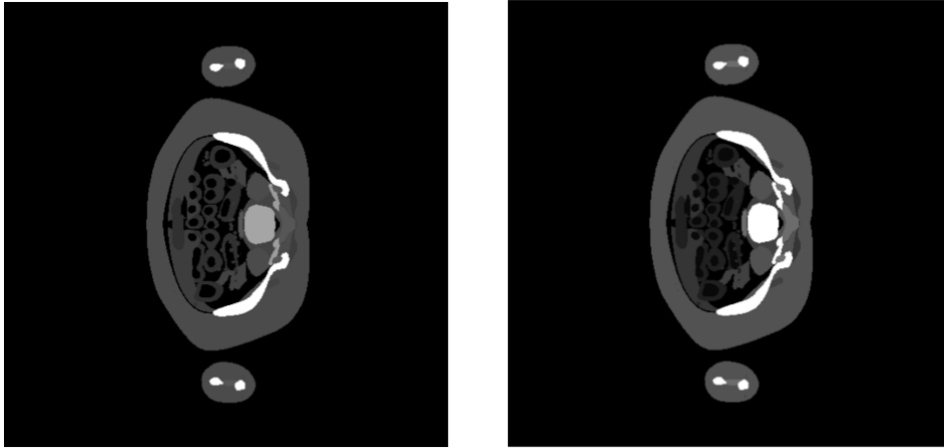


Figure 76 On the left the gamma corrected section 83 ($\gamma=0.40$), on the right the section 83 obtained by the binary file “*mat_HU.bin*”.

The assembly of the sequence of sections obtained by the binary file “*mat_HU.bin*” was also performed.

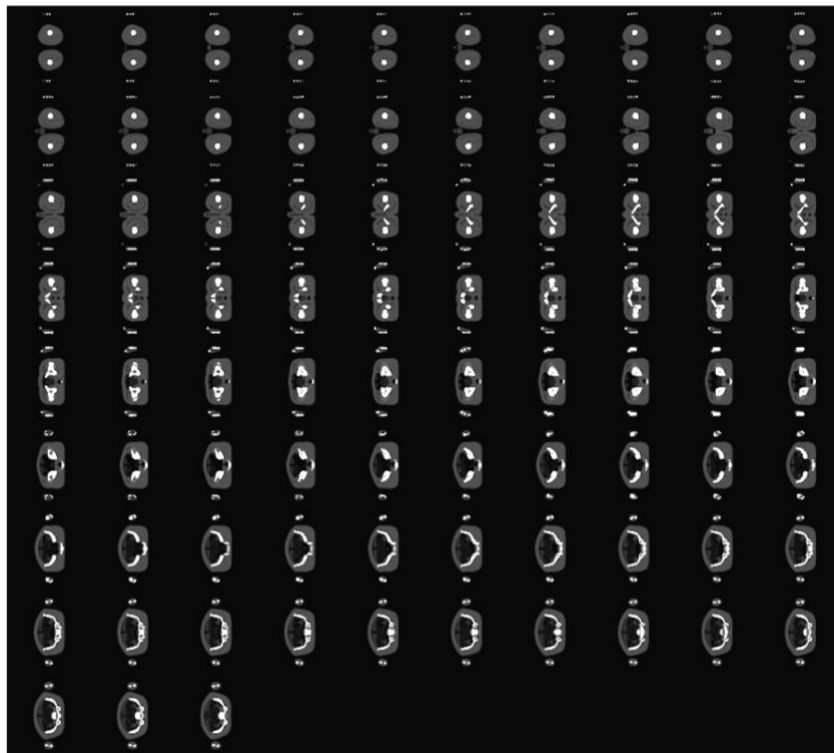


Figure 77 Assembly of the sequence of sections obtained by the binary file “*mat_HU.bin*”.

For the binary file “*mat_ID.bin*” has been scale the data by setting a minimum value, 0, and a maximum value, 50, the reference MATLAB script is “*ID_prostate*”.

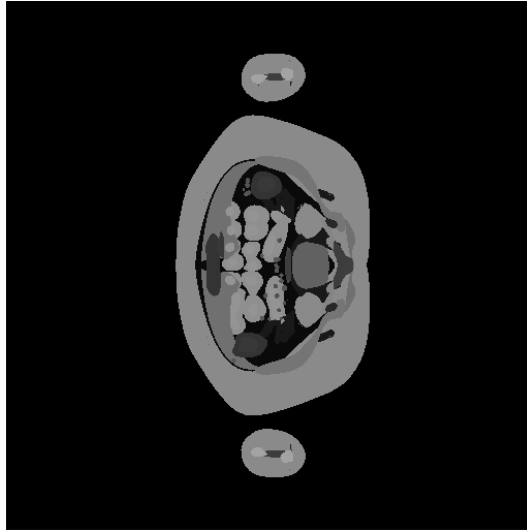


Figure 78 Section 83 obtained by the binary file “mat_ID.bin”.

Figure 70 is different from Figure 68 because the ID vector assign a cardinal number to each organ.

Subsequently the assembly of the sequence of sections obtained by the binary file “*mat_ID.bin*” was also performed.

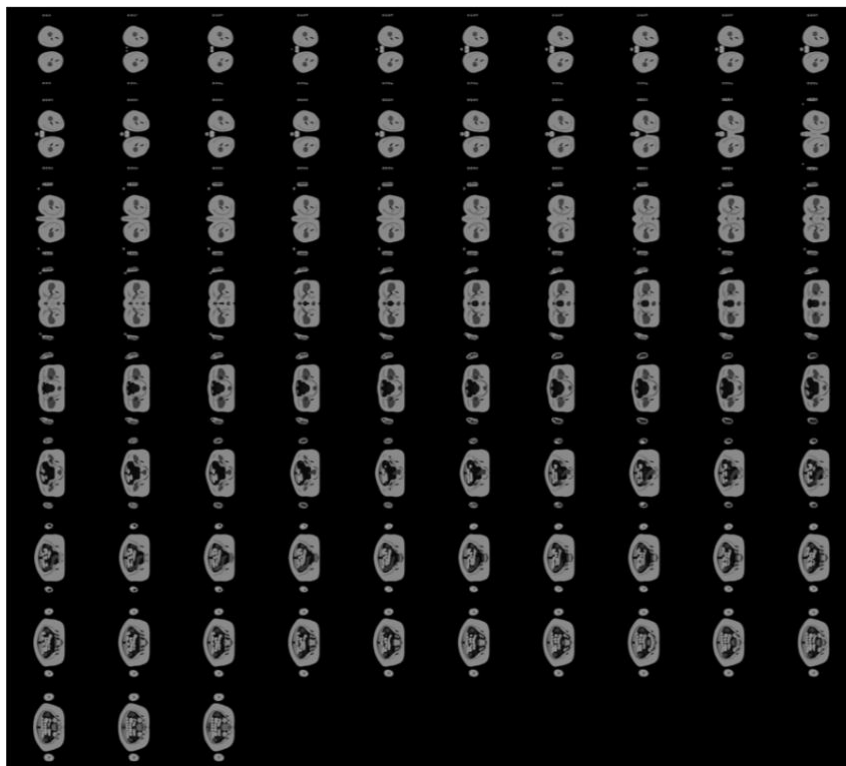
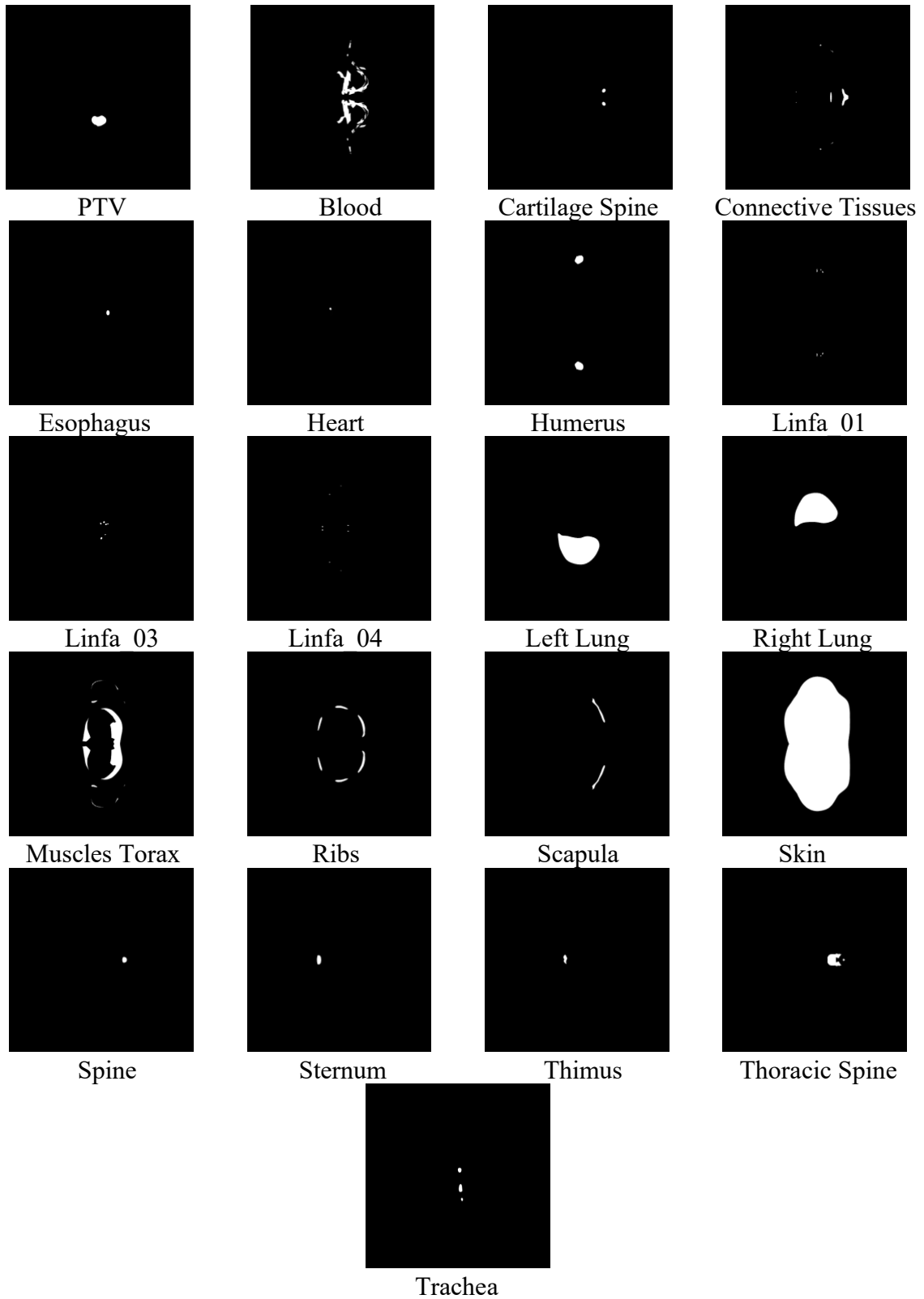


Figure 79 Assembly of the sequence of sections obtained by the binary file “mat_ID.bin”.

5.3.4 Case 3: Left Lung

The frames generated are 97 and the organs involved in the 54th section are the following:



The section obtained through the use of the MATLAB codes “*vol_conversion*” and “*compositing*” is:

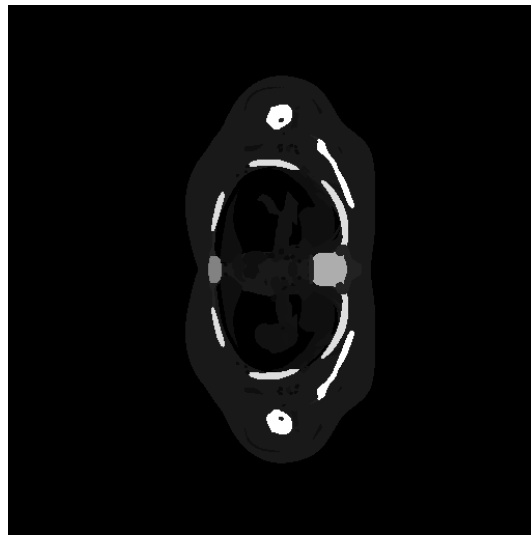


Figure 80 Case 3 "Left Lung" - Section 54.

The Figure 80 hasn't a good contrast, for this reason it has been necessary to apply the *gamma correction*, in the script “*Filtro_gammalog_left_lung*”.

In this case γ has been assumed equal to 0.50 thanks to which is possible to obtain a good contrast.

In the following figure is possible to notice the difference between the original picture and the corrected one.

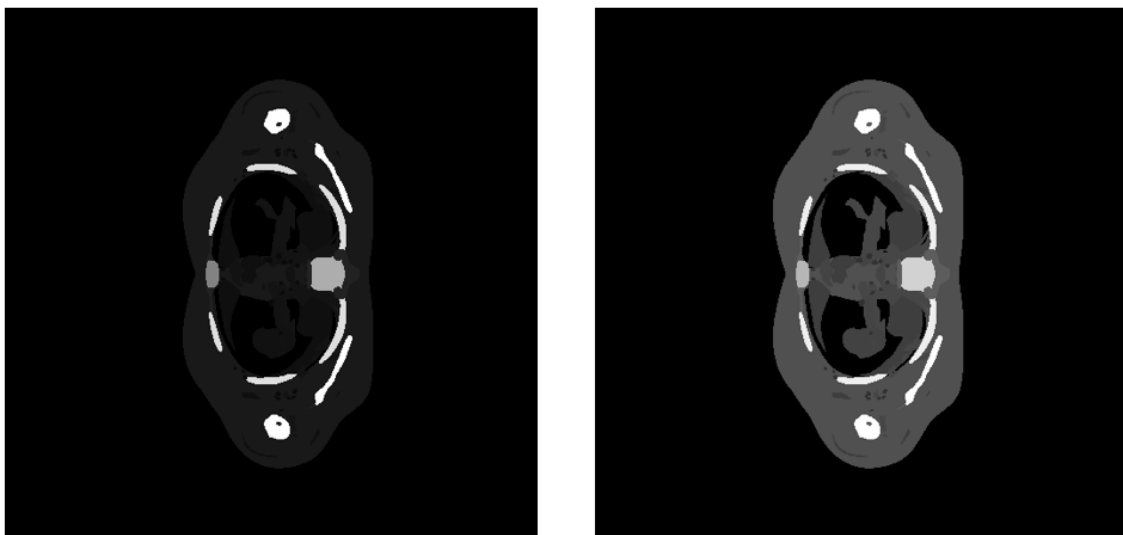


Figure 81 On the left the original section 54, on the right the gamma corrected section 54 ($\gamma=0.50$).

The previous procedure has been reiterated for each section.

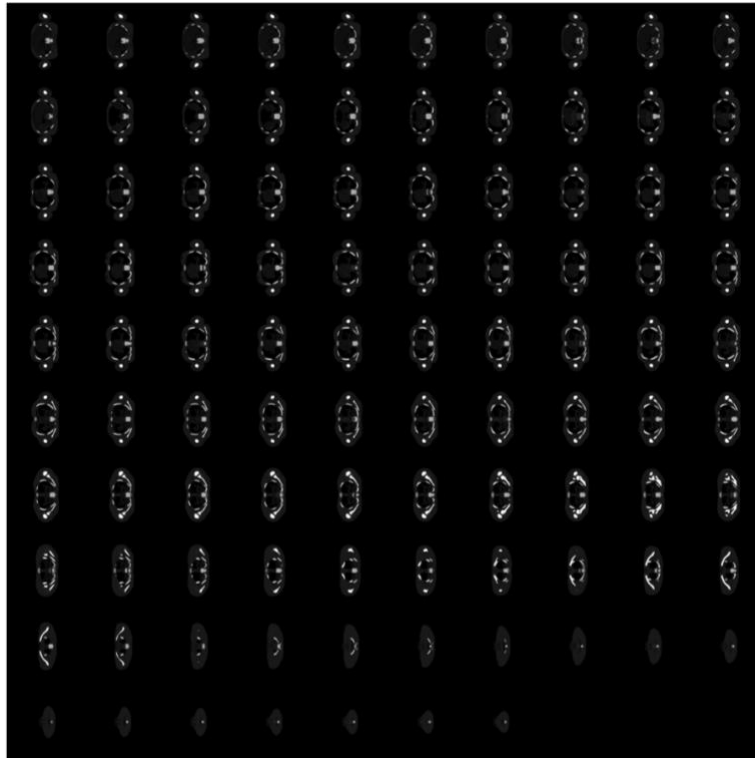


Figure 82 Assembly of original sections.

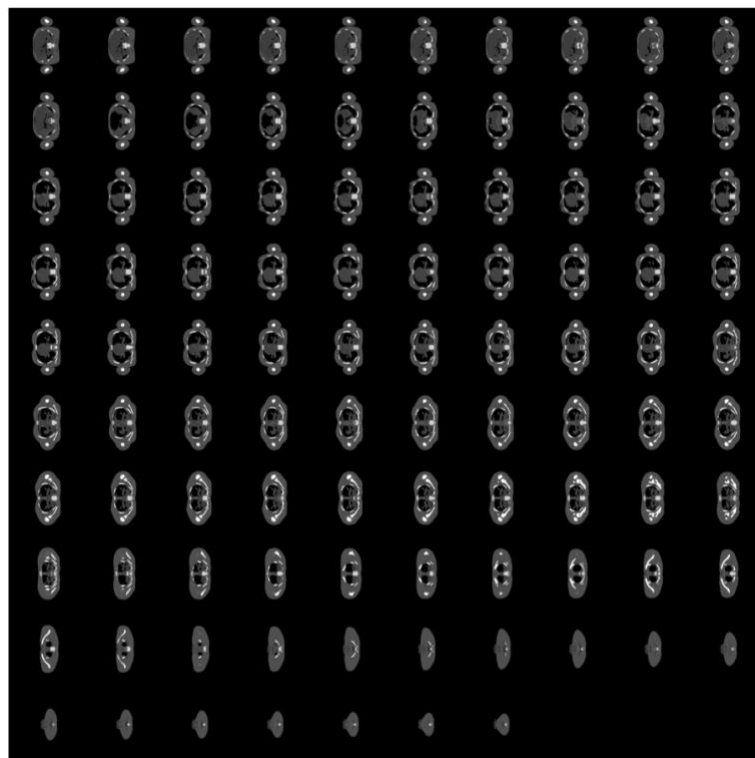
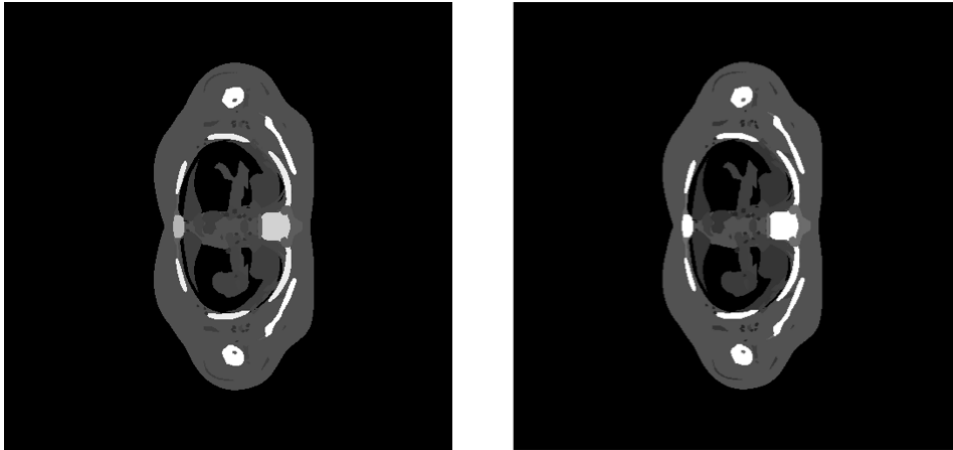


Figure 83 Assembly of gamma corrected sections ($\gamma=0.50$).

The following steps regards the processing of files in binary format “*mat_HU.bin*” and “*mat_ID.bin*”, obtained in “*compositing*” from 3D matrices.

In the MATLAB script “*HU_left_lung*” it was first memorized the binary file “*mat_HU.bin*” in 97 2D matrices, each of which of the size 512 X 512. Among all the section has been chosen the 54th to be in line with the previous example.



*Figure 84 On the left the gamma corrected section 54 ($\gamma=0.50$), on the right the section 54 obtained by the binary file “*mat_HU.bin*”.*

The assembly of the sequence of sections obtained by the binary file “*mat_HU.bin*” was also performed.

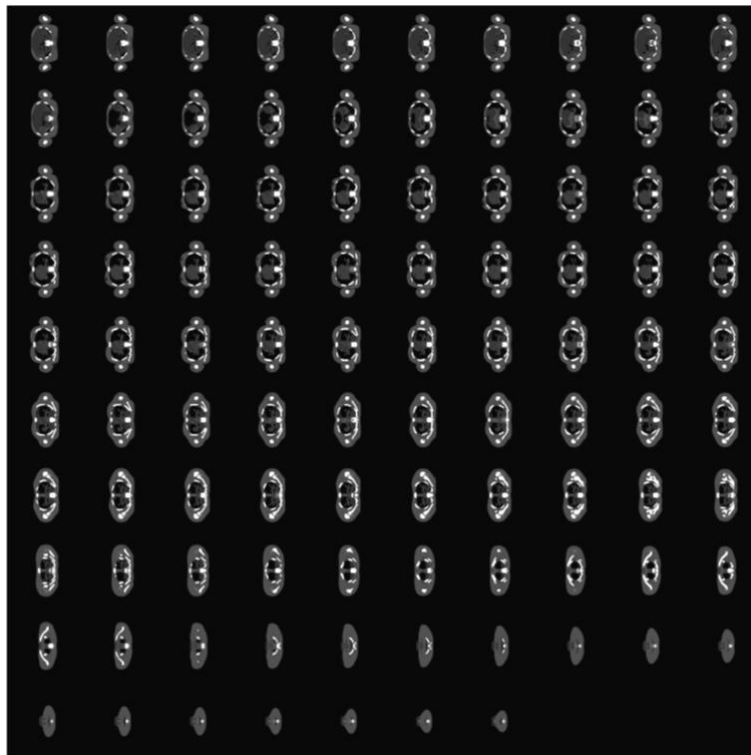


*Figure 85 Assembly of the sequence of sections obtained by the binary file “*mat_HU.bin*”.*

For the binary file “*mat_ID.bin*” has been scale the data by setting a minimum value, 0, and a maximum value, 70, the reference MATLAB script is “*ID_left_lung*”.

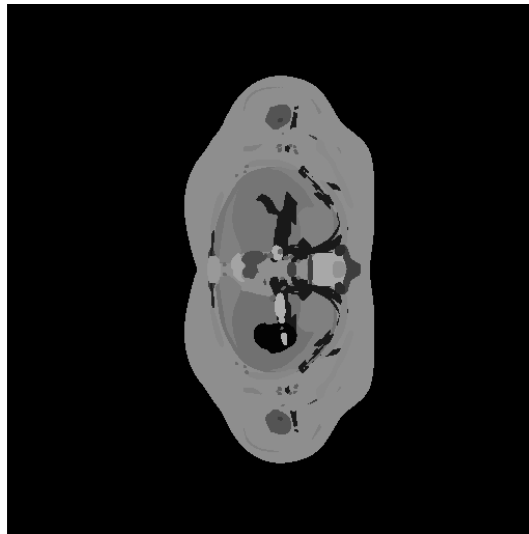


Figure 86 Section 54 obtained by the binary file “mat_ID.bin”.

Figure 86 is different from Figure 84 because the ID vector assign a cardinal number to each organ. Subsequently the assembly of the sequence of sections obtained by the binary file “*mat_ID.bin*” was also performed.

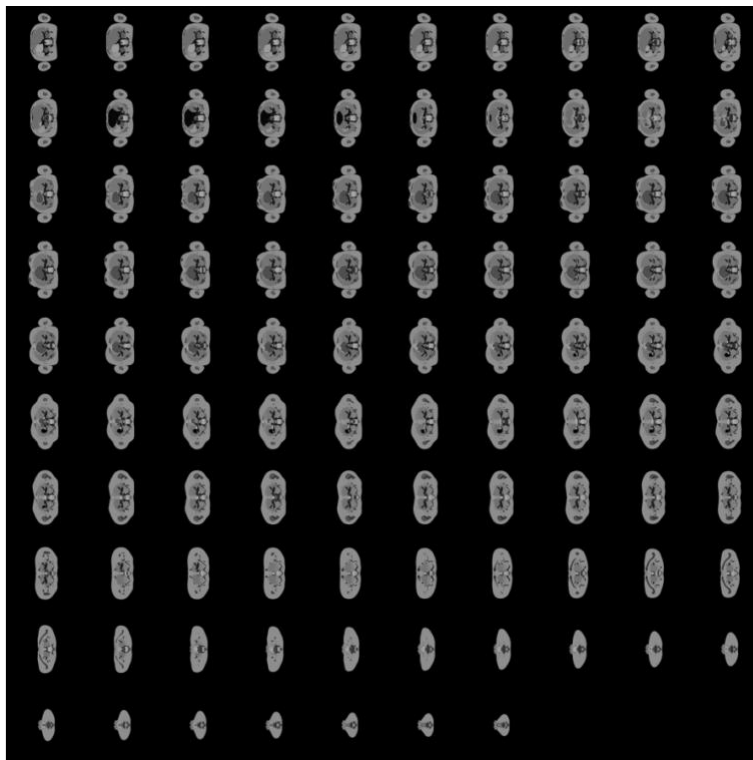


Figure 87 Assembly of the sequence of sections obtained by the binary file “mat_ID.bin”.

Chapter 6

Workflow VPatient

6.1 4SeePlan

The planning CT is first converted in DICOM and in second place exported in 4SeePlan, where the contouring, optimization and simulation are performed.

The VPatient is able to convert the .png images in DICOM using functions of the library of the *Image Processing Toolbox* MATLAB, like *dicomread*, *dicomwrite* and *dicominfo*.

4SeePlan is the Treatment Planning System conceived and programed by the *I-See*, whose aim is to simulate the deposition of protons' energy into the patient.

Through the intuitive GUI, Graphical User Interface, called ForToGo, is possible to use an analytical and a statistical approach to evaluate with high accuracy the delivered dose and to optimize it.

The software is stored on a local server and its interface is web based, so that the commands can be imparted easily through the web browser and also the results can be visualized on it.

The contouring process regards the surrounding of both the organs at risk and the target, it is a very important passage in TPS because a high precision in contouring allow to have a more realistic dose estimation, Figure 88.

The software is composed of 4 main modules, Figure 89:

- Image Registration, where the CT images with contoured OARs and target are visualized;
- Fast Optimization interface, where are shown the graphical and data output of FO;

- Montecarlo Simulation interface, where are plotted the profile depth of the dose in 3D and in 2D;
- Dose Engine interface, where are shown the graphical and data output of MC.

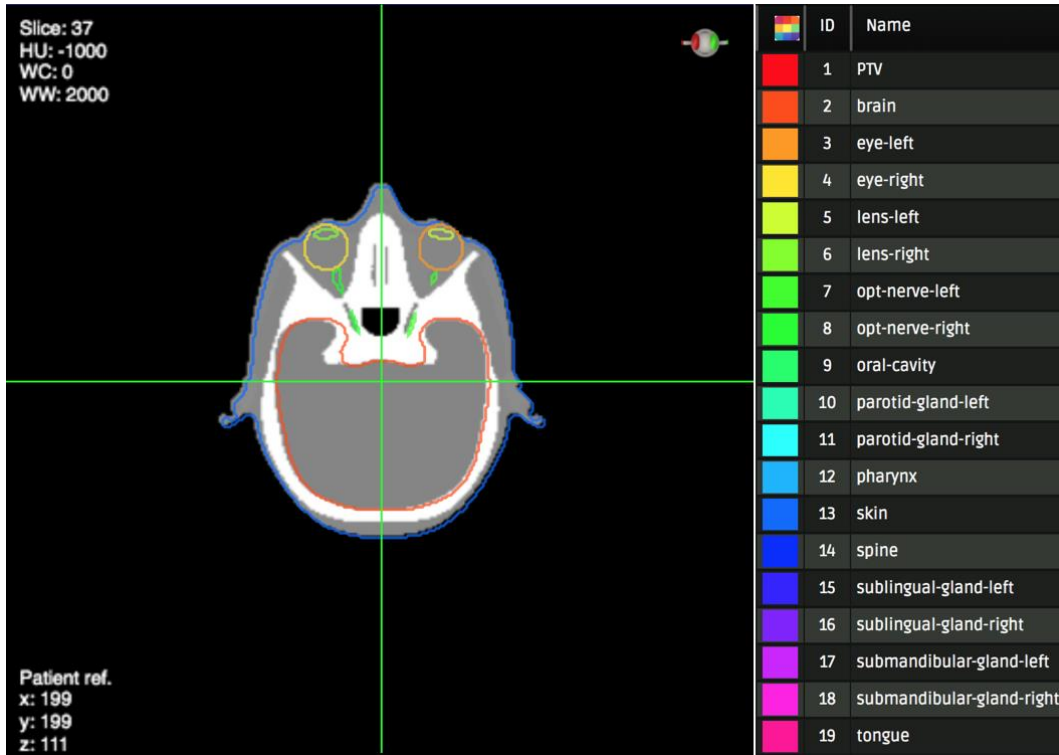


Figure 88 Contouring of OARs.

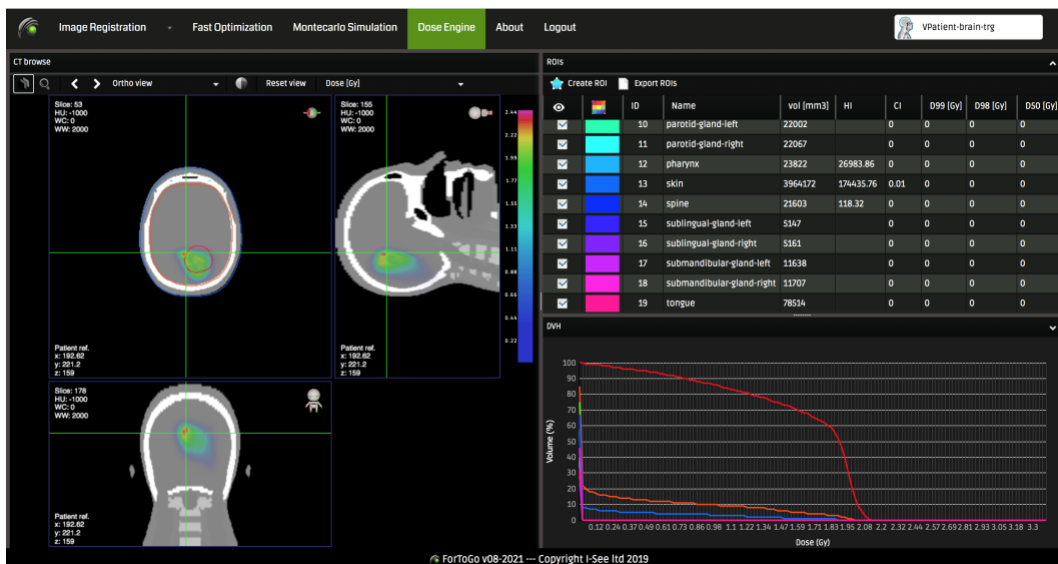


Figure 89 4SeePlan GUI.

The second part of this master thesis is based on the deepening of the treatment planning through a comparative analysis between Fast Optimization and Monte Carlo simulation and a study analysis on a new tumour treatment technique.

6.1.1 Comparative analysis between Fast Optimization and Monte Carlo simulation

Thanks to the testing version of 4SeePlan it has been possible to compare the Fast Optimization and the Monte Carlo simulation, through the treatment planning of a brain tumour located in the parietal lobe.

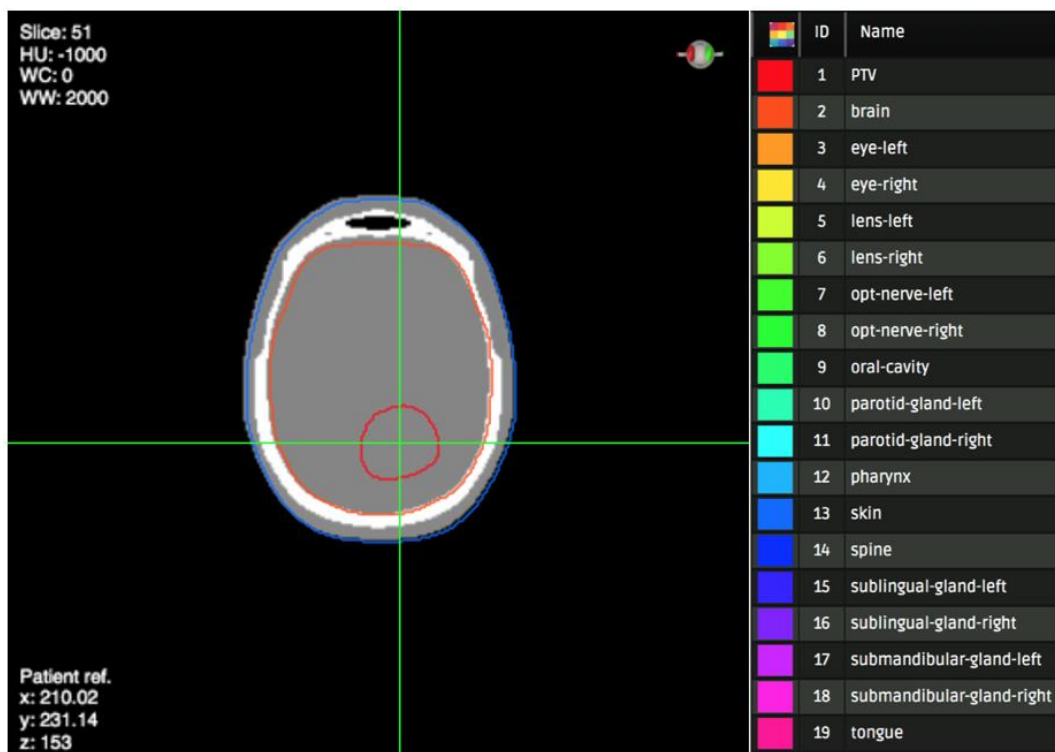


Figure 90 Contouring of Target 1.

The first step is to set the prescribed dose at 2 Gy and to define the best angle for the incident radiation. Fixing the direction of the couch at 0°, the choice fell on the standard orthogonal gantry $268.97^\circ \approx 270^\circ$ and the less usual gantry $168.92^\circ \approx 169^\circ$.

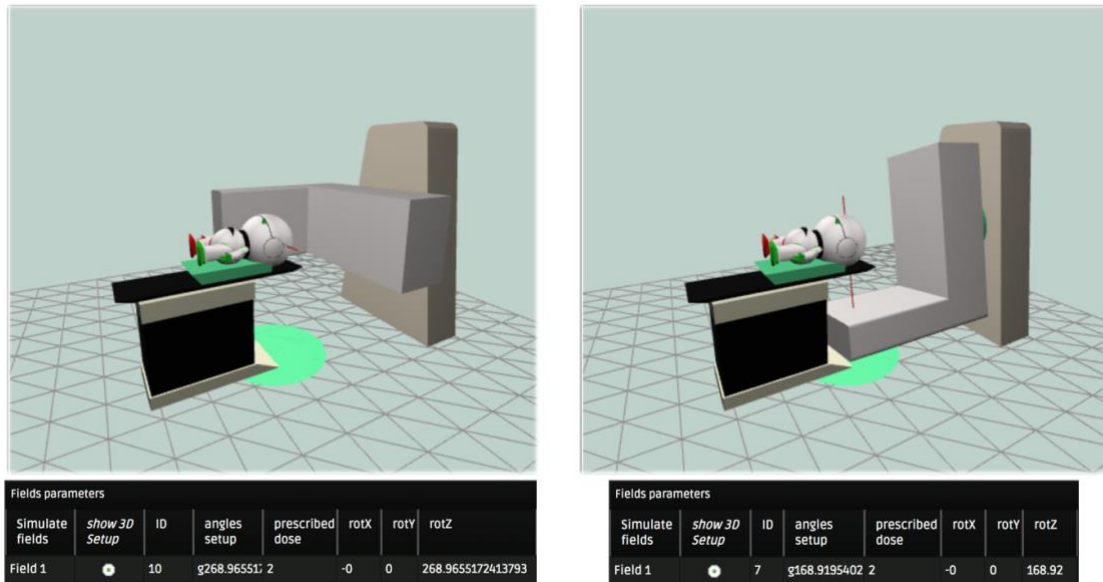


Figure 91 Angles setup.

The second step is the simulation of the treatment through the Fast Optimization and the Monte Carlo Method.

The output generated in both cases are the isodoses, the DVHs and the tables where are listed the values of the Homogeneity Index (HI), the Conformity Index (CI) and the quantity of dose received by the 99%, 98%, 50%, 2% and 1% of the volume for each ROI, Region Of Interest.

Isodose

In the following images are represented the isodoses in 2D sections from different point of view obtained thanks to Fast Optimization. As we can see the target results to absorb homogeneously the radiation in both cases of directions.

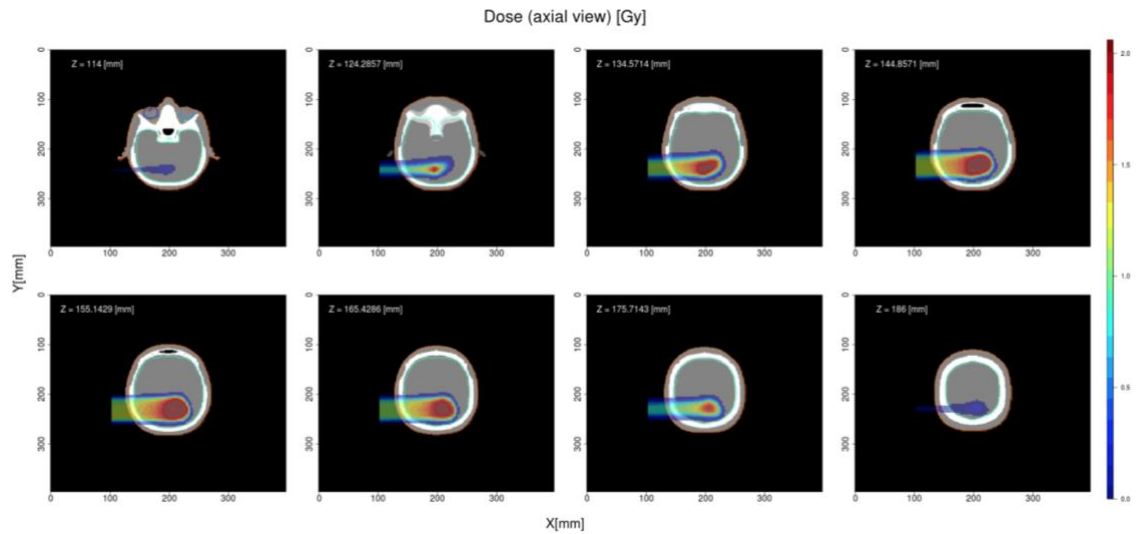


Figure 92 Axial view, gantry 270° , couch 0° .

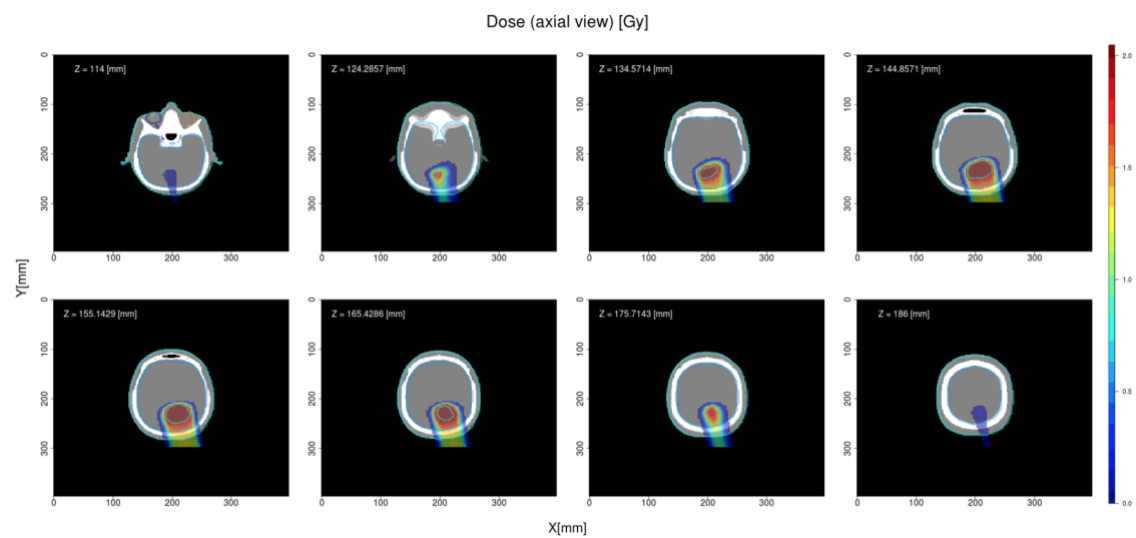


Figure 93 Axial view, gantry 169° , couch 0° .

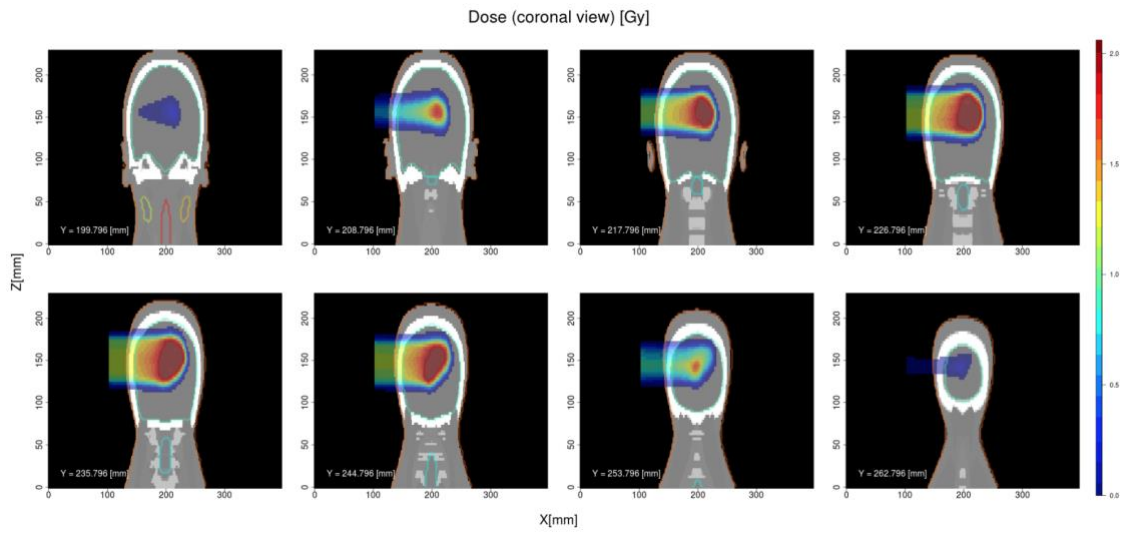


Figure 94 Coronal view, gantry 270° , couch 0° .

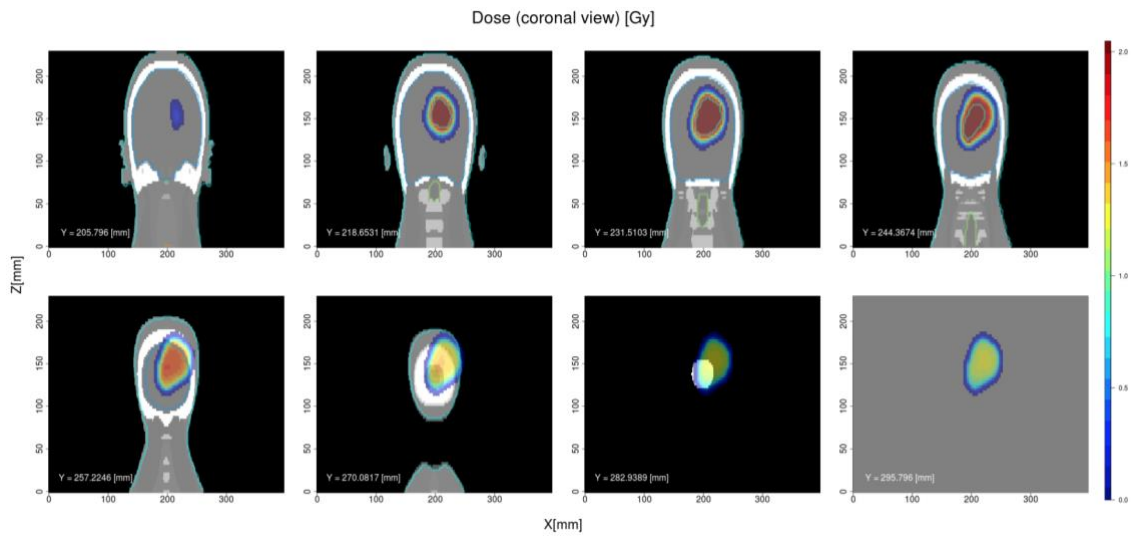


Figure 95 Coronal view, gantry 169° , couch 0° .

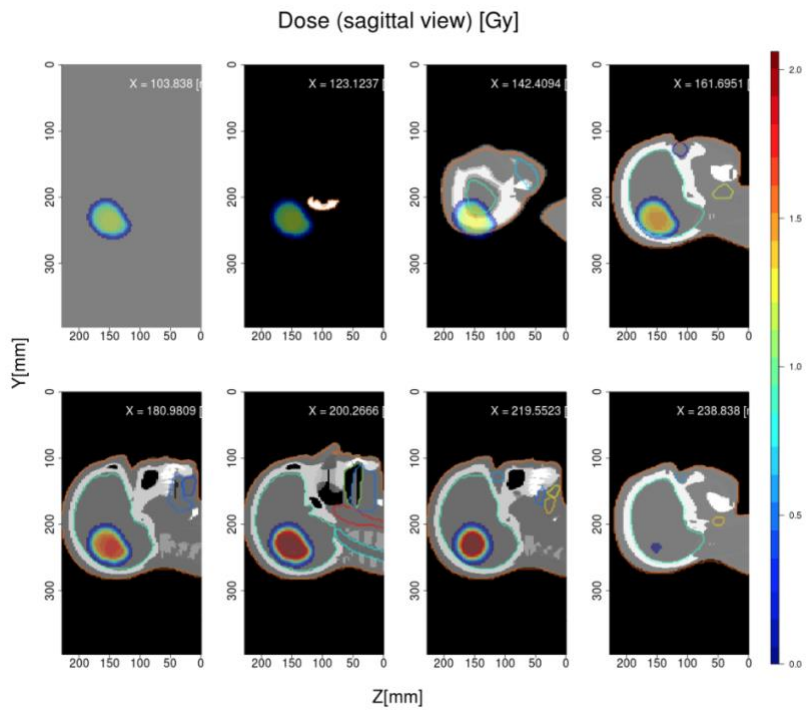


Figure 96 Sagittal view, gantry 270°, couch 0°.

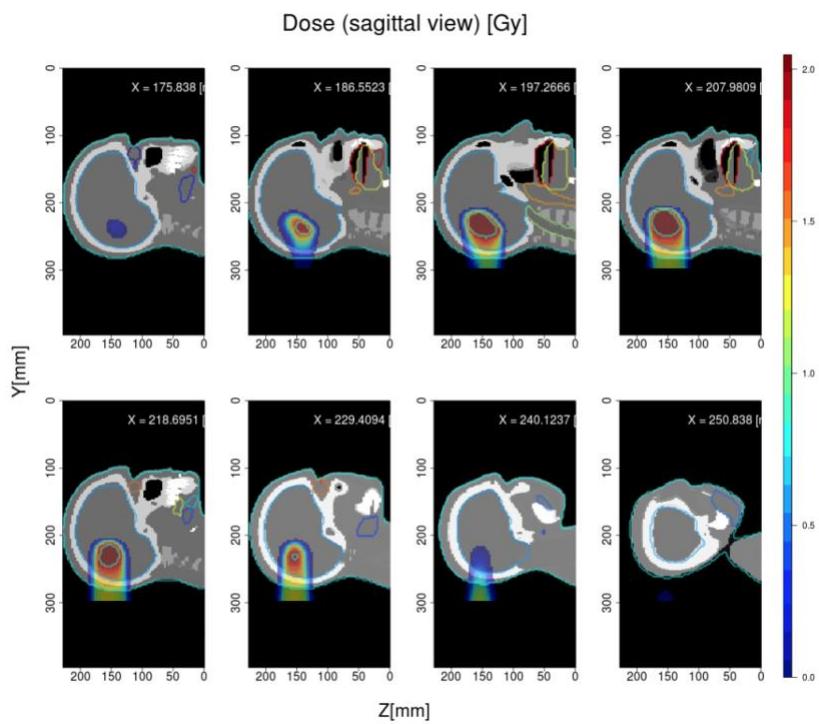


Figure 97 Sagittal view, gantry 169°, couch 0°.

The isodoses generated by the Monte Carlo simulation are different because they show visible discrepancies in the dose distribution, as we can see by the discontinuity of the red colour in the following images, due to the fact that MC takes into account the real densities of the organs.

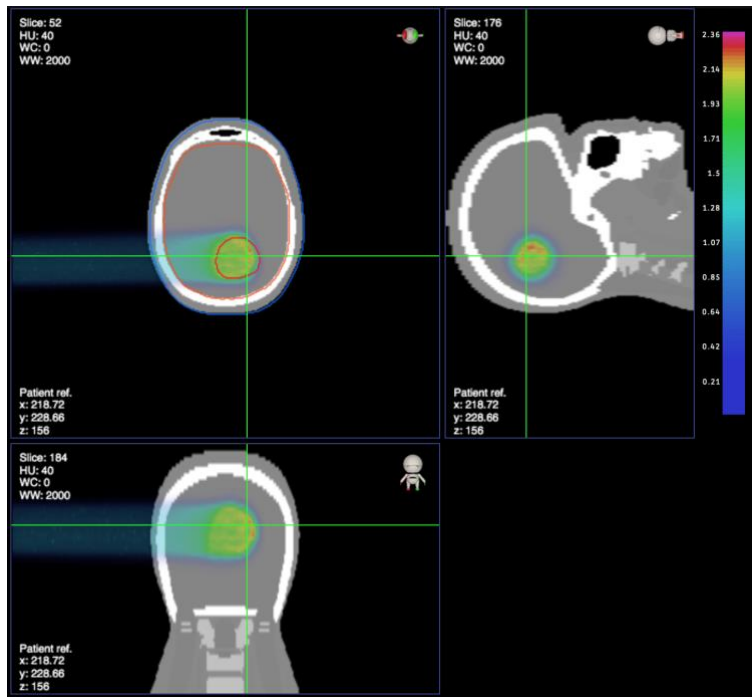


Figure 98 Ortho view, gantry 270°, couch 0°.

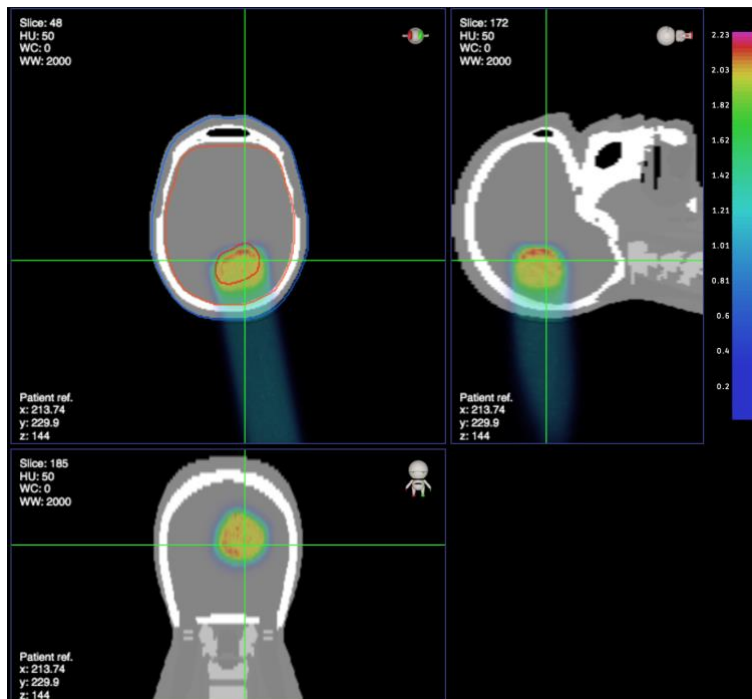


Figure 99 Ortho view, gantry 169°, couch 0°.

DVHs

The following DVHs are generated through MATLAB elaborating the .txt files obtained from 4SeePlan. Each DVHs is accompanied by a table containing the punctual values of the dose absorbed by the 99 %, 98 %, 50%, 2% and 1 % of the volume. Let's remember that the target ideal trend should be similar to a rectangle, while the OARs one should decrease rapidly to 0.

- Comparison between Fast Optimization and Monte Carlo Method results with the same orientation of the beam

1. Gantry 270°, couch 0°

Referring to the table, all the target values belonging to the Fast Optimization simulation results to be nearer to the ideal ones, as the D99, D98 and D50 are higher and D2 and D1 decrease faster to generate the rectangular shape.

For what regards the OAR, that in this specific case is the brain, it records values nearer to the ideal one in the Monte Carlo.

The “skin” in this case represents the “external contour”, that gives an idea of the irradiation impact all over the body. Also this component shows values nearer to the ideal one in the Monte Carlo method.

Gantry 270°, couch 0°					
	D99 [Gy]	D98 [Gy]	D50 [Gy]	D2 [Gy]	D1 [Gy]
Fast Optimization					
PTV	1.9476	1.957	1.9989	2.0394	2.0459
Brain	0	0	0	1.9916	2.0098
Skin	0	0	0	1.5415	1.9596
Monte Carlo Method					
PTV	0.91	1.1	1.97	2.14	2.18
Brain	0	0	0	1.97	2.01
Skin	0	0	0	1.49	1.91

Table 5 Punctual values of the dose absorbed by the 99%, 98%, 50%, 2% and 1% of the volume, for gantry 270°, couch 0°.

Obviously the punctual value can give only a partial view of the reality, for this reason the DVHs are analysed.

The comparison of the DVHs shows that the dose received by the percentage of volume of the target is nearer to the prescribed dose in the Fast Optimization case. This phenomenon verifies because, as said before, the MC takes into account the effective inhomogeneity of the tissues.

Differently the brain and external contour curves are lower and so nearer to the ideal trends in the Monte Carlo simulation.

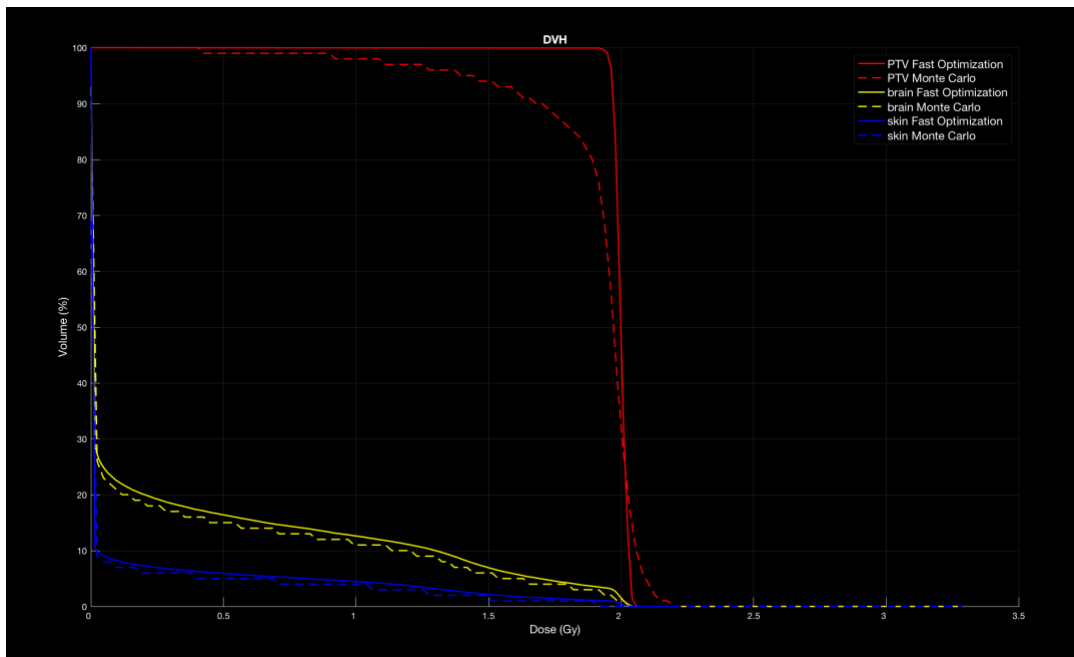


Figure 100 DVHs of PTV, brain and skin (external contour) obtained with Fast Optimization and Monte Carlo, for gantry 270°, couch 0°.

2. Gantry 169°, couch 0°

The comment regarding the gantry 169°, couch 0° are the same reported for the gantry 270 °, couch 0°.

Gantry 169°, couch 0°					
	D99 [Gy]	D98 [Gy]	D50 [Gy]	D2 [Gy]	D1 [Gy]
Fast Optimization					
PTV	1.9649	1.9678	1.9996	2.0294	2.0329
Brain	0	0	0	1.9939	2.0075
Skin	0	0	0	1.5167	1.965

Monte Carlo Method					
PTV	0.81	1.01	1.97	2.1	2.13
Brain	0	0	0	1.97	2
Skin	0	0	0	1.44	1.92

Table 6 Punctual values of the dose absorbed by the 99%, 98%, 50%, 2% and 1% of the volume, for gantry 169°, couch 0°.

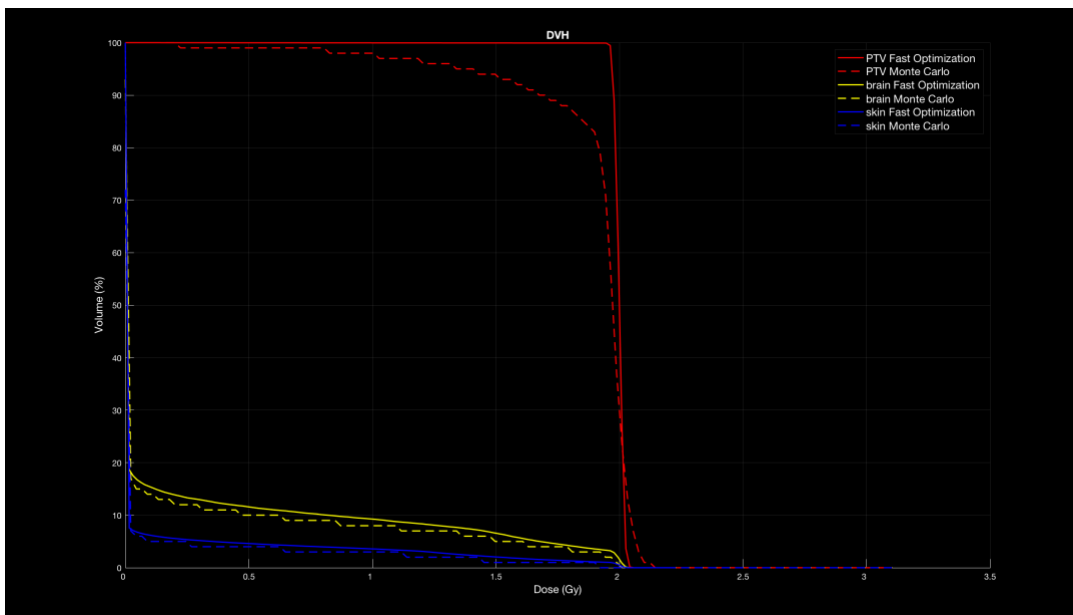


Figure 101 DVHs of PTV, brain and skin (external contour) obtained with Fast Optimization and Monte Carlo, for gantry 169°, couch 0°.

- Comparison between Fast Optimization results with gantry 270°, couch 0° and gantry 169°, couch 0°

Looking at the table, all the target values belonging to the gantry 169°, couch 0° results to be nearer to the ideal ones, as the D99, D98 and D50 are higher and D2 and D1 decrease faster.

For what regards the brain and the external contour, since we only own the D2 and D1 values, it is better to refer to the DVHs to define their trends.

Fast Optimization					
	D99 [Gy]	D98 [Gy]	D50 [Gy]	D2 [Gy]	D1 [Gy]
Gantry 270°, couch 0°					
PTV	1.9476	1.957	1.9989	2.0394	2.0459
Brain	0	0	0	1.9916	2.0098
Skin	0	0	0	1.5415	1.9596
Gantry 169°, couch 0°					
PTV	1.9649	1.9678	1.9996	2.0294	2.0329
Brain	0	0	0	1.9939	2.0075
Skin	0	0	0	1.5167	1.965

Table 7 Punctual values of the dose absorbed by the 99%, 98%, 50%, 2% and 1% of the volume, for gantry 270°, couch 0° and gantry 169°, couch 0° calculated with Fast Optimization.

The comparison of the DHV shows a curve of gantry 169°, couch 0° nearer to a rectangle and a lower curve for the brain and the skin. So both for the target and the OAR the results nearer to the prescribed one are obtained with gantry 169°, couch 0°.

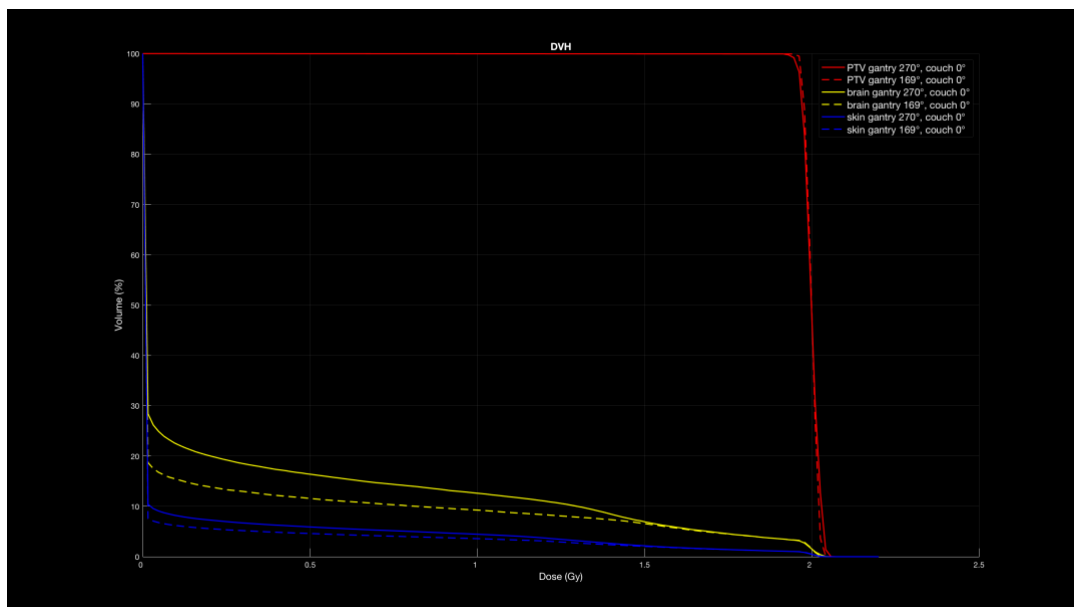


Figure 102 DVHs of PTV, brain and skin (external contour) obtained with Fast Optimization, for gantry 270°, couch 0° and gantry 169°, couch 0°.

- Comparison between Monte Carlo Method results with gantry 270°, couch 0° and gantry 169°, couch 0°

The data listed in the table show that in the initial phase of the target the gantry 270°, couch 0° has higher values and so nearer to the prescribed one. While in the final phase the values nearer to the ideal ones are those belonging to the gantry 169°, couch 0°, because they decrease faster.

For what regards the brain and the external contour, since we only own the D2 and D1 values also in this case, it is better to refer to the DVHs to define their trends.

Monte Carlo Method					
	D99 [Gy]	D98 [Gy]	D50 [Gy]	D2 [Gy]	D1 [Gy]
Gantry 270°, couch 0°					
PTV	0.91	1.1	1.97	2.14	2.18
Brain	0	0	0	1.97	2.01
Skin	0	0	0	1.49	1.91
Gantry 169°, couch 0°					
PTV	0.81	1.01	1.97	2.1	2.13
Brain	0	0	0	1.97	2
Skin	0	0	0	1.44	1.92

Table 8 Punctual values of the dose absorbed by the 99%, 98%, 50%, 2% and 1% of the volume, for gantry 270°, couch 0° and gantry 169°, couch 0° calculated with Monte Carlo method.

The comparison of the DVHs shows that the curve of gantry 169°, couch 0° relative to the target is nearer to a rectangle. This last statement denotes the fact that often the punctual values cannot define the totalitarian reality of the trend of the curve, for this reason the DVHs become of fundamental importance.

The curve relative to the external contour and the brain are lower and consequently nearer to the prescribed values in the case of gantry 169°, couch 0°.

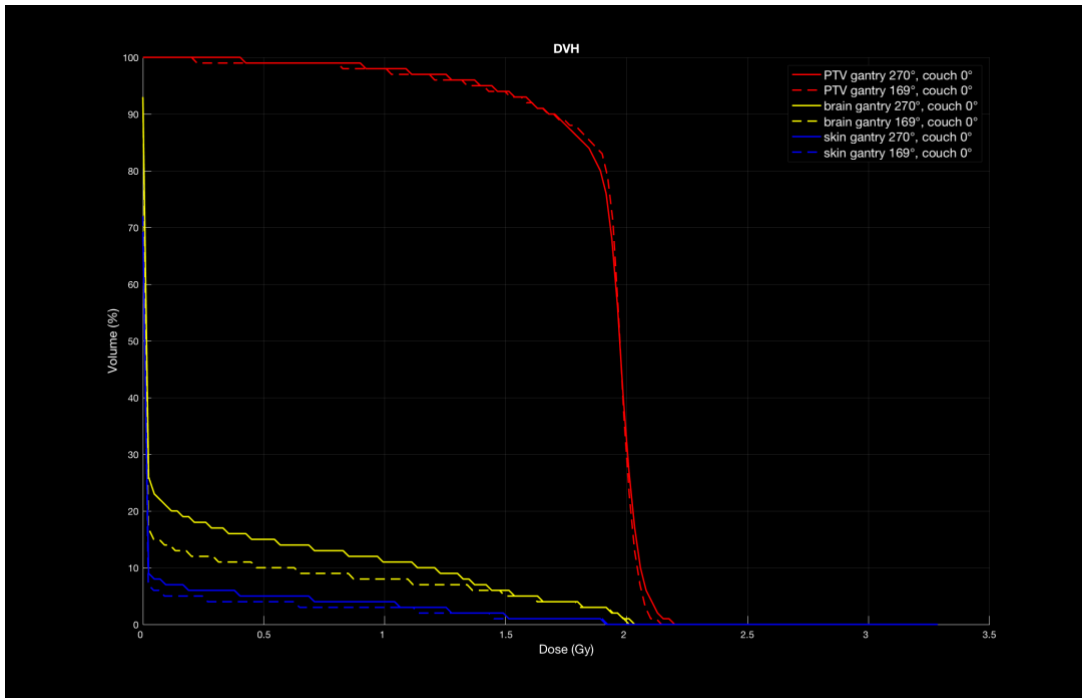


Figure 103 DVHs of PTV, brain and skin (external contour) obtained with Monte Carlo, for gantry 270°, couch 0° and gantry 169°, couch 0°.

Evaluation Indices

In the following table are listed the value of Homogeneity and Conformity Indices, that respectively allow to have an idea of the irradiation homogeneity of the tissues and of the real volume irradiated.

	Fast Optimization		Monte Carlo Method	
	HI	CI	HI	CI
Gantry 270°, couch 0°	0.0412	1	0.53	0.82
Gantry 169°, couch 0°	0.0308	1	0.55	0.84

Table 9 HI and CI for gantry 270°, couch 0° and gantry 169°, couch 0° calculated with Fast Optimization and Monte Carlo method.

- Comparison between Fast Optimization and Monte Carlo Method results with the same orientation of the beam
 1. Gantry 270°, couch 0°

For the Planned Target Volume, in the Fast Optimization the value of HI is nearer to the ideal value, 0, because the water phantom is homogenised for definition, instead in Monte Carlo Simulation the value of HI is higher but always in the allowed limit. The value of CI in Monte Carlo Case is under 0.9, while in Fast Optimization case the CI is equal to the ideal value, 1, this because in FO the volume irradiated is equal to the volume prescribed.

2. Gantry 169°, couch 0°

The comment regarding the gantry 169°, couch 0° are the same reported for the gantry 270 °, couch 0°.

- Comparison between Fast Optimization results with gantry 270°, couch 0° and gantry 169°, couch 0°

Being the CI value equal in both case, this comparison reveals that the gantry 169°, couch 0° has a HI value nearer to the prescribed one.

- Comparison between Monte Carlo Method results with gantry 270°, couch 0° and gantry 169°, couch 0°

In this case it's possible to notice that the HI value is nearer to the ideal 0 in the gantry 270°, couch 0° case, while the CI value is nearer to the ideal 1 in the gantry 169°, couch 0° case.

Comments

The tools provided by 4SeePlan allow to have a multi-perspective view of the treatment plan from which it is possible to evaluate the goodness of it.

First of all, isodoses give a visual perception of the treatment and give a chance to vary the direction of the beam choosing a better one.

Instead, the evaluation indices define the homogeneity of the treatment and the conformity of the treated volume respect to the prescribed one. and they give a first sight on the percentage of the volume irradiated.

The DVHs return a comprehensive idea of the results of the simulations giving both a numerical and a visual perspective of the quality of the treatment.

In this specific case the better direction of the treatment result to be gantry 169°, couch 0°.

Through this first case study has been possible to underline the differences between the Fast Optimization and the Monte Carlo method. This last one allow to optimize the TPS clearly obtaining results less near to the ideal values respect to Fast Optimization, because it takes into account the real densities of the organs.

6.1.2 Study analysis on a new tumour treatment technique

The aim of the engineer is to find new techniques able to increase the efficiency of the tumour treating. For this reason it has been chosen to analyse what would happen hitting the target from different angles.

In this second part of the study to better see the effects of the treatment it has been decided to position the target in the frontal area of the brain, nearer to sensible organs like eyes.

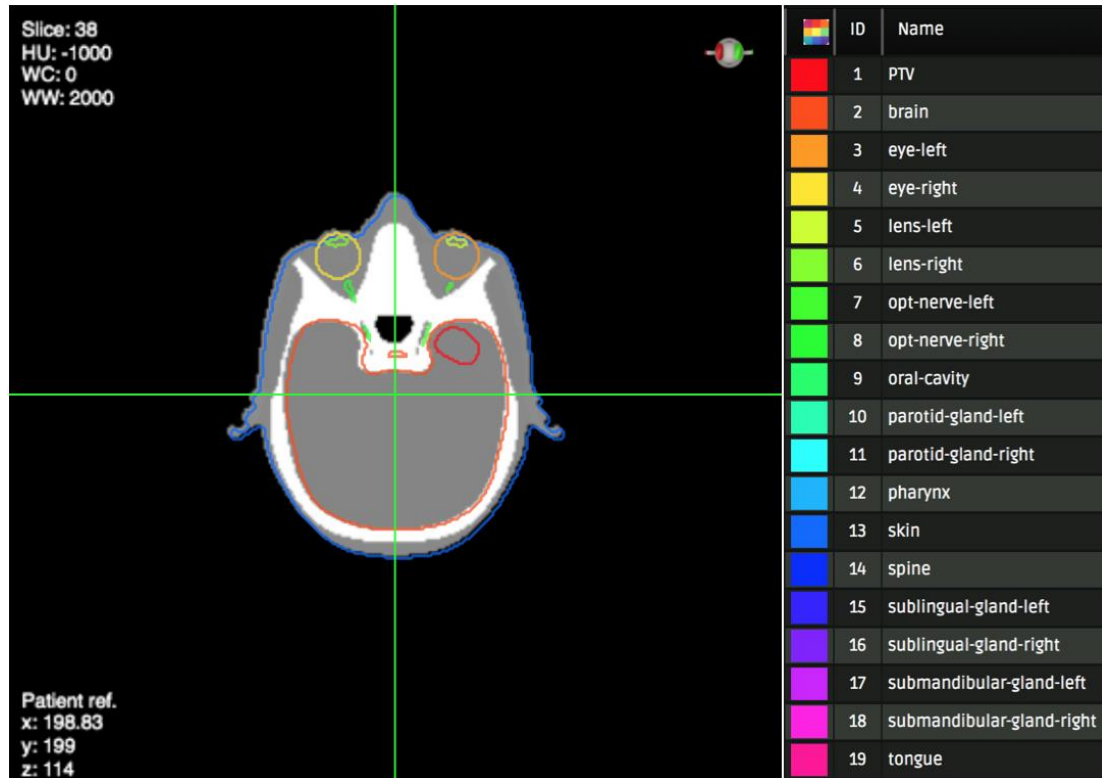


Figure 104 Contouring of Target 2.

The first step is defining the best angles for the incident radiation, the choice fell on the following ones:

- gantry $48.28^\circ \approx 48^\circ$, couch 0°
- gantry $68.87^\circ \approx 69^\circ$, couch 0°
- gantry $80.64^\circ \approx 81^\circ$, couch 0°
- gantry $124.78^\circ \approx 125^\circ$, couch 0°

The dose has been set at 1 Gy for each direction, for a total dose of 4 Gy.

Simulate fields	show 3D Setup	ID	angles setup	prescribe dose	rotX	rotY	rotZ
Field 1	<input checked="" type="radio"/>	26	g48.28c0	1	-0	0	48.28
Field 2	<input type="radio"/>	27	g68.87c0	1	-0	0	68.87
Field 3	<input type="radio"/>	28	g80.64c0	1	-0	0	80.64
Field 4	<input type="radio"/>	29	g124.78c0	1	-0	0	124.78

Figure 105 Fields parameters.

The second step is the simulation of the treatment through the Fast Optimization and the Monte Carlo Method.

The set of irradiation angles will be compared to a classical single irradiation angle, that in this case is the best one between the four defined previously, that is the gantry $124.78^\circ \approx 125^\circ$, couch 0° .

The data analysed in this section belong to the Monte Carlo simulation.

In the following images are represented the 3D Dose Deposition respectively for the 1 field and the 4 fields technique. From the comparison it can be deduced that the dose absorbed by each organs' particles result to be lower in the 4 fields technique. This concept permits to not overlap the dose limit established to preserve the OARs.

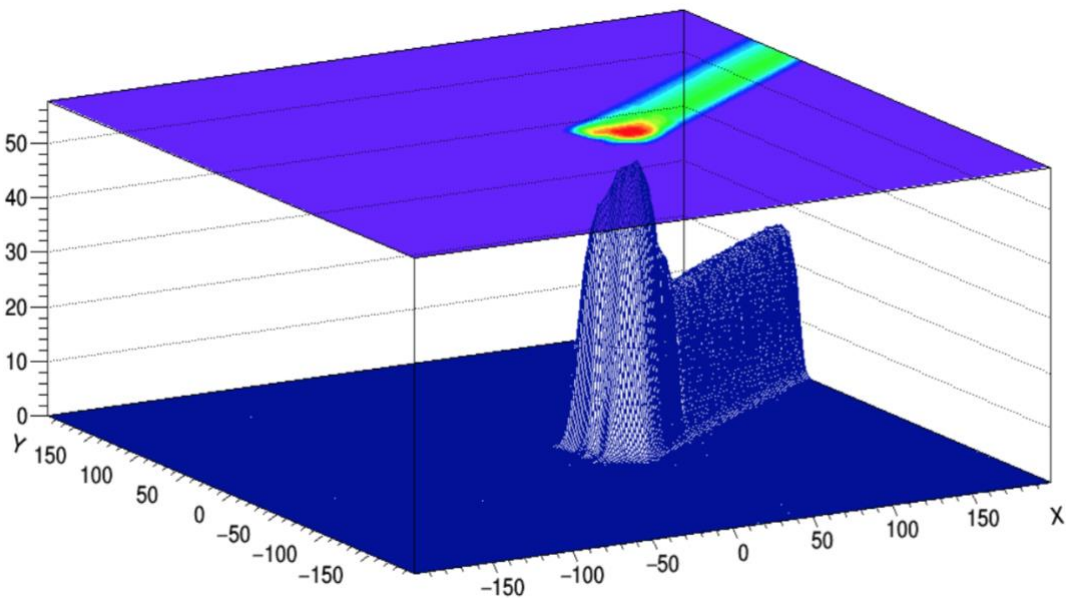


Figure 106 Dose Deposition All Fields yx projection for gantry 1 field technique.

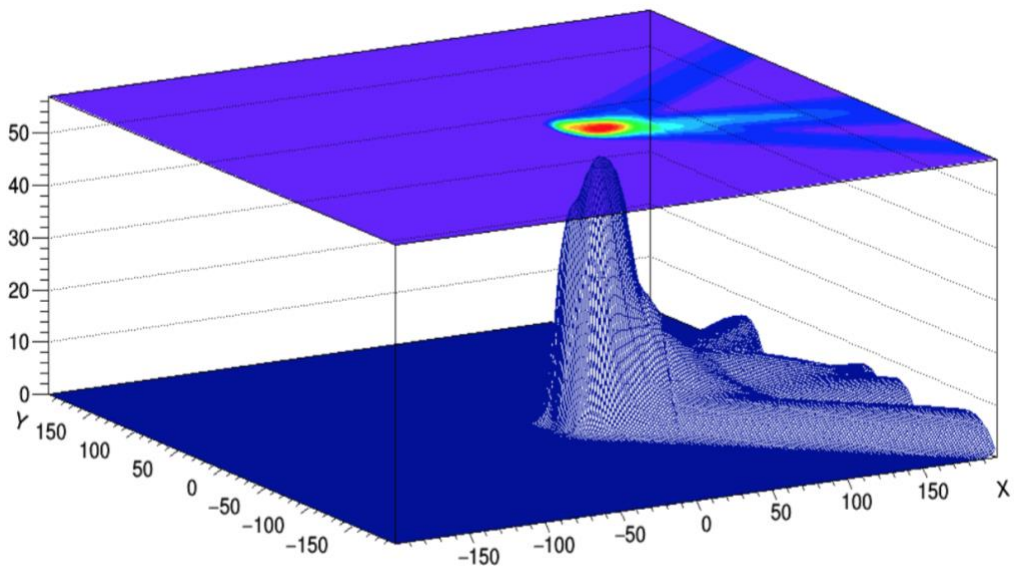


Figure 107 Dose Deposition All Fields yx projection for 4 fields technique.

Isodose

The same concept can be observed through the isodoses. In correspondence of the same slices $(x,y,z)=(224.93, 182.68, 123)$ at first sight seem that the pick of dose absorbed by the target is higher in the single angle irradiation case, while the dose absorbed by the other organs is lower in the four angles irradiation case.

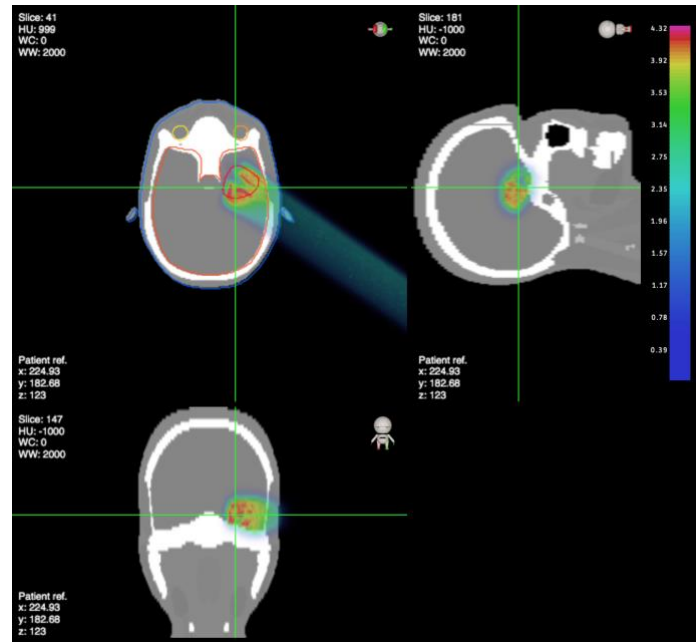


Figure 108 Ortho view, 1 field technique.

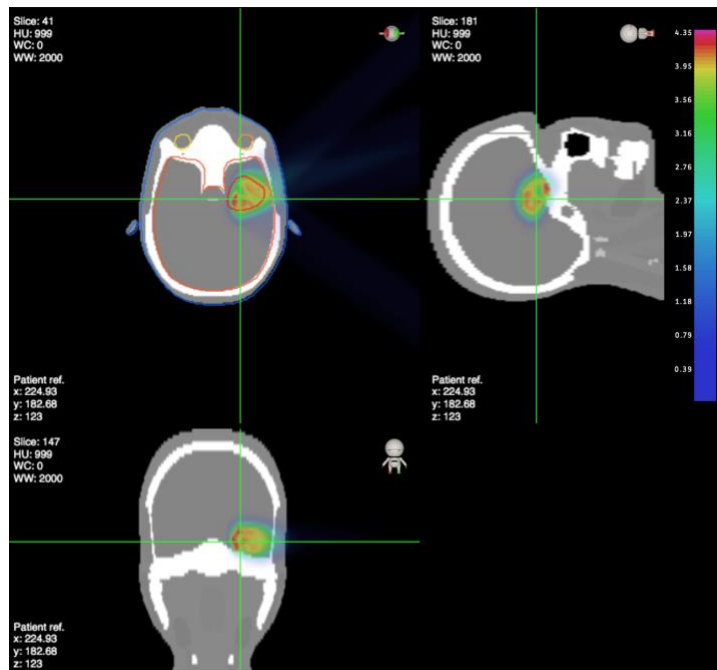


Figure 109 Ortho view of 4 fields technique.

DVHs

Thanks to the data generated by 4SeePlan and reported in the tables is possible to see that the target has a dose absorption nearer to the ideal one in the 4 fields case. In fact in this last case the PTV presents higher values for D99, D98 and D50, and lower values in D2 and D1, which means it goes down faster.

The OARs involved in these techniques are the brain, the left eye and the left optical nerve. All the organs register values nearer to the prescribed one with the 4 fields technique except for the left eye that presents a dose of the order of cents, because of the use of gantry 48°, couch 0°.

The skin, that also in this case represents the external contour, gives results nearer to the ideal one in the 4 fields case.

1 Field Technique					
	D99 [Gy]	D98 [Gy]	D50 [Gy]	D2 [Gy]	D1 [Gy]
Monte Carlo Method					
PTV	1.23	1.47	3.81	4.14	4.19
Brain	0	0	0	3.43	3.82
Eye-left	0	0	0	0	0
Opt-nerve-left	0	0	0.06	1.33	1.37
Skin	0	0	0	1.82	2.85

Table 10 Punctual values of the dose absorbed by the 99%, 98%, 50%, 2% and 1% of the volume, for 1 Field.

4 Fields Technique					
	D99 [Gy]	D98 [Gy]	D50 [Gy]	D2 [Gy]	D1 [Gy]
Monte Carlo Method					
PTV	1.77	2.05	3.84	4.13	4.18
Brain	0	0	0	3.27	3.81
Eye-left	0	0	0	0.03	0.05
Opt-nerve-left	0	0	0.05	0.46	0.47
Skin	0	0	0	1.13	2.36

Table 11 Punctual values of the dose absorbed by the 99%, 98%, 50%, 2% and 1% of the volume, for 4 Fields.

Thanks to the DVHs comparison is possible to see that using more than one fields gives better results, because the target behaviour is more similar to a rectangle and the dose deposited in the OARs is lower.

Let's remember that the optical nerve is a serial organ, that is an organ that if damaged in one point is damaged completely, clearly exist a dose limit to which it can be subjected. So, the more we can save it the more we improve the patient quality of life and through the 4 fields technique the improvement is substantial.

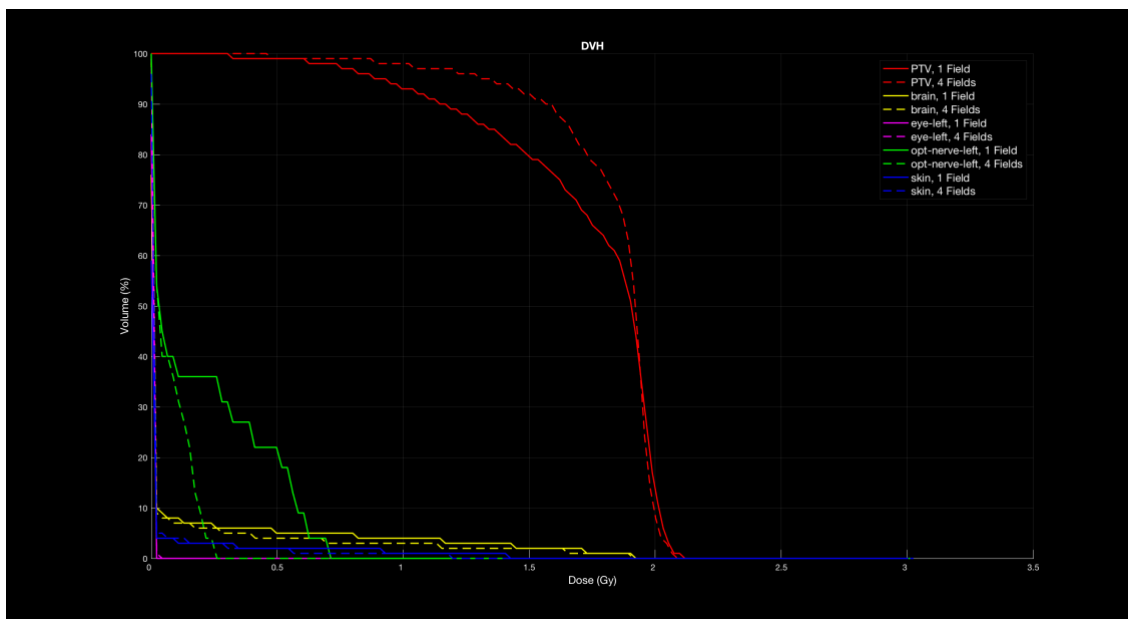


Figure 110 DVHs of PTV, brain, left eye, left optical nerve and skin (external contour) obtained with Monte Carlo, for 1 field and 4 fields.

Evaluation Indices

For what regards the evaluation indices, the target presents a lower value of HI in the 4 fields case, nearer to the ideal 0 value, obtaining a more homogeneously irradiated PTV. Instead the CI has a higher value, nearer to the ideal 1 value, that allow to have an irradiated zone more similar to the planned one.

	1 Field	4 Fields
HI PTV	0.7	0.54
CI PTV	0.56	0.66

Table 12 HI and CI for 1 Field and 4Fields.

Comments

The idea of involving more than one fields of irradiation takes its cue from the Arc Therapy, a very efficient technique belonging to radiotherapy which makes use of photons.

Thanks to the results obtained by the study effectuated in this master thesis is possible to assert that the use of more than one field to irradiate the tumour, in particular if it is posed near serial organs or more in general OARs, increases the efficiency of the treatment.

Therefore this could be a starting point to deepen this technique in the field of proton therapy.

Chapter 7

Conclusions

Radiotherapy is continuously developing new strategies to treat with high efficiency the tumour. The aim of the nuclear engineer in this field is to develop software able to simulate and optimize the treatment planning.

Thanks to the cooperation with the *I-See s. r. l.* has been possible to deepen the more technical aspects that hide behind the radiotherapy.

The company plays this role approaching the private world by providing an updated and highly efficient platform.

In this thesis all the fundamental steps related to radiotherapy simulation were retraced. The first part consists in the generation of CT images thanks to the use of the *VPatient 3D*, a virtual phantom created by the collaboration with the *National Institute of Nuclear Physics*. Generate virtual CT images is important because it allow not to refer to real CTs which, due to privacy, are very difficult to obtain. Moreover, the *VPatient 3D* gives the possibility to model the target with different shapes and to place it in different body positions.

The study effectuated regards the post processing of the compositing in terms of improvement of the grey contrast for images and of verification of the goodness of the binary matrices generated by Matlab scripts.

In the second part the simulation development of a normal treatment plan was undertaken through the platform provided by the *I-See* company, *4SeePlan*.

The treatment planning involves firstly the use of Fast Optimization and secondly of Monte Carlo method. The results generated by the *4SeePlan* are the isodoses, which give an optical view of the treatment, the plan evaluation indices, which numerically define the goodness of the plan, and the DVHs that outline in the clearest way the efficiency of the plan.

The comparisons effectuated in this section regards the utilisation of two gantry orientations, one more classical and another one more particular. The study effectuated on results obtained has shown that the best angle is the more particular one, that implies that the radiotherapy must work also from the most disparate directions to allow a higher efficiency of the treatment.

Against this, another radiotherapy technique was considered, the multiple field irradiation. It consists in irradiating the tumour through several directions of treatment, in our case has been studied the 4 fields case. The study effectuated has underlined the high efficiency of this new technique and its benefits, which consist in a greater irradiation of the tumour and a lower irradiation of the organs at risk.

In conclusion, nowadays radiotherapy has a fundamental role in the cancer treatment so it's important to study new techniques and to improve the efficiency of them. The *I-See* searches to do this work for medicine and to provide a software accessible to all, that allows to plan a radiotherapy treatment in the simplest and most intuitive way for the user.

Bibliography

- [1] H. Sung, J. Ferlay, R. L. Siegel, M. Laversanne, I. Soerjomataram, A. Jemal and F. Bray – “*Global Cancer Statistics 2020: GLOBOCAN Estimates of Incidence and Mortality Worldwide for 36 Cancers in 185 Countries*” – CA CAN J CLI 2021; Volume 71, 209-249
- [2] <https://www.dovecomemicuro.it/enciclopedia/benessere/radiazioni-ionizzanti-pericoli> visited on 19/05/2021
- [3] <https://www.amedeolucente.it/pdf/Radiazioni.pdf> visited on 19/05/2021
- [4] David S. Chang, Foster D. Lasley, Indra J. Das, Marc S. Mendonca, Joseph R. Dynlacht – “*Interactions of Electromagnetic Radiation with matter*” – Basic Radiotherapy Physics and Biology pp 35-41
- [5] F. A. Attix – slides “*Introduction to Radiological Physics and Radiation Dosimetry: Chapter 1*”
- [6] https://www.tes.com/lessons/h_TakkwoD7hepA/bremsstrahlung-production visited on 01/02/2021
- [7] <https://thoracickey.com/biological-basis-of-fractionation-and-timing-of-radiotherapy/> visited on 01/02/2021
- [8] R. F. Laitano – “*Fondamenti di dosimetria delle radiazioni ionizzanti*” – 4° Edizione, ENEA, 2015
- [9] http://www.fisica.uniud.it/~cobal/Lezione_IV_triESTE.pdf
- [10] Dott. Salzano Gianfranco – “*Elementi di radiobiologia, radioprotezione e controlli di qualità*” – Facoltà di scienze matematiche, fisiche e naturali, Università degli studi di Salerno
- [11] http://www-naweb.iaea.org/nahu/DMRP/documents/slides/Chapter_14_Basic_Radiobiology.pdf visited on 03/03/2021
- [12] “Effetti biologici delle radiazioni” – Ann. Ist. Super. Sanità – Vol. 23, N. 2 (1987), pp. 207-252
- [13] https://www.researchgate.net/figure/Figura-21-II-grafico-mostra-limportanza-relativa-delleffetto-fotoelettrico_fig1_282292390 visited on 20/05/2021
- [14] <http://www.upmcsanpietro.it/en/cellule-tumorali-vs-cellule-normali-qual-la-differenza/> visited on 03/03/2021
- [15] https://training.seer.cancer.gov/anatomy/cells_tissues_membranes/cells/structure.html visited on 03/03/2021
- [16] <https://www.scienceforpassion.com/2012/02/il-dna-e-il-ciclo-vitale-di-una-cellula.html> visited on 03/03/2021

- [17] <http://www.med.unipg.it/ccl/Materiale%20Didattico/Radioterapia/Radiobiologia.pdf> visited on 20/05/2021
- [18] Dr. Francesco di Rosa – “*Effetti Biologici delle Radiazioni*” – ASP Caltanissetta, Università degli studi di Palermo
- [19] <http://www.fisiokinesiterapia.biz/download/radiazionizz.pdf> visited on 21/05/2021
- [20] https://it.wikipedia.org/wiki/Storia_della_radioterapia visited on 21/05/2021
- [21] <https://www.airc.it/cancro/affronta-la-malattia/guida-alle-terapie/radioterapia> visited on 21/05/2021
- [22] Wonhee Hur, Seung Kew Yoon – “*Molecular Pathogenesis of radiation-Induced Cell Toxicity in Stem Cells*” – International Journal of Molecular Sciences 2017, 18, 2749
- [23] <http://fisica.unipv.it/eventi/Incontri-martedi/2017-12-12-Baiocco-Babini-slides.pdf> visited on 20/07/2020
- [24] <http://www.med.unipg.it/ccl/Materiale%20Didattico/Radioterapia/Radiobiologia.pdf> visited on 9/03/2021
- [25] Maiorino Carla – “*Studio degli effetti subletali indotti da radiazioni ad alto LET e diverso Z nell’ambito del progetto MiMo-BRAGG*” – Facoltà di Scienze Matematiche, Fisiche e Naturali – Università degli Studi di Napoli “Federico II”
- [26] Dirk Mussig – “*Re-scanning in scanned ion beam therapy in the presence of organ motion*” – 2014 Technische Universität Darmstadt
- [27] <https://informa.airicerca.org/it/2016/03/14/adroterapia-nuova-frontiera-radioterapia/> visited on 10/02/2020
- [28] Tesi di Valeria Rosso – “*Un sistema PET per il monitoraggio del trattamento in adroterapia: simulazione Monte Carlo e confronto con i dati sperimentali*” – 2013/2014 Corso di Laurea Magistrale in Fisica Medica, Università degli Studi di Pisa
- [29] Ahmedin Jemal, Lindsey Torre, Isabelle Soerjomataram, Freddie Bray – “*The Cancer Atlas*” – Third edition, American Cancer Society
- [30] <https://fondazionecao.it/news/quali-sono-patologie-trattabili-adroterapia> visited on 10/03/2021
- [31] <https://scienzapertutti.infn.it/6-adroterapia-in-italia> visited on 10/03/2021
- [32] Tesi di Riccardo Ridolfi – “*Adroterapia: principi e applicazioni*” – 2014/2015 Corso di Laurea in Fisica, Università di Bologna
- [33] https://it.wikipedia.org/wiki/Acceleratore_di_particelle#Storia visited on 21/05/2021
- [34] <https://bilimfili.com/hiperfizik/hbase/magnetic/cyclot.html> visited on 10/03/2021
- [35] <https://fondazionecao.it/adroterapia/sincrotrone> visited on 21/07/2020
- [36] <https://cnx.org/contents/dP0ocxV9@11.19:p3nizZII@9/Particle-Accelerators-and-Detectors> visited on 10/03/2020
- [37] Tesi di Martina Sequenza - “*Progettazione di un sistema di schermatura per un acceleratore lineare a protoni per adroterapia*” – 2012/2013 Tesi di Laurea in Ingegneria Biomedica, Università degli Studi di Roma La Sapienza
- [38] <http://www.frascati.enea.it/accelerators/Repository/TOP-IMPLART/TOP-PDF/CAP5enea.pdf> visited on 10/03/2021

- [39] https://indico.cern.ch/event/697187/contributions/2866410/attachments/1616714/2569745/2018OMAworkshopPSI_EO.pdf visited on 10/03/2021
- [40] <https://fondazionecnao.it/adroterapia/sale-di-trattamento> visited on 10/03/2021
- [41] “Definition of target volumes and organs at risk” – IAEA-
https://humanhealth.iaea.org/HHW/RadiationOncology/Treatingpatients/Treatment_planning_and_techniques/Training_Course/12_Defining_target_volumes_and_organs_at_risk.pdf
- [42] <https://protonterapia.provincia.tn.it/Per-i-pazienti/Come-funziona-il-trattamento> visited on 22/04/2021
- [43] <https://www.psi.ch/en/protontherapy> visited on 22/04/2021
- [44] “Corso di Diagnostica per Immagini” – Facoltà di Medicina e Chirurgia -
<http://unina.stidue.net/Diagnostica%20e%20Radioterapia/raggi%20x.pdf>
- [45] https://www.researchgate.net/figure/Schematics-of-a-conventional-X-ray-tube-the-electrons-e-are-emitted-from-the_fig1_327816840 visited on 26/04/2021
- [46] Michael Overdick – “*Detectors for X-Ray imaging and computed tomography*” – Advances and Key Technologies, Philips Research, Aachen, Germany
- [47] https://www.ge.infn.it/~squarcia/DIDATTICA/FM2/10_Radiografia.pdf visited on 26/04/2021
- [48] E. Shefer, A. Altman, R. Behling, R. Goshen, L. Gregorian, Y. Roterman, I. Uman, N. Wainer, Y. Yagil, O. Zarchin – “*State of the Art of CT Detectors and Sources: A Literature Review*” – Advances in CT Imaging (NJ PELC, SECTION EDITOR) – 1 February 2013
- [49] Vikki Harmonay – “*It’s All About CT Detectors*” – Atlantis Worldwide, Sensible Solutions for Refurbished Radiology, 2 December 2020
- [50] <https://www.affidea.it/le-prestazioni/diagnostica-per-immagini/tac-tomografia-computerizzata/> visited on 26/04/2021
- [51] <https://www.youtube.com/watch?v=EUz8zBuq64g> visited on 26/04/2021
- [52] <https://www.airc.it/cancro/affronta-la-malattia/guida-agli-esami/tc-tomografia-computerizzata> visited on 19/05/2021
- [53] K-H. Chang, W. Lee, D-M. Choo, C-S. Lee, Y. Kim – “*Dose reduction in CT using Bismuth shielding: Measurements and Monte Carlo simulations*” – Radiation Protection Dosimetry (2010), Vol. 138, No. 4, pp. 382-388
- [54] Shu-Ang Zhou, Anders Brahme – “*Development of phase-contrast X-ray imaging techniques and potential medical applications*” – Physica Medica (2008) 24, 129-148, Science Direct
- [55] W. Schneider, T. Bortfeld and W. Schlegel – “*Correlation between CT numbers and tissue parameters needed for Monte Carlo simulations of clinical dose distributions*” – Phy. Med. Biol. 45 (2000) 459-478
- [56] Mattia Cretoni - “*Radiopharmaceuticals diffusion inside human body and problem modelling*” - Tesi magistrale in Ingegneria Energetica e Nucleare – Politecnico di Torino 2018 – 2019
- [57] https://it.wikipedia.org/wiki/Tomografia_computerizzata visited on 26/04/2021

- [58] <https://line.17qq.com/articles/shshhwwky.html> visited on 26/04/2021
- [59] Scannicchio - “*Fisica biomedica*” – EdiSES 2013, Cap. 28 “*Strumentazione biomedica*”
- [60] Marco Serafini – “*Dosi in TC multislice con tecniche di modulazione automatica della corrente*” – Servizio Sanitario Regionale Emilia Romagna, Azienda Unità Sanitaria Locale di Modena, Unità Operativa Fisica Sanitaria
- [61] Professor Gianni Coppa – “*Biomedical and industrial applications of radiation*” – Politecnico di Torino, 2019/2020
- [62] Prof. J. Hornak - “*The Basics of MRP*” - University of Rochester, NY
- [63] Prof. Filippo Molinari – Slides “*Fondamenti di risonanza magnetica*” – Modulo di Bioimmagini – Politecnico di Torino
- [64] <http://www.andreaforneris.com/appunti-rm/2009/pdf/A-Parte2Apparecchiature.pdf> visited on 18/05/2021
- [65] Francesco Paolo Sellitti - “*Apparecchiature e Tecnologie di Risonanza Magnetica per immagini*” – Federazione Nazionale Colledi Tecnici Sanitari di Radiologia Medica
- [66] <https://upmc salvatormundi.it/diagnostica-per-immagini/risonanza-magnetica-aperta-e-chiusa-differenze> visited on 14/05/2021
- [67] https://it.wikipedia.org/wiki/Imaging_a_risonanza_magnetica visited on 29/04/2021
- [68] https://www.youtube.com/watch?v=E44W54z_Ykw visited on 30/04/2021
- [69] <https://www.istituto-besta.it/risonanza-magnetica-cosa-e-e-come-funziona-la-risonanza-magnetica-> visited on 18/05/2021
- [70] Urschütz – “*SIEMENS Healthcare particle therapy*” – Modified
- [71] Claudia Pardi – “*Effetto della modellazione della linea di fascio sull’ottimizzazione del piano di trattamento in radioterapia*”- Tesi magistrale in Ingegneria Energetica e Nucleare – Politecnico di Torino 2017 – 2018
- [72] <https://www.youtube.com/embed/FcS7dx7NuJE?rel=0> visited on 16/11/2021
- [73] Yi-Lan Lin – “*Proton beam therapy of periorbital sinonasal squamous cell carcinoma: Two case reports and review of literature*” – World Journal of Clinical Oncology, Aug 24, 2020; 11 (8): 655-672
- [74] F. Bourhaleb, F. Marchetto, A. Attili, G. Pittà, R. Cirio, M. Donetti, et al. – “*A treatment planning code for inverse planning and 3D optimization in hadrontherapy*” – Computers in Biology and Medicine 38 (2008) 990 – 999
- [75] S. Scoccianti, B. Detti, D. Gadda, D. Greto et al. – “*Organs at risk in the brain and their dose-constrained in adults and children: A radiation oncologist’s guide for delineation in everyday practice*” – Radiotherapy and Oncology 114 (2015) 230 - 238
- [76] G. Ruvio, R. Solimene, A. Cuccaro, G. Fiaschetti, A. J. Fagan, S. Cournane, J. Cooke, M. J. Ammann, J. Tobon and J. E. Browne – “*Multimodal Breast Phantoms for Microwave, Ultrasound, Mammography, Magnetic Resonance and Computed Tomography Imaging*” – Sensors 2020
- [77] <https://www.ojs.unito.it/index.php/jbp/article/view/4654> visited on 16/08/2021
- [78] A. Elter, S. Dorsch, P. Mann, A. Runz, W. Johnen, C. K. Spindeldreier, S. Klüter and C. P. Karger – “*End-to-end test of an online adaptive treatment procedure in MR-*

- guided radiotherapy using a phantom with anthropomorphic structures” – Physics in Medicine & Biology 64 (2019) 225003 (13 pp)
- [79] <https://insimu.com> visited on 16/08/2021
- [80] <https://www.bellevuecollege.edu/news/2019/07/29/radiation-therapy-in-the-virtual-world/> visited on 16/08/2021
- [81] https://www.youtube.com/watch?v=a4uq_AkYzCg visited on 16/08/2021
- [82] <https://www.vertual.co.uk/products/vert/> visited on 16/08/2021
- [83] F. Lewis, et al – “Anxiety and its time courses during radiotherapy for non-metastatic breast cancer: A longitudinal study” - 2014 Elsevier Ireland
- [84] Alexander Raith – “VIPER – Virtual Patient Education in Radiotherapy” – Master Thesis, St. Polten University of Applied Sciences
- [85] L.P. Neves, A. B. Franco, M. França, M. R. Soares, W. Belinato, W. S. Santos, L. V. E. Caldas and A. P. Perini – “Computational dosimetry in a pediatric i-CAT procedure using virtual anthropomorphic phantoms” – Radiation Physics and Chemistry 167 (2020)
- [86] <https://www.i-seecomputing.com/products.html> visited on 30/11/2021
- [87] Annals of the ICPR, ICPR Publication 110 – “Adult References Computational Phantoms” – Editor C. H. Clement, 2009
- [88] <https://www.i-seecomputing.com/web-application.html> visited on 30/11/2021
- [89] <https://nicetomeetu21.github.io/2020/02/13/Image%20Processing/> 《Digital-Image-Processing-Gonzalez-》 -第3章-学习笔记/ visited on 16/11/2021

Appendix

- *Filtro_gammalog_brain*

```
%%%%%%%%%%%%%%%%%%%%%%%%%%%%%%%%%%%%%%%%%%%%%%%%%%%%%%%%%%%%%%%%%%%%%%%%%%%%%%
% Author: Isabel De Pasquale %
% Description: The code receives as input a set of .png %
% images from the "output" folder to which a 0.45 "gamma" %
% filter is applied. %
% Edited images are saved in the "filtro" folder. Lastly the%
% serial montage of the edited images is produced. %
%%%%%%%%%%%%%%%%%%%%%%%%%%%%%%%%%%%%%%%%%%%%%%%%%%%%%%%%%%%%%%%%%%%%%%%%%%%%%%

close all
clear all
clc

slices = dir(['output/', '*.png']);
N_slices = length(slices);
c=1;
gamma=0.45;

for s=1:N_slices
    immagine = imread(['output/', slices(s).name]);
    imd = im2double(immagine);
    im_out = c * imd .^ gamma;
    filepath=['filtro/', sprintf('%04.0f', s), '.png'];
    imwrite((im_out), filepath)
    A(:,:,s)=im_out;
End

figure (1)
montage(A);
```

- *HU_brain*

```
%%%%%%%%%%%%%%%%%%%%%%%%%%%%%%%%%%%%%%%%%%%%%%%%%%%%%%%%%%%%%%%%%%%%%%%%%%%%%%
% Author: Isabel De Pasquale %
% Description: The code memorizes the "mat_HU.bin" binary %
% file in 64 2D matrices, each of which of the size 512X512 %
% pixels. The first section is shown specifying the display %
% range between 0 and 300. Lastly the serial montage of the %
% edited images is produced. %
%%%%%%%%%%%%%%%%%%%%%%%%%%%%%%%%%%%%%%%%%%%%%%%%%%%%%%%%%%%%%%%%%%%%%%%%%%%%%%
```

```

clear all
close all
clc

fileID = fopen('mat_HU.bin');
for ii=1:64
    A(:,:,ii)=fread(fileID,[512 512],'int16');
end

figure(1)
imshow((A(:,:,1)),[0 300]);
fclose(fileID);

figure (2)
montage(reshape(uint16(A),[size(A,1),size(A,2),1,size(A,3)]),
'DisplayRange',[0 300]);
set(gca,'clim',[0 300]);
drawnow;
shg;

```

- *ID_brain*

```

%%%%%%%%%%%%%%%%%%%%%%%%%%%%%%%%%%%%%%%%%%%%%%%%%%%%%%%%%%%%%%%%%%%%%%%%
% Author: Isabel De Pasquale %
% Description: The code memorizes the "mat_ID.bin" binary %
% file in 64 2D matrices, each of which of the size 512X512 %
% pixels. The first section is shown specifying the display %
% range between 0 and 35. Moreover a 3.5 "gamma" filter is %
% applied to improve image quality. Lastly the serial %
% montage of the edited images is produced. %
%%%%%%%%%%%%%%%%%%%%%%%%%%%%%%%%%%%%%%%%%%%%%%%%%%%%%%%%%%%%%%%%%%%%%%%%

clear all
close all
clc

fileID = fopen('mat_ID.bin');

for ii=1:64
    A(:,:,ii)=fread(fileID,[512 512],'int16');
end

figure(1)
imshow((A(:,:,1)),[0 35]);
fclose(fileID);

```

```

c=1;
gamma=3.5;
immagine = imread('Figura4.png');
imd = im2double(immagine);
im_out = c * imd .^ gamma;
imwrite(im_out, 'Figure4_pro3.5.png')

figure (2)
montage(reshape(uint16(A), [size(A,1), size(A,2), 1, size(A,3)]),
'DisplayRange', []);
set(gca, 'clim', [0 35]);
drawnow;
shg;

```

- *Filtro_gammalog_prostate*

```

%%%%%%%%%%%%%%%%%%%%%%%%%%%%%%%%%%%%%%%%%%%%%%%%%%%%%%%%%%%%%%%%%%%%%%%%
% Author: Isabel De Pasquale %
% Description: The code receives as input a set of .png %
% images from the "output" folder to which a 0.40 "gamma" %
% filter is applied. Edited images are saved in the "filtro"%
% folder. Lastly the serial montage of the edited images is %
% produced. %
%%%%%%%%%%%%%%%%%%%%%%%%%%%%%%%%%%%%%%%%%%%%%%%%%%%%%%%%%%%%%%%%%%%%%%%%

close all
clear all
clc

slices = dir(['output/', '/*.png']);
Nslices = length(slices);
c=1;
gamma=0.40;

for s=1:Nslices
    immagine = imread(['output/', slices(s).name]);
    imd = im2double(immagine);
    im_out = c * imd .^ gamma;
    filepath=['filtro/', sprintf('%04.0f', s), '.png'];
    imwrite((im_out), filepath)
    B(:, :, s)=imd;
    A(:, :, s)=im_out;
end

figure (1)

```

```
montage(A);
figure (2)
montage(B);
```

- *HU_prostate*

```
%%%%%%%%%%%%%%%%%%%%%%%%%%%%%%%%%%%%%%%%%%%%%%%%%%%%%%%%%%%%%%%%%%%%%%%%
% Author: Isabel De Pasquale %
% Description: The code memorizes the "mat_HU.bin" binary %
% file in 83 2D matrices, each of which of the size 512X512 %
% pixels. The first section is shown specifying the display %
% range between -10 and 250. Lastly the serial montage of %
% the edited images is produced. %
%%%%%%%%%%%%%%%%%%%%%%%%%%%%%%%%%%%%%%%%%%%%%%%%%%%%%%%%%%%%%%%%%%%%%%%%

clear all
close all
clc

fileID = fopen('mat_HU.bin');

for ii=1:83
    A(:, :, ii)=fread(fileID, [512 512], 'int16');
end

figure(1)
imshow(A(:, :, end), [-10 250]);
fclose(fileID);

figure (2)
montage(reshape(uint16(A), [size(A,1), size(A,2), 1, size(A,3)]),
'DisplayRange', []);
set(gca, 'clim', [-10 250]);
drawnow;
shg;
```

- *ID_prostate*

```
%%%%%%%%%%%%%%%%%%%%%%%%%%%%%%%%%%%%%%%%%%%%%%%%%%%%%%%%%%%%%%%%%%%%%%%%
% Author: Isabel De Pasquale %
% Description: The code memorizes the "mat_ID.bin" binary %
% file in 83 2D matrices, each of which of the size 512X512 %
% pixels. The first section is shown specifying the display %
% range between 0 and 50. Lastly the serial montage of the %
% edited images is produced. %
%%%%%%%%%%%%%%%%%%%%%%%%%%%%%%%%%%%%%%%%%%%%%%%%%%%%%%%%%%%%%%%%%%%%%%%%
```

```

clear all
close all
clc

fileID = fopen('mat_ID.bin');
for ii=1:83
    A(:,:,ii)=fread(fileID,[512 512],'int16');
end

figure(1)
imshow((A(:,:,83)),[0 50]);
fclose(fileID);

figure (2)
montage(reshape(uint16(A),[size(A,1),size(A,2),1,size(A,3)]),
'DisplayRange',[0 50]);
set(gca,'clim',[0 50]);
drawnow;
shg;

```

- *Filtro_gammalog_left_lung*

```

%%%%%%%%%%%%%%%%%%%%%%%%%%%%%%%%%%%%%%%%%%%%%%%%%%%%%%%%%%%%%%%%%%%%%%%%
% Author: Isabel De Pasquale %
% Description: The code receives as input a set of .png %
% images from the "output" folder to which a 0.50 "gamma" %
% filter is applied. Edited images are saved in the "filtro"%
% folder. Lastly the serial montage of the edited images is %
% produced. %
%%%%%%%%%%%%%%%%%%%%%%%%%%%%%%%%%%%%%%%%%%%%%%%%%%%%%%%%%%%%%%%%%%%%%%%%

close all
clear all
clc

slices = dir(['output/', '/*.png']);
Nsllices = length(slices);
c=1;
gamma=0.50;

for s=1:Nsllices
    immagine = imread(['output/',slices(s).name]);
    imd = im2double(immagine);
    im_out = c * imd .^ gamma;
    filepath=['filtro/', sprintf('%04.0f', s), '.png'];

```

```

        imwrite((im_out), filepath)
        B(:,:,s)=imd;
        A(:,:,s)=im_out;
end
figure (1)
montage(A);
figure (2)
montage(B);

```

- *HU_left_lung*

```

%%%%%%%%%%%%%%%%%%%%%%%%%%%%%%%%%%%%%%%%%%%%%%%%%%%%%%%%%%%%%%%%%%%%%%%%%%
% Author: Isabel De Pasquale %
% Description: The code memorizes the "mat_HU.bin" binary %
% file in 97 2D matrices, each of which of the size 512X512 %
% pixels. The first section is shown specifying the display %
% range between -10 and 250. Lastly the serial montage of %
% the edited images is produced. %
%%%%%%%%%%%%%%%%%%%%%%%%%%%%%%%%%%%%%%%%%%%%%%%%%%%%%%%%%%%%%%%%%%%%%%%%%%

clear all
close all
clc

fileID = fopen('mat_HU.bin');

for ii=1:97
    A(:,:,ii)=fread(fileID,[512 512],'int16');
end

figure(1)
imshow((A(:,:,54)), [-10 250]);
fclose(fileID);

figure (2)
montage(reshape(uint16(A), [size(A,1), size(A,2), 1, size(A,3)]),
'DisplayRange', []);
set(gca, 'clim', [-10 250]);
drawnow;
shg;

```

- *ID_left_lung*

```

%%%%%%%%%%%%%%%%%%%%%%%%%%%%%%%%%%%%%%%%%%%%%%%%%%%%%%%%%%%%%%%%%%%%%%%%%%
% Author: Isabel De Pasquale %

```

```

% Description: The code memorizes the "mat_ID.bin" binary %
% file in 97 2D matrices, each of which of the size 512X512 %
% pixels. The first section is shown specifying the display %
% range between 0 and 70. Lastly the serial montage of the %
% edited images is produced. %
%%%%%%%%%%%%%%%%%%%%%%%%%%%%%%%%%%%%%%%%%%%%%%%%%%%%%%%%%%%%%%%%%%%%%%%%

clear all
close all
clc

fileID = fopen('mat_ID.bin');

for ii=1:97
    A(:,:,ii)=fread(fileID,[512 512],'int16');
end

figure(1)
imshow((A(:,:,54)),[0 70]);
fclose(fileID);

figure (2)
montage(reshape(uint16(A),[size(A,1),size(A,2),1,size(A,3)]),
'DisplayRange',[0 70]);
set(gca,'clim',[0 70]);
drawnow;
shg;

```